WIENER KERNEL ANALYSES OF THE FUNCTIONAL MICROSTRUCTURE OF A CRUSTACEAN VISUAL FIELD

Thesis by

David Sheby

In Partial Fulfillment of the Requirements

for the Degree of

Doctor of Philosophy

California Institute of Technology

Pasadena, California

1978

(Submitted December 19, 1977)

ACKNOWLEDGEMENTS

Wives are usually acknowledged last in theses, but I cannot let that convention override my appreciation of the unflinching support and encouragement that my wife, Deborah, gave to me throughout my tenure as a graduate student at Caltech. Without her, I would not now be able to savor the satisfaction and honor of acknowledging the following people who, in different ways, guided and/or assisted my thesis research. Thank you, Deb!

I am very much indebted to my thesis advisor, Dr. Gilbert D. McCann, for having provided me with the unique opportunity of studying within the extremely exciting and stimulating interdisciplinary atmosphere of the Bioinformation Systems group at Caltech, envisioned, created and guided by his keen foresight and intelligence. I am also grateful to Dr. McCann for: his continued financial support throughout my graduate studies; and for many invaluable conversations that assisted me in carrying out this research.

I wish to thank Professors Derek Fender and Nicholas George for the unique blends of friendship and scientific counsel that they variously supplied at times of need.

I've particularly enjoyed my relatively recent association with Dr. CAG Wiersma who has patiently tolerated my white noise assault on his crayfish and who has provided me with much invaluable information about nervous systems. I wish to thank Dr. Wiersma's associate, Ms. Joan Roach, for many conversations about crayfish physiology and for

allowing me to access her reprint file. I wish to thank my friend, Dr. Donald Rafuse (Loma Linda University) for many enjoyable conversations about 038, and for his unselfish supplies of photographs and field maps of the crayfish eye.

I wish to thank Dr. Amnon Yariv for allowing me the use of his laboratory, for working on my optic fibers and LEDs', and for allowing me to question, at length, his graduate students, post docs, and technicians about various aspects of electro-optic technology. Through Dr. Yariv, I met Drs. Jacques Pankove and David Medved who were very helpful to me in my research.

My day-to-day successes in the laboratory could not have been achieved without the help of the following individuals: Mr. Daniel Aranovich, who designed my LEDs' current drivers and who kept my electronic equipment operational; Mr. Albert Broers, who transformed many of my vague ideas about mechanical devices into operational working realities; and Mr. Dale Knutsen, who provided me with many additional programs to supplement his LAB and GAS data collection and analyses systems which made research at Caltech a pleasure.

Much of my special purpose equipment was donated to me by some very generous people and organizations: Dr. Jacques Pankove of RCA's David Sarnoff Research Laboratories (Princeton, N.J.) provided me with samples of his experimental blue GaN LEDS; Dr. David Medved of Meret, Inc. (Santa Monica, CA) provided me with a constant supply of Pilkington optic fibers; Mr. Enrique J. Flesch of United Detector Technology, Inc. (Santa Monica, CA) provided me with supplies of PIN

photo diodes; various sized hypodermic needles were provided by The Huntington Hospital (Pasadena, CA) and American Hospital Supply (Irvine, CA); odd sized optic fibers for my early stimulus designs were provided by: Corning Glass Works (Corning, N.Y.); Dr. Ronald Chesler of Fiber Communications, Inc. (East Orange, N.J.); Dr. Michael Barnoski of Hughes Research Laboratories (Malibu, CA); and International Fiber Optics, Inc. (Oxnard, CA).

I would like to thank Drs. Vasilis Marmarelis and Syozo Yasui for many enlightening conversations about Wiener kernels. I would also like to thank Drs. Dick Nassel (University of Lund, Sweden) and Richard Olivo (Smith College) for long distance correspondences and conversations which cleared up many questions about crayfish anatomy and physiology, respectively.

Last, but not least, I would like to thank the California Institute of Technology for being what it is; and the National Institutes of Health for the various grants that supported this work.

ABSTRACT

The microstructure of the excitatory field of the crayfish sustaining fiber 038 was studied by Wiener kernel analysis. By treating the receptive field as a multi-input single-output system, Volterra's, and Wiener's, nonlinear functional formalisms for such systems could be invoked to define the canonical types of interactions that could, and do, underlie the field.

A light emitting diode/fiber optic stimulus package was developed for these experiments to:provide the required spatial configurations of independently (noise-) modulated sources; optimally excite the crayfish's yellow-sensitive visual system; and to eliminate the artifacts that might arise from conventional light sources' spectral dependence on drive current.

The second-order cross kernels computed from 2-, and 4-input experiments indicate that a lateral excitation phenomenon is predominant in the field. Evidence for lateral inhibition (between yellow channels) is indirect, but suggestive that inhibition manifests itself through a third-order cross term. 038 does receive inputs from yellow and blue channels, and their is evidence of yellow channel inhibition of the blue channel. Periodic structure found in 038's spike train response to multiple stimuli can be modelled by first and second-order self kernels without the use of cross terms.

Analysis of the kernel dynamics leads to a model of the functional microstructure subserving 038's excitatory field.

TABLE OF CONTENTS

Chapter 1

INTRODUCTION: THE MICROSTRUCTURE OF RECEPTIVE FIELDS

1.1 Basic Concepts

Visual systems are comprised of two basic parts: a photoreceptor layer of light sensitive cells which transduce photon absorption into electrical signals; and a cascaded plexus of cells which process those signals into a representation of the visual environment of interest to the animal. That representation is determined by the "receptive field" properties of those afferent cells which transmit the processed signals from the animal's eye to its brain. A receptive field for a visual system cell is defined in terms of the locus of points on the photoreceptor array whose stimulation by light induces a response in the particular cell under study. To "decipher" the messages used by an animal in reconstructing its visual environment it is necessary to study the spatial and temporal encoding properties of the component receptive fields comprising its visual system and providing the sole inputs to the animal's brain.

Receptive fields were first described for the retinal ganglion cells of vertebrates by Hartline (1938), and since then most concepts on the organization of receptive fields have evolved from the particulars found in the vertebrate system, thus making comparisons with other systems (i.e., invertebrate and non-biological) based on universal processing concepts difficult. In the vertebrate eye the most commonly found receptive field structure is that of the center-on

surround-off variety which consists of two concentric circular regions on the retina. Light stimulation of the "center" region induces an excitation in the cell; stimulation of the surrounding annulus inhibits the cell. Architectures exist with the roles of center and surround reversed, with slightly different geometries, or with the regions individually displaying more complex, or, perhaps, not so well delineated, behaviors.

Most of the early functional studies on receptive fields concentrated on the temporal properties of the center and surround and the mutual antagonism between them. In such studies a sinusoidal light stimulation is presented diffusely over the entire field of a particular receptive field unit, or selectively to the field's center or surround, and the ganglion cell's response is recorded as a function of stimulus temporal frequency. The mutual interaction between a center and surround is studied by observing changes in the center's (surround's) dynamic response induced by presentation of a stationary illumination to the surround (center). In such experiments the sinusoid signals have had a low depth of modulation to insure the linearity of the system.

Vision, however, in all but the simplest biological systems, is a two-dimensional spatial process charged with the detection of forms, textures, and motions which involve processing techniques not easily analyzed by a single temporally fluctuating signal. Textural information, for example, is contained in the two-dimensional spatial joint probability distributions of a pattern's luminance flux: camouflage is a widely employed survival technique which takes advantage of a preda-

tor's inability to discriminate between an object and a background when both share certain statistical similarities in their luminance compositions.

When receptive fields are viewed from this perspective, i.e., their ability or inability to encode properties of incident patterns, all previous barriers to comparisons between vertebrate and invertebrate systems disappear. For now the object of a receptive field study is not the elucidation and study of a particular architecture, but of the basic information and signal processing schemes which determine the types of patterns that can be processed by a visual system. Consider, for example, Rodieck's (1965) model of retinal receptive fields in which a ganglion cell's response results from a linear summation of the excitation and inhibition within the field, and weighed by appropriate sensitivity coefficients. Such systems have been extensively studied by Minsky and Papert (1969) in their work on the nonbiological pattern recognition devices known as perceptrons, and have been shown to be severely limited in their ability to encode geometrical features of patterns. Such linear summation mechanisms cannot detect connectivity or certain topological invariants (under rotation), nor can these systems separate overlapping figures from one another (Abelson, 1977). A visual system constructed as Rodieck envisioned would suffer from severe processing limitations. Perhaps nature's awareness of the simplicity of this scheme is demonstrated by the existence of "Y"-type ganglion cells in the cat retina, which possess widespread nonlinear summation properties throughout their receptive fields (Enroth-Cugell & Robson, 1966; Hochstein & Shapley, 1976a,b).

As yet, Minsky and Papert's (1969) approach to analyzing geometrical encoding limitations has not been extended to these types of nonlinear systems.

The neural substrate of visual systems is involved in a great amount of lateral signal processing among disparate retinal regions for the extraction of spatio-temporal relationships from the induced electrical activity in photoreceptors to reflect real world objects and events. What the exact nature of these interactions is largely unknown. Attention has been turning from overall temporal field properties to the local functional microstructure from which receptive fields are built. This has involved the use of small spot stimuli or sine-wave gratings positioned within a particular subregion to examine the "summation" properties of the field (Stone & Fabian, 1968; Easter, 1968; Grusser, et al, 1970; Glantz, 1971; Levine & Abramov, 1975; Hochstein & Shapley, 1976a,b). Such studies have important implications for the understanding of the processing capabilities and limitations of receptive fields in encoding information about the structure of patterns incident upon them.

1.2 Nonlinear Summation Phenomena

In most studies on the spatial summation properties of receptive fields the experimental procedure has been to stimulate two (equisensitive) areas of a receptive field subregion (usually an on-center region) independently and then simultaneously, and to observe the ganglion cell's response, R, to each situation (Stone & Fabian, 1968; Easter, 1968; Grusser, et al, 1970; Levine & Abramov, 1975). The two stimulated

areas of the center are identified by the nomenclature "area 1" and "area 2", and the light intensity incident on each is I_1 and I_2, respectively. R_i denotes the ganglion cell's response (in spikes per second) when "area i" is illuminated with I_i. R_{1+2} is the response when areas 1 and 2 are illuminated simultaneously (with $I_1=I_2$). The objective of such experiments has been to compare R_{1+2} to the algebraic sum of the R_i. If

$$R_{1+2} = R_1 + R_2 \qquad (1.2.1)$$

then the system is said to be linear, and no interactions appear to be taking place between the two areas in the receptive field. If, however,

$$R_{1+2} \neq R_1 + R_2 \qquad (1.2.2)$$

then the receptive field summation is said to be nonlinear, because superposition (i.e., addition) of the two areas' elicited responses did not occur. Equation 1.2.2 is rewritten as

$$R_{1+2} = R_1 + R_2 + \Delta \qquad (1.2.3)$$

where Δ is a distortion factor reflecting the nonlinear interaction between the two areas. If $\Delta > 0$, then an increase in the spike rate has occurred, indicating a facilitory (i.e., excitatory) interaction between the two areas. If, however, $\Delta < 0$, then R_{1+2} reflects a reduction in the spike rate which could indicate: 1) an inhibitory interaction between the two areas; or 2) a spike rate compression resulting from the cell's inability to exceed a maximum firing rate, R_{max}, due

to its refractory period (i.e., $R_1 + R_2 > R_{max} = R_{1+2}$). For $\Delta < 0$ the source of the nonlinear summation needs to be determined and various strategies have been used to accomplish that (Grusser, et al, 1970; Abramov & Levine, 1975; Levine & Abramov, 1975).

Such multi-spot paradigms have been used to examine the microstructure of the cat (Stone & Fabian, 1968; Grusser, et al, 1970), the goldfish (Easter, 1968; Abramov & Levine, 1975; Levine & Abramov, 1975), and a crustacean's retinal receptive fields (Glantz, 1971). Cats appear to have extensive lateral interactions in the receptive fields of their Y-type ganglion cells (e.g., Hochstein & Shapley, 1976a), but the source of the goldfish's nonlinear summation appears to be spike compression (Abramov & Levine, 1975). That different results should be found in animals from different environments is not surprising, but other than identifying a nonlinear summation and its possible source, these experiments have provided little insight into the encoding properties of receptive fields, nor do they freely yield any information about the interactions' dynamics. Their limited scope of interpretability has stemmed, in part, from the absence of a formalistic conceptual framework for defining and classifying canonic types of interactions that might exist within a visual system and for examining the processing capabilities of each. How, for example, might a 4-spot stimulus used by Grusser, et al (1970) differ from a 2-spot configuration in its theoretical and practical effectiveness in exciting and extracting functionally distinct interaction phenomena in a receptive field? Such a question cannot be posed nor examined without an appro-

priate formalism in which to set such a question.

1.3 Volterra Descriptors for Receptive Field Interactions

The Volterra series expansion for multi-input systems is an appropriate formalism for describing the rich variety of spatial interactions in a visual system through the mechanism of "cross kernels". The need for cross kernels is underscored by the fact that even the simple eye of Limulus has lateral inhibition containing a second-order nonlinearity (Barlow & Lange, 1974) with nontrivial properties (Barlow & Quarles, 1975). For a system with a single input $x(t)$, the output $y(t)$ can be written as a Volterra series of the form

$$y(t) = \sum_{n=1}^{\infty} \int_{-\infty}^{\infty} \cdots \int_{-\infty}^{\infty} g_n(\tau_1, \cdots \tau_n) \prod_{j=1}^{n} x(t-\tau_j) d\tau_1 \cdots d\tau_n \qquad (1.3.1)$$

where the kernels $g_n(\tau_1, \tau_2, \cdots, \tau_n)$ describe the system's response for any input. In such a single input system there are no other input channels for cross-channel (i.e., lateral) interactions to take place, hence there is no need for "cross kernels". For a system with N input channels, the Volterra series expansion for $y(t)$ includes such interaction terms and is written as

$$y(t) = \sum_{k_1=0}^{N} \cdots \sum_{k_N=0}^{N} \int_{-\infty}^{\infty} \cdots \int_{-\infty}^{\infty} g_{k_1 k_2 \cdots k_n}(\tau_{1,1}, \tau_{1,2}, \cdots, \tau_{1,k_1}; \cdots;$$

$$\cdot\ \tau_{k_n,1},\tau_{k_n,2}\cdots,\tau_{k_n,k_n})$$

$$\cdot\ x_1(t-\tau_{1,1})x_1(t-\tau_{1,2})\cdots x_1(t-\tau_{1,k_1}) \qquad (1.3.2)$$

$$\cdots$$

$$\cdot\ x_N(t-\tau_{k_N,1})x_N(t-\tau_{k_N,2})\cdots x_N(t-\tau_{k_N,k_N})\,d\tau_{1,1}\cdots d\tau_{k_N,k_N}$$

(In this notation a zero subscript, i.e., $k_i=0$, eliminates the corresponding integration and input (Parente, 1970).)

Such a notation, however, is cumbersome: the elegance and utility of the Volterra series for multi-input systems is better realized by rewriting equation 1.3.2 as a sum of nonlinear interactions of lower order (Poggio & Reichardt, 1976):

$$y(t) = g_o + \sum_{k=1}^{N} g_k * x_k + \sum_{k,j}^{N} g_{kj} *^2 x_k x_j + \cdots$$

$$+ \sum_{k_1\cdots,k_n}^{N} g_{k_1,k_2,\cdots,k_n} *^n x_{k_1}\cdots x_{k_n} + \cdots \qquad (1.3.3)$$

where

$$g_{k_1\cdots k_p} *^p x_{k_1}\cdots z_{k_p} = \int_{-\infty}^{\infty}\cdots\int_{-\infty}^{\infty} g_{k_1\cdots k_p}(\tau_1,\cdots,\tau_p)$$

$$\cdot \prod_{j=1}^{p} x_{k_j}(t-\tau_j)\,d\tau_1\cdots d\tau_p \qquad (1.3.4)$$

(The dc term, g_0, can be eliminated from this expansion if one wishes to avoid the possibility of a system response without a causative input (Bedrosian & Rice, 1971).)

In equations 1.3.1 and 1.3.3 the kernels $g_{k_1 \ldots k_n}$ are the self-kernels (of order n) for channel r when all the subscripts are identical (i.e., $k_1=k_2=\ldots=k_n=r$) and describe the system response R_r of the previous section. In this manner the notation for the (n-) order of the kernel is indicated by the number of subscripts. Hence, $g_{k_1 \ldots k_n}$ of equations 1.3.1 and 1.3.3 is identical to g_n of equation 1.3.1 when $k_1=k_2=\ldots=k_n=1$. The second term of equation 1.3.3 contains kernels with only one subscript and reflects the first-order "self" kernels for each of the N input channels. Interaction among channels can only occur when there are two or more input channels to the system. Interaction terms, i.e., cross kernels, are defined by those terms $g_{k_1 \ldots k_n}$ $(n \geq 2)$ possessing different subscripts, and reflects the "distortion" previously denoted by Δ. Hence $g_{ij}(\tau_1,\tau_2)$ describes the second-order interaction between channels i and j; $g_{ijk}(\tau_1,\tau_2,\tau_3)$ describes a third-order interaction between channels i, j, and k; $g_{iij}(\tau_1,\tau_2,\tau_3)$ describes a third-order interaction between two channels (i and j). The p-order of a system (Poggio & Reichardt, 1976; Abelson, 1977) is defined as the number of different channels providing inputs to an interaction term: $g_{iij}(\tau_1,\tau_2,\tau_3)$ is a third-order (i.e., n-order 3) kernel of p-order 2.

The Volterra series of equation 1.3.3 can be truncated to any desired value of n to reflect the degree of the highest nonlinearity of interest.

Hence for n=1, equations 1.3.1 and 1.3.3 reflect the convolution integral of linear systems theory, and is the system that Minsky and Papert (1969) studied (the threshold mechanism included in their perceptron is easily incorporated by cascading the pulse encoder described in Chapter 3). Discussions of the Volterra kernels' availability (through the closely related non-linear G-functionals of Wiener (1958)) are deferred until Chapter 3.

Retinal receptive fields, composed of multiple (photoreceptor) inputs and a single cell's output, may be thought of as multi-input single-output systems with their own Volterra series expansions. The cross kernels of equation 1.3.3 reveal that such a system's response may depend on interactions among signals arising from various combinations of input ports. If multi-spot "response-summation" experiments, described in Section 1.2, used sufficiently small stimuli to stimulate single (or, practically, very small numbers of) input channels, then equation 1.3.3 suggests that there are classes of interactions (of p-order 3 and greater) which, if existent within a tested system, could not be excited nor detected by 2-spot configurations. How many of these higher p-order interactions are actually operating in a visual system is a question that has not been widely or directly studied in the past. Poggio and Reichardt (1976) have speculated extensively on the nature of the neural interactions that underlie certain aspects of the optokinetic response of flies. They have postulated on p-order 4 lateral inhibitory networks subserving the position dependent component of the fly's pattern fixation behavior, and on similar networks underlying the fly's ability to discriminate between a

figure and ground, but no neurophysiological experiments have been performed to confirm their speculations. (p-order 2 cross kernels, underlying motion detection in flies, have been identified by Marmarelis and McCann (1973).)

Julesz (1975), in a set of experiments specifically designed to examine such processing limitations (vis-a-vis a particular visual processing task),used pairs of computer-generated "random" textures to examine the classes of textures that a (human) visual system could not process. He was able to demonstrate that two textures were distinguishable from each other if they differed in either their first-, or second-order luminance probability distributions; if, however, the textures were identical in their first-, and second-order statistics, but differed in their third-order distributions, then they were indistinguishable from each other. This set a surprisingly low upper limit on the number of adjacent points whose luminance patterns a (human) visual system could keep track of. Julesz was unable to ascertain whether this limitation was cortical in origin or stemmed from retinal receptive field properties. Julesz (1975) suggested a simple experiment to distinguish between the two possibilities: that his computer generated textures be presented to a retinal receptive field whose response to each could be examined to determine which textures the field saw as different or the same. Thus far his suggestion has not been taken up by vertebrate researchers.

The closest a neurophysiological study has come to examining higher p-order interactions in a receptive field was Grusser et al's

(1970) which used a 4-spot stimulus (arranged in a square configuration) and its 15 permutation subsets to examine nonlinear summation on the cat ganglion cell receptive fields. Grusser found nonlinear summation (i.e., $R \sum_{i=1}^{j} \neq \sum_{i=1}^{j} R_i$, $j = 2,3,4$) and conjectured that it arose from lateral interactions within the field and not from spike compression. (From the second harmonic contents in y-cell responses to sinusoid grating stimuli, Hochstein and Shapley (1976b) have postulated a network of "small field" "rectifier" elements, of otherwise nondescript nature, subserving nonlinear spatial summation in cat receptive fields.)

Aside from these investigations and the extensive studies on lateral inhibition in the horseshoe crab Limulus (cf. Ratliff, 1974) which have provided the basic insights into the microcosm of interactions that subserve visual systems, no other studies have concerned themselves directly with identifying the extent and nature of the n- , and p-, order interactions in a receptive field and their effect on encoding stimulus parameters. This thesis attempts to partially fill that void by a direct study of the Volterra (-Wiener) kernels subserving a receptive field especially suited for dissecting the type of microstructure that has been alluded to.

1.4 The Compound Eye for Functional Microstructure Studies

The compound eye of certain invertebrates (i.e., the arthropods) is an ideal system for studying neural interactions underlying organizational phenomena common to many visual systems. Its highly patterned

geometrical array of ommatidial facets (cf. Chapter 2) permits easy access to, and stimulation of, the eye's input channels, via optic fibers, individually or in combination, with a precision and flexibility that is unavailable in the inverted retina structure of the vertebrates. With such control over the stimulated input port configurations, subtle microstructures of neural interactions can be dissected: lateral inhibition (in Limulus (Ratliff, 1974)) and motion detection (in flies (McCann and Marmarelis, 1973)) are two classic examples of the types of processes whose study has been greatly facilitated in the compound eye.

When compared with the vertebrate eye, the compound eye appears, at first, deceptively simple. Such a conclusion is quickly negated when the latter's form and motion detection capabilities are realized, as represented by the pattern recognition ability of bees , and chasing behavior of flies. That such neural processing is localized to discrete foveal regions which utilize only a part of the eye's total ommatidial pool, makes the compound eye particularly interesting for studying the differences in neural activity (and interaction paths) introduced by specific permutations of stimulus configurations onto these restricted parts of the eye.

Although receptive fields, per se, have not been a primary area of research in the compound eye, they certainly do exist therein, and to some degree resemble the organizations found in vertebrates eyes (Arnett, 1972; Wiitanen, 1974). The receptive fields of a particular class of visual interneurones in the crustacean, Procambarus clarkii (the swamp crayfish--a moderately evolved arthropod) have been particu-

larly well studied by Wiersma and his colleagues (e.g., Wiersma & Yamaguichi, 1968; Wiersma & McCann, in preparation). These interneurones, known as sustaining fibers (cf. Chapter 2) generate spike trains and may be thought of as analogous to the ganglion cells found in vertebrate retina. Their receptive fields display nonlinear summation phenomena (Glantz, 1971) which, from studies on the bursting properties of sustaining fibers (Glantz and Nudelman, 1976), are thought to arise from a rich lattice of lateral (inhibitory) interactions (cf. Chapters 5 and 7).

The well studied properties of the sustaining fibers, coupled with the general experimental advantages afforded by the compound eye (and several attributes discussed in Chapter 2) make the crayfish eye a particularly amenable preparation for studying how a receptive field organization is built up from the microstructure of interactions identified by the Volterra formalism of Section 1.3.

Using the crayfish eye, this thesis undertakes, for the first time, a concerted study of such interactions subserving a particular fiber ("Q38", cf. Wiersma & Yamaguichi, 1967; cf. Chapter 2) through the use of Wiener's nonlinear G-functionals (Chapter 3) and a specially designed optic fiber/LED package for optimally eliciting the responses of interest (Sheby & McCann, 1976: cf. Chapter 2).

The optic fiber stimulus configurations presented to the crayfish include various geometrical arrangements as well as the "patterns" of Julesz (1975) to demonstrate the universality of the approach to receptive field studies initiated here.

Using various combinations of (1-,)2-, 3-, and 4-optic fibers for presenting appropriate "white noise" stimuli (cf. Chapter 3) the order, dynamics, and extent of signal processing interactions subserving a higher order (arthropod) visual interneuron become available through Wiener kernels (cf. Chapter 3) in a manner previously unavailable to past investigations. In particular, the characteristics of the dynamics of cross talk between two (or more) input channels can be examined for changes as additional retinal regions are excited with controlled stimulus configurations. The ability to examine the effect and structure of equation 1.3.3's cross kernels introduces a new technique for examining the complexities of (multi-input) single-output (spike generating) systems invisible to the past investigations of nonlinear spatial summation phenomena.

1.5 Thesis Outline

Chapter 2 reviews the physiology of the crayfish's visual system to introduce the stimulus package used in the following experiments. Chapter 3 reviews basic concepts of Wiener and Volterra kernels and their inter-relationship, with special emphasis on how lateral interactions and spike train data affect kernel analyses.

Chapter 4 studies the basic properties of the single channels underlying 038's receptive field and Chapter 5 studies dual channel interactions. Chapter 6 extends dual channel interactions to color interactions; and Chapter 7 studies the interactions underlying 038's response to 3-, 4-, and multi-spot configurations. Chapter 8 discusses

and summarizes the results.

Chapter 2

THE PHYSIOLOGY AND STIMULATION OF THE CRAYFISH EYE

2.1 The Crayfish Eye

2.1.1 Overview of the Crayfish Visual System

The crayfish (Figure 2.1.1) is a freshwater decapod crustacean whose visual system is primarily located in two eye stalk structures that protrude laterally from the animal's head. At the distal end of the stalk is a hemispheroidally-shaped compound eye (Figure 2.1.2) which, in the fully grown adult, is composed of about 2500 ommatidia (Roach & Wiersma, 1974). An ommatidium is the functional sensory unit of the compound eye and consists of a transparent lens system (the dioptric apparatus) for collecting and directing light to its underlying cluster of eight photoreceptors (i.e., retinular cells, denoted as R1-R8, cf. Figure 2.1.3) known collectively as retinula. The retinula are surrounded by pigment cells containing screening pigments which migrate with changes in environmental illumination, thus controlling the amount of light reaching the photoreceptors (e.g., Arechiga, et al, 1974). Seven of the retinular cells surround a structure known as the rhabdom, which is the photosensitive part of the ommatidium. The rhabdom is composed of tightly packed microvilli projections of the retinular cell membranes and contains the visual pigments. The eighth retinular cell forms a separate rhabdom (Nassel, 1976). The corneal facets are the surface elements of the dioptric apparatus and, in the crayfish, are square-shaped with diameters ranging from 45 microns (Eguichi, et al, 1973) to 61.5 microns (Wald, 1968).

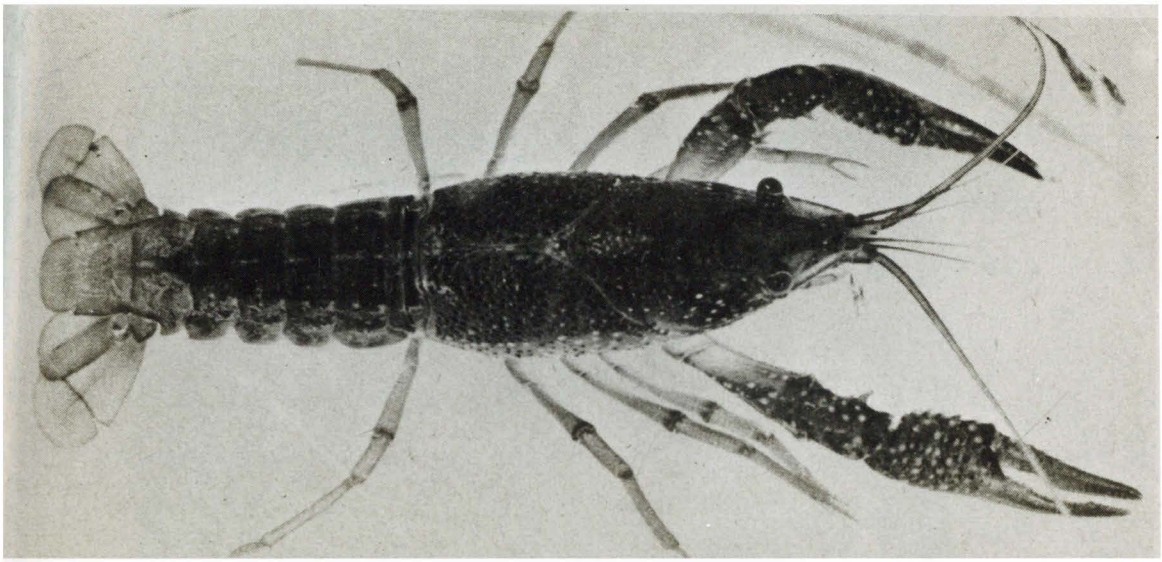

Fig. 2.1.1 An adult crayfish

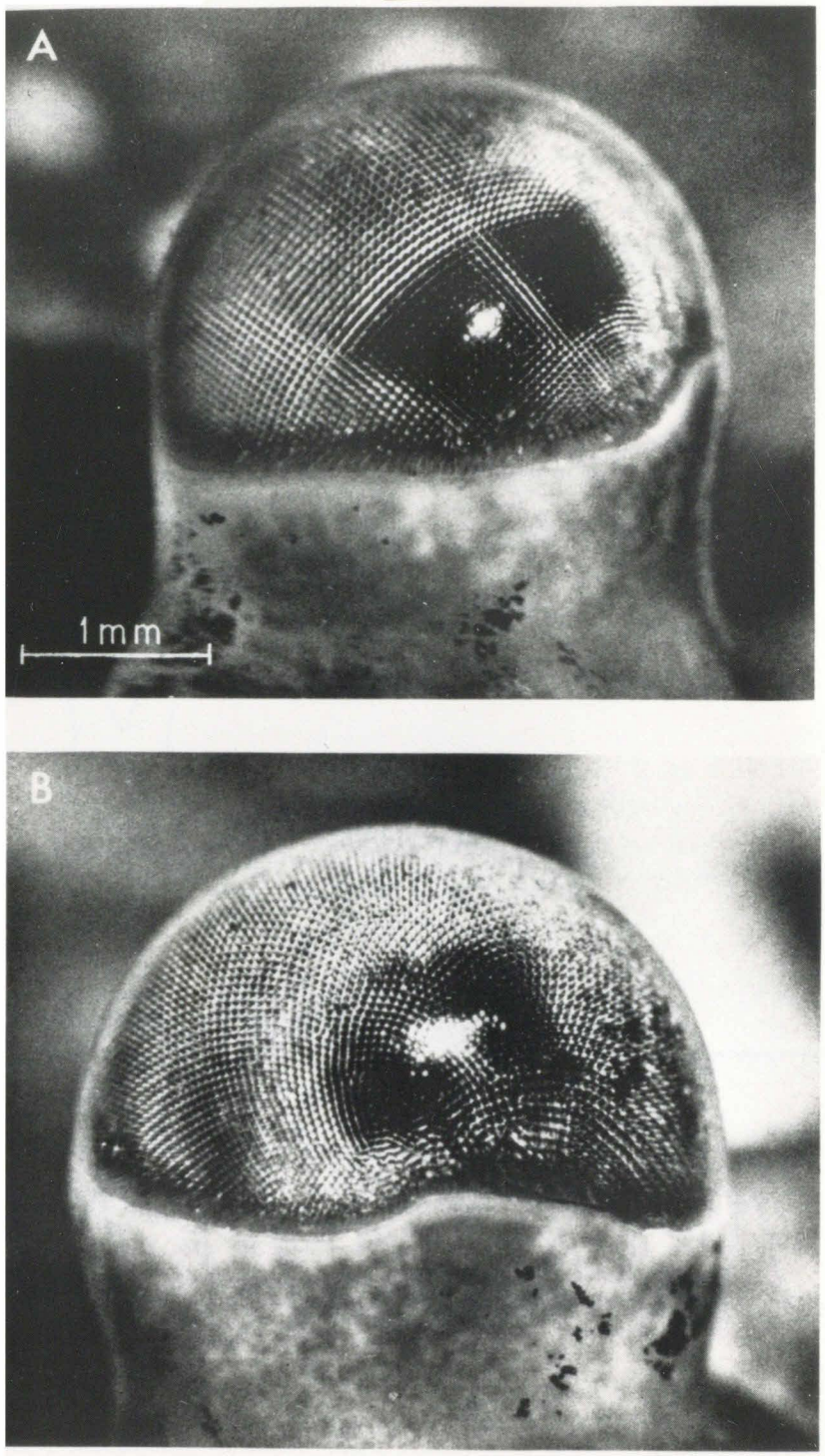

Fig. 2.1.2 Compound eye of the crayfish
(from Waterman and Fernandez (1970))
A. anterior view; B. dorsal quadrant
038's field is to right of indentation

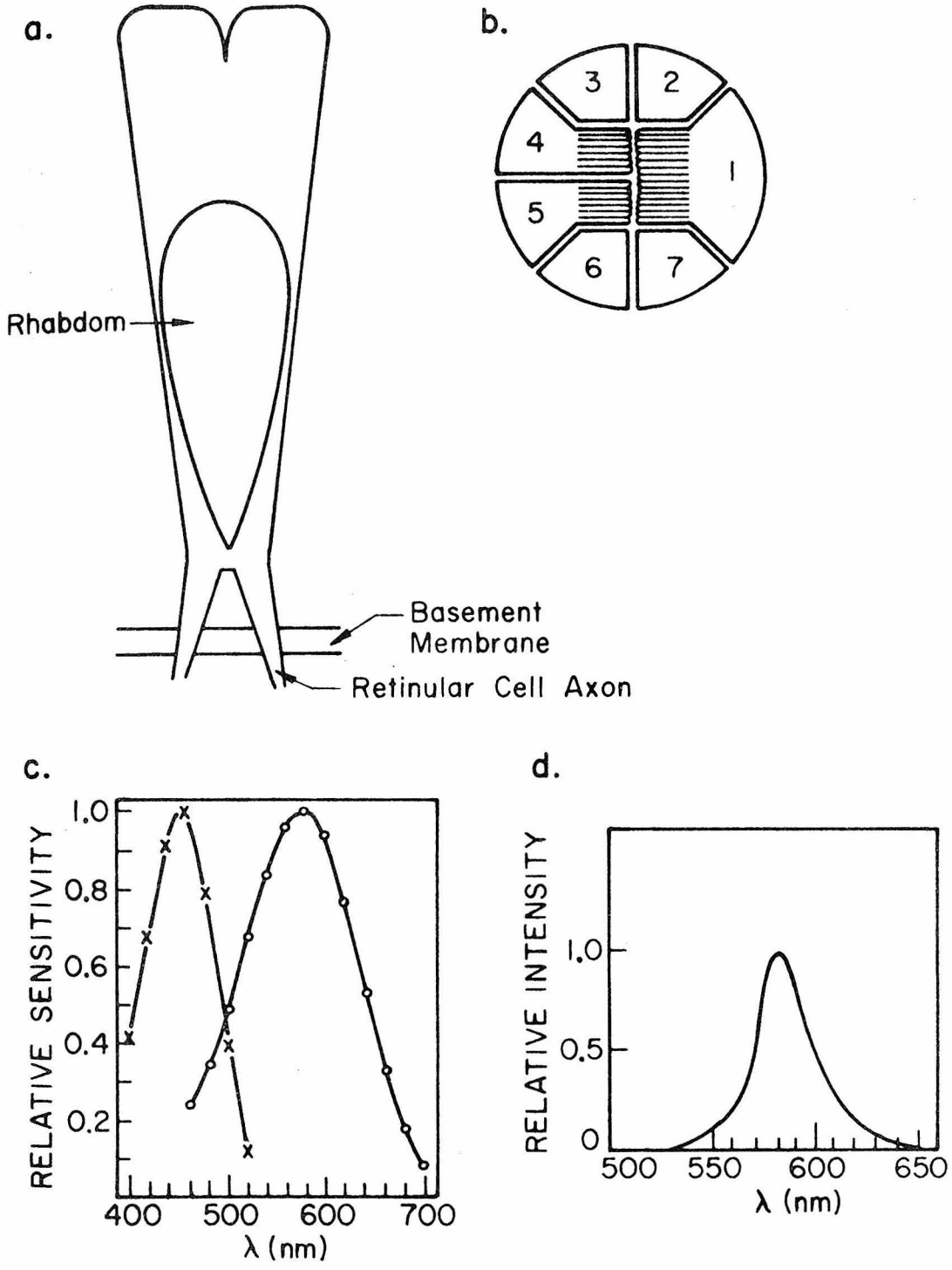

Fig. 2.1.3 Eye Physiology (a-c after Eguichi et al (1973)). (a) rhabdom; (b) retinula numbering; (c) sensitivity of "blue" and "yellow" retinular cells; (d) yellow LED spectrum

The facets are arranged in two orthogonally oblique rows (cf. Figure 2.1.4b) which, in small eye regions, appear as an array of squares.

Behind the retina lie four cascaded neural ganglia and two hormonal storage sites (the X-organ and the sinus gland). The first and most distal of the optic ganglia is the lamina ganglionaris, followed by (in increasingly proximal order) the medulla externa, the medulla interna, and the medulla terminalis (Figure 2.1.5). Exiting each eye stalk and entering the brain are approximately 17,000 fibers (Nunnemacher, et al, 1962), a small subset of which has been electrophysiologically studied by Wiersma and Yamaguichi (1966) and classified into four functional groups. One of these groups, the sustaining fibers, is composed of 14 visual interneurones whose axons run together in a single bundle (Wiersma & Yamaguichi, 1966; D. Rafuse, unpublished). These sustaining fibers are characterized by their response to a step in illumination consisting in an initial high frequency burst (with a rate of about 200-500 spikes per second) resulting in a steady-state firing rate. The firing rate of the initial burst and subsequent steady-state, as well as the latency of the response,depends on the intensity of the stimulus: the higher the intensity, the shorter the latency and the higher the firing rate. Each sustaining fiber has its own distinctive receptive field (Wiersma & Yamaguichi, 1966) which is used to uniquely define the fiber studied (e.g., cf. Woodcock & Goldsmith, 1973). The sustaining fibers are identified by a nomenclature consisting of a one or two digit code preceded by the letter "O" (Wiersma & Yamaguichi, 1966).

The most commonly found, and presumably the largest, of the sustaining fibers is known as O38. O38's receptive field consists of an

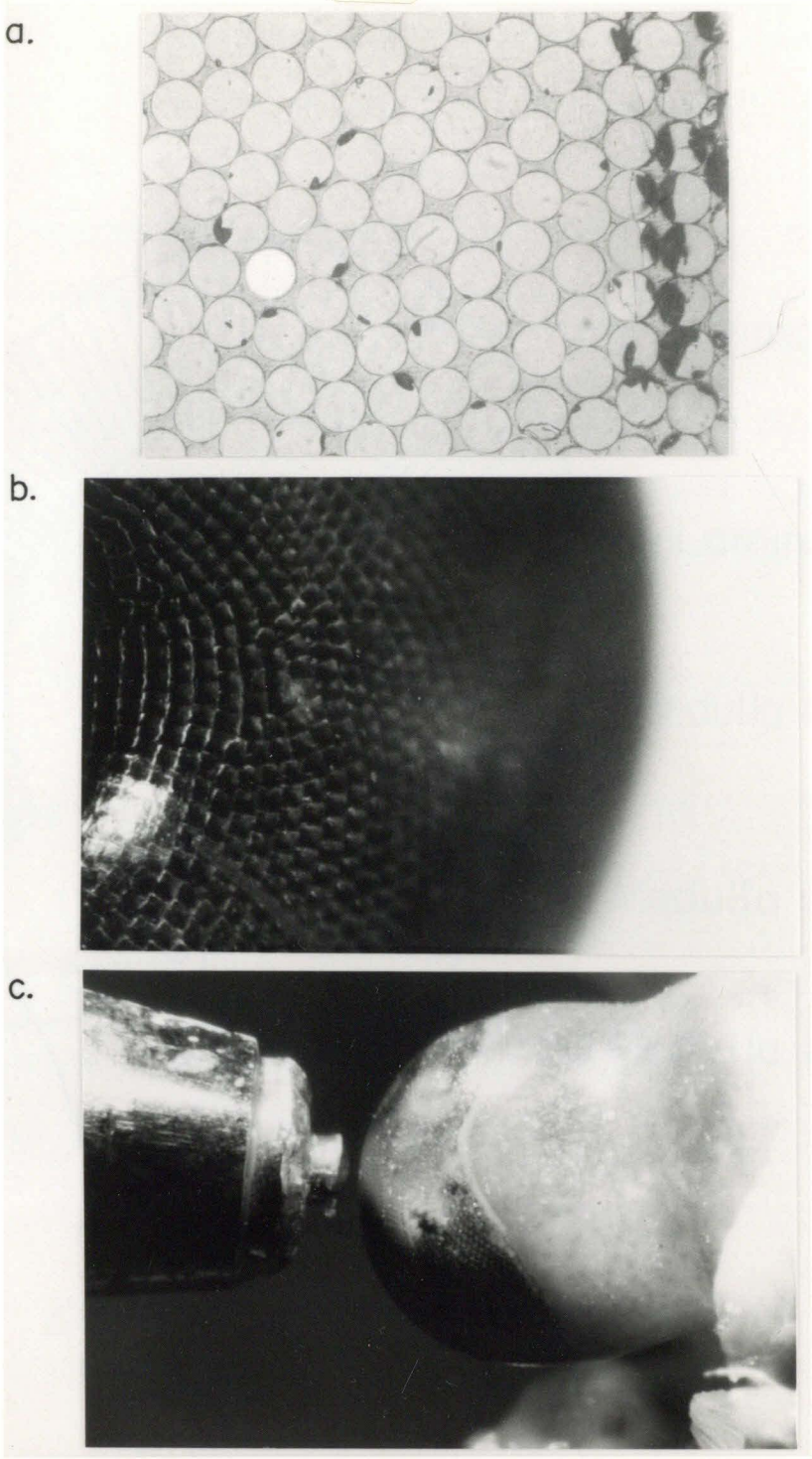

Fig. 2.1.4 a) array of 20μ diameter optic fibers; b) 20μ fiber against a single ommatidium; c)array against eye (not on 038)

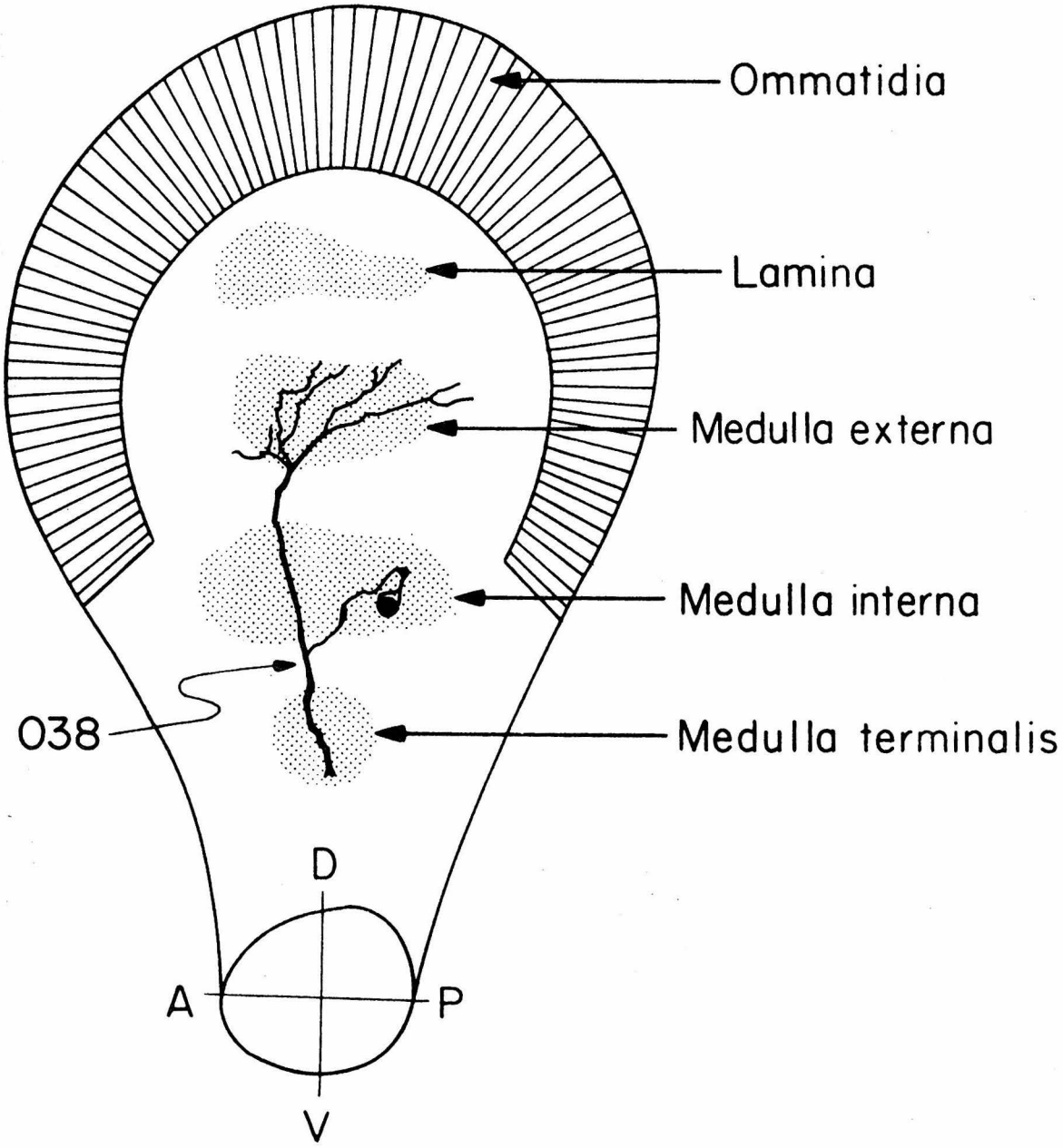

Fig. 2.1.5 Crayfish Optic Ganglia and Schematized Representation of 038

ovoid region running along the dorso-posterior (i.e., upper rear) rim of the eye (Figure 2.1.6). The length of the field is about 1600 microns and it extends, maximally, in width for about 800 microns (cf. Chapter 4). Illumination within the ovoid's boundaries excites the sustaining fiber; illumination beyond the ovoid results in inhibition of the fiber (Wiersma & Yamaguichi, 1967).

The sustaining fibers are thought to arise from the medulla externa (Wiersma, unpublished; D. Rafuse, unpublished) but beyond that little else is known about their synaptic contacts with other neural elements.

038 was chosen as the object of study in these experiments because of its size, physical durability, and quickly identifiable characteristics (all of which minimizes time consuming and damage-inflicting microelectrode probing), and its well reported behavior in the literature. With 038 as the representative sustaining fiber a greater number of experimental controls could be placed on the experiments to analyze the constituent microstructure of its field, thus eliminating the need to examine possible differences among sustaining fiber types.

2.1.2 Spectral Sensitivity of the Retinular Cells

The crayfish compound eye contains two types of retinular cells: a yellow(-green) receptor with a maximum spectral sensitivity at 565-570 ηm (or possibly at 594 ηm); and a blue-violet cell with a peak sensitivity at 430-460 ηm. Nosaki (1969), in intracellular recordings of retinular cells, found the peak spectral sensitivity of the yellow receptor to be at 560 ηm (in winter, and to be greater than 600 ηm in summer);

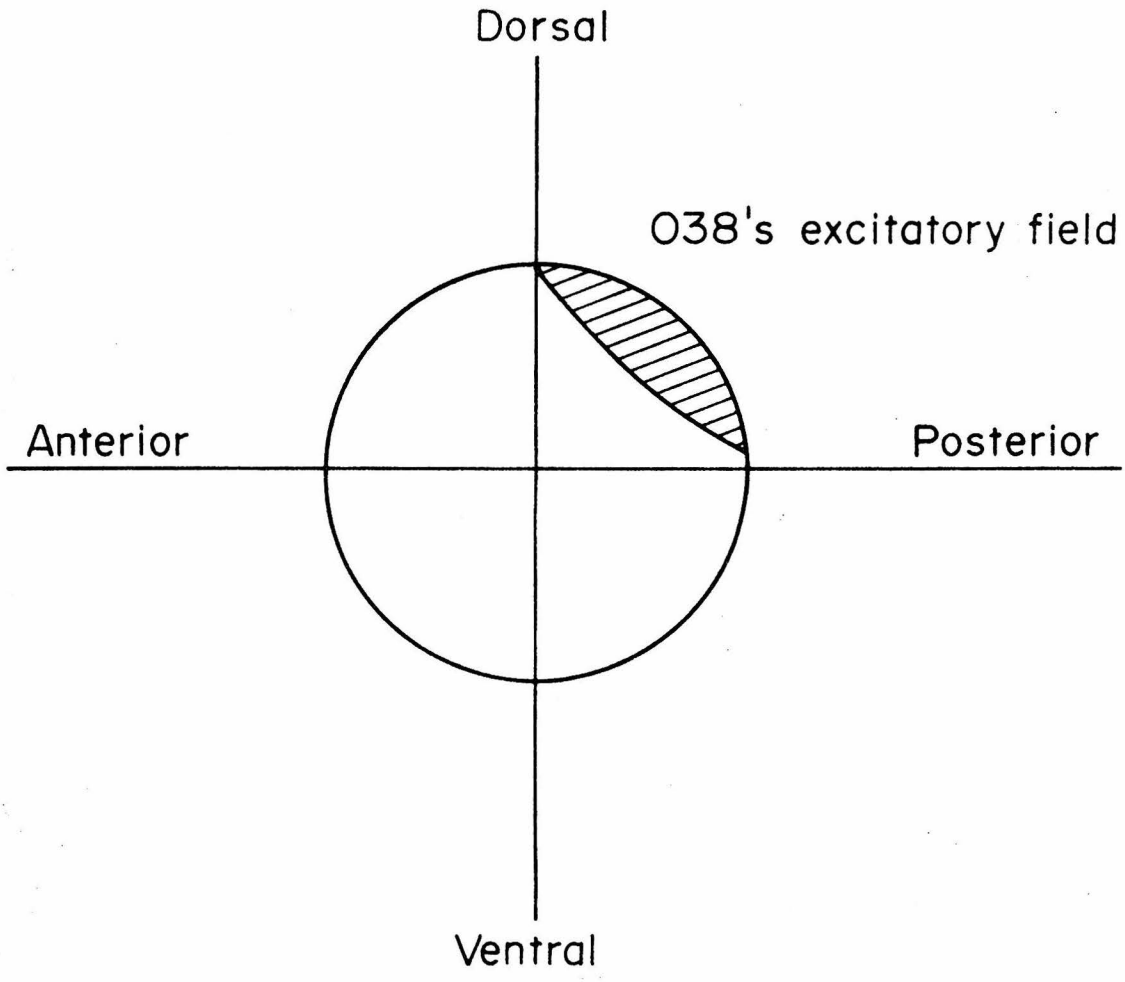

Fig. 2.1.6 Location of 038's Excitatory Receptive Field

and the blue receptor to have a peak sensitivity at 460 nm. Waterman and Fernandez (1970), also using intracellular recordings, found the yellow receptor to have an average peak sensitivity at 594 nm. Their blue cells responded maximally at 440 nm. Typical spectral sensitivities for their cells are shown in Figure 2.1.3c. Waterman and Fernandez (1970) did not observe the seasonal variability in the yellow-sensitive cells as reported by Nosaki (1969). Ultraviolet sensitivity has not been observed in the crayfish eye (Goldsmith, 1972).

The higher penetration rate of yellow cells in intracellular recordings (90%, Nosaki, 1969; 81%, Waterman & Fernandez, 1970) as compared with the lower penetration rate (10-19%) for the blue-violet, has suggested that the yellow-sensitive retinular cells are the predominant variety present in the crayfish.

In an elaborate measurement of the densities of certain cytoplasmic organelles resulting from selective chromatic light adaptation, Eguichi, et al (1973) have attempted to identify which retinular cells in an ommatidium are the blue-, and yellow-sensitive cells. They concluded that R3 and R4 (cf. Figure 2.1.3) were violet-sensitive and that the other retinular cells (R1,2,5,6,7) were yellow-sensitive (R8 was not studied). They divided the yellow-sensitive group into two categories: pure yellow receptors (R1 and R7); and a class of cells that seemed to have mixed sensitivity to both yellow and violet (R2,5,6). Eguichi, et al (1973) pointed out, however, that a mixed yellow-violet group was inconsistent with other studies: 95% of all intracellularly recorded cells had single peak wavelength sensitivities and only 5% had double peaks.

The presence of 3 mixed yellow-blue receptors (out of 7) should have resulted in at least 42% of all intracellular penetrations to reveal double peaks. Hence, Eguichi, et al (1973) offered an analysis of their data suggesting that the yellow-blue grouping arose from an inconsistency in the violet cells' localizations in one ommatidium to another.

Goldsmith (in press) has performed extensive microspectrophotometric experiments on the isolated crayfish rhabdom (bleached and unbleached) and has found all absorption spectra to match the spectral sensitivity curves for the yellow receptors. Hence, it may be that R1-R7 are all yellow sensitive and that R8 is the blue receptor: such a scheme would account for the recording rates of the two cells.

2.1.3 The Spectral Sensitivity of the Sustaining Fiber (038)

The spectral sensitivity of the sustaining fibers of the crayfish (Procambarus) has been extensively studied (Trevino & Larimer, 1970; Woodcock & Goldsmith, 1970, 1973) and, fortuitously, the characteristics of 038 have been examined in all of these investigations.

In the dark-adapted state, 038 is maximally sensitive in the yellow-green (λ_{max} = 575 nm, Trevino & Larimer, 1973; λ_{max} = 560-580 nm, Woodcock & Goldsmith, 1970) and upon adaptation with red light its sensitivity shifts to the blue (λ_{max} = 465 nm, Trevino & Larimer, 1970). These findings suggest that 038 receives inputs from the crayfish's two types of retinular cells. Woodcock and Goldsmith (1970) reported two 038 units, in different animals, which had peak (dark adapted) sensitivities in the blue, and later reported (Woodcock & Goldsmith, 1973) that about 10% of all sustaining fibers (without a breakdown of their types)

demonstrated a peak sensitivity at 460-480 ηm. It should be noted that all 36 sustaining units studied by Trevino and Larimer (1970) consistently demonstrated peak sensitivities in the yellow (e.g., λ_{max} for sustaining fiber "01" was 565 ηm).

Using two test wavelengths (473 and 573 ηm), Woodcock and Goldsmith (1973) examined the constancy of the sustaining fibers' spectral sensitivity within different regions of their receptive fields. While they found no major differences within a field, they did find a slight preference for yellow in those receptive field parts falling in the ventral regions of the eye, and a slight increase in blue sensitivity for field regions falling within the dorsal half of the eye. Noting that 038's field is along the dorso-posterior rim, it is essential to explain the differences of these findings in view of the yellow sensitivity previously described (Trevino & Larimer, 1970; Woodcock & Goldsmith, 1970). Woodcock and Goldsmith have attempted to explain these different findings via differences in the experimental procedures they used versus those used by Trevino and Larimer (1970).

Woodcock and Goldsmith (1973) measured the average number of impulses in a sustaining fiber's response to a 1 second stimulus. Such a measure erases all the fine structure of a spike train (cf. Chapter 3). Hence, they could not observe contributions in a spike train that might be spectrum related as did Trevino and Larimer (1970; see below). Woodcock and Goldsmith have pointed out that test stimuli with wavelengths 473 and 573 ηm that they used, do not selectively excite the blue and yellow sensitive photoreceptors, respectively. Instead, the spectral sensitivity curves of both retinula cell types

(Fig.2.1.3) show that 473 nm excites both classes of photoreceptors, but a yellow stimulus at 573 nm has less effect on blue sensitive receptors than does its reciprocal experiment (i.e., 473 on yellow-sensitive cells). Hence, any measurement of response to blue light based solely on spike count reflects the activity of both the blue and yellow sensitive cells, but a response to yellow light primarily reflects the activity of the yellow sensitive cells (see Chapter 6).

Trevino and Larimer (1970) studied spectral sensitivity in the "hotspot" (i.e., center) of a field in two ways. For the dark-adapted spectral sensitivity curve of 038 they measured the energy required of a 20 msec light pulse to elicit two spikes in a dark-adapted animal. They chose that near-threshold condition so that they could examine the contribution of the blue receptors to 038; Goldsmith and Fernandez (1968) found that the blue sensitive retinulae saturated only 1.5 log units above threshold. A second method examined the fine temporal pattern of the sustaining fibers' spike trains. In the dark-adapted state, 038's response to the brief flash of red or blue light is a burst of spikes. When the eye is red-adapted (thus decreasing the sensitivity of the yellow photoreceptors) the sustaining fibers' response to a blue flash breaks into two components: a late and an early phase (Trevino & Larimer, 1970). The response of a red-adapted fiber to a flash of red light lacks the late burst; in a dark-, or violet-adapted eye, the late burst is also absent. This suggests that the late burst is a contribution from blue-sensitive retinular cells. Such an observation could not be made by the gross spike counting procedure employed by Woodcock and

Goldsmith (1973). Woodcock and Goldsmith's finding of a favored blue sensitivity in the dorsal regions of the crayfish eye cannot easily be reconciled with the literature indicating a preponderant population of yellow-sensitive retinular cells as inputs to the sustaining fibers. The question of color channels is explored further in Chapter 6.

2.2 Light Stimulus

2.2.1 Introduction to Optic Fibers and LEDs

Single and pairs of optic fibers have been extensively employed as light guides in studies of arthropod visual systems (e.g., Barlow, 1969; Shapley, 1971). The experimental procedures and designs used in those applications were, unfortunately, unsuited for the purposes of this thesis. For example, the sources used were often incandescent lamps whose spectra were current dependent or extremely broad banded (e.g., 400-700 μm). Section 2.1's discussion of the crayfish eye's spectral sensitivity suggests the misinterpretations that could result when 038's response is correlated to a stimulus of varying intensity that also fluctuates in spectral composition. To overcome this problem, and the nontrivial task of presenting nonrandom configurations of multiple small spot stimuli to the restricted area of 038's receptive field, a specially designed optic-fiber, light-emitting diode (LED) stimulus was built (Sheby & McCann, 1976), with particular care to exploit both 038's and the retinula's predominant yellow sensitivity.

Step index optic fibers are composed of a glass core of uniform refractive index, n_1, surrounded by a glass cladding of

slightly lower index of refraction, n_2. Light launched into the fiber core at an angle less than the critical acceptance angle, θ_{max} (the numerical aperture) is internally reflected upon striking the core-cladding interface and continues to propagate down the fiber core. The numerical aperture is the basic parameter for describing the characteristics of an optic fiber. The numerical aperture is defined by

$$NA = \sin \theta_{max} = (n_1^2 - n_2^2)^{1/2} / n_0 \qquad (2.2.1)$$

where n_0 is the index of refraction of a uniform medium located between the fiber core and the incident (or exit) beam of light.

When an electromagnetic field propagates in an unclad fiber, the field extends beyond the boundary of the transmitting glass and any material in contact with the fiber would disrupt the field. When unclad fibers are packed close together in an orderly array, light will pass from one to the other, because evanescent waves that exist close to the fiber surface can be trapped by an adjacent fiber. This optical cross-talk is highly undesirable when it comes time to compute the (Wiener) kernels of the system (Chapter 3); it can also result in the accidental stimulation of a region that was to remain unexcited during an experiment.

The amount of light that can be launched into an optic fiber is limited by the number of modes, N, that the fiber can support. N is determined by a dimensionless parameter, V, where

$$N = V^2/2 \qquad (2.2.2)$$

and

$$V = 2D(n_1^2 - n_2^2)^{1/2} / \lambda \qquad n_1 > n_2 \qquad (2.2.3)$$

and D is the fiber core diameter, and λ is the wavelength of the incident light. For $V < 2.5$ only one mode can be supported on the fiber.

High radiance light emitting diodes are ideal sources for fiber optic systems. Their Lambertian radiance profiles can excite a great number of modes in an optic fiber. Their nearly linear drive current-output light intensity relationship allows them to be accurately and simply controlled by direct amplitude modulation of their drive current (Figure 2.2.1). The Gaussian white noise intensities required for Wiener kernel analyses (Chapter 3) are easily obtained by connecting the LEDs' current sources to the appropriate noise generator(s) Most important, the LEDs' spectra do not shift with drive current as do other incandescent sources (Figure 2.2.2). Hence, all visual phenomena studied with LEDs are intensity dependent and not spectrum dependent. Furthermore, LEDs are inexpensive and have half-lives approaching 100,000 hours.

Unlike other incandescent sources, LEDs convert electrical energy directly into light without the production of heat and intermediate conversion from thermal energy; thus the need for heat absorbing filters is eliminated.

Optic fibers are easily coupled to LEDs by butting the input fiber end directly against the emitting surface of the LED. Since LED surface emitting areas are usually larger than that of a fiber core, only a fraction of the LED's total radiated light can be coupled to the fiber.

The efficiency, η, of a fiber optic–LED coupling is proportional to the numerical aperture, i.e.,

$$\eta \propto A_{fiber}(NA)^2 / A_{source} \qquad (2.2.4)$$

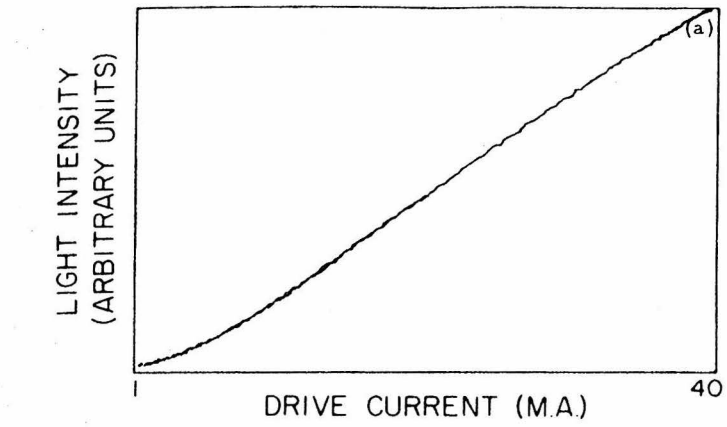

LED drive current vs. output fiber intensity.

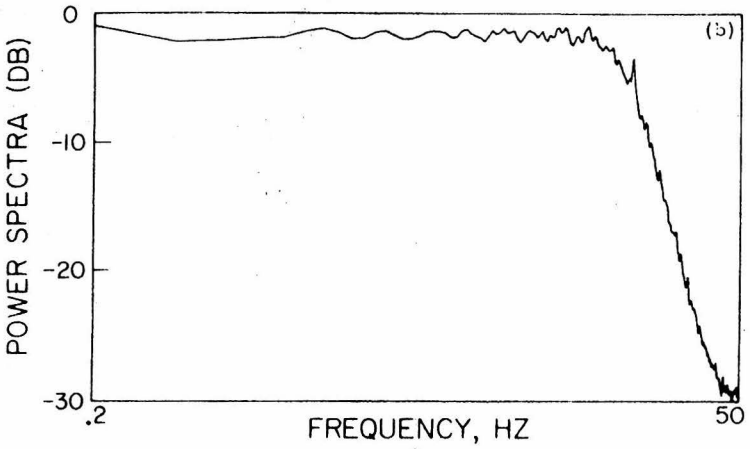

Power spectrum of output fiber intensity.

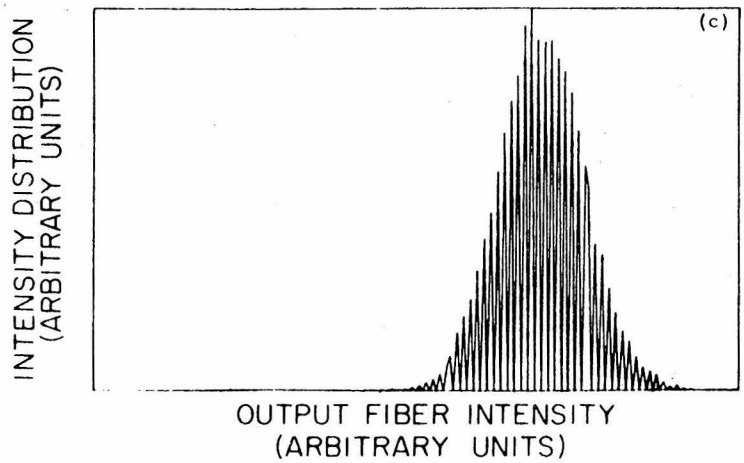

Gaussian distribution of output fiber intensity.

Fig. 2.2.1 Characteristics of Output Intensity from an Optic Fiber

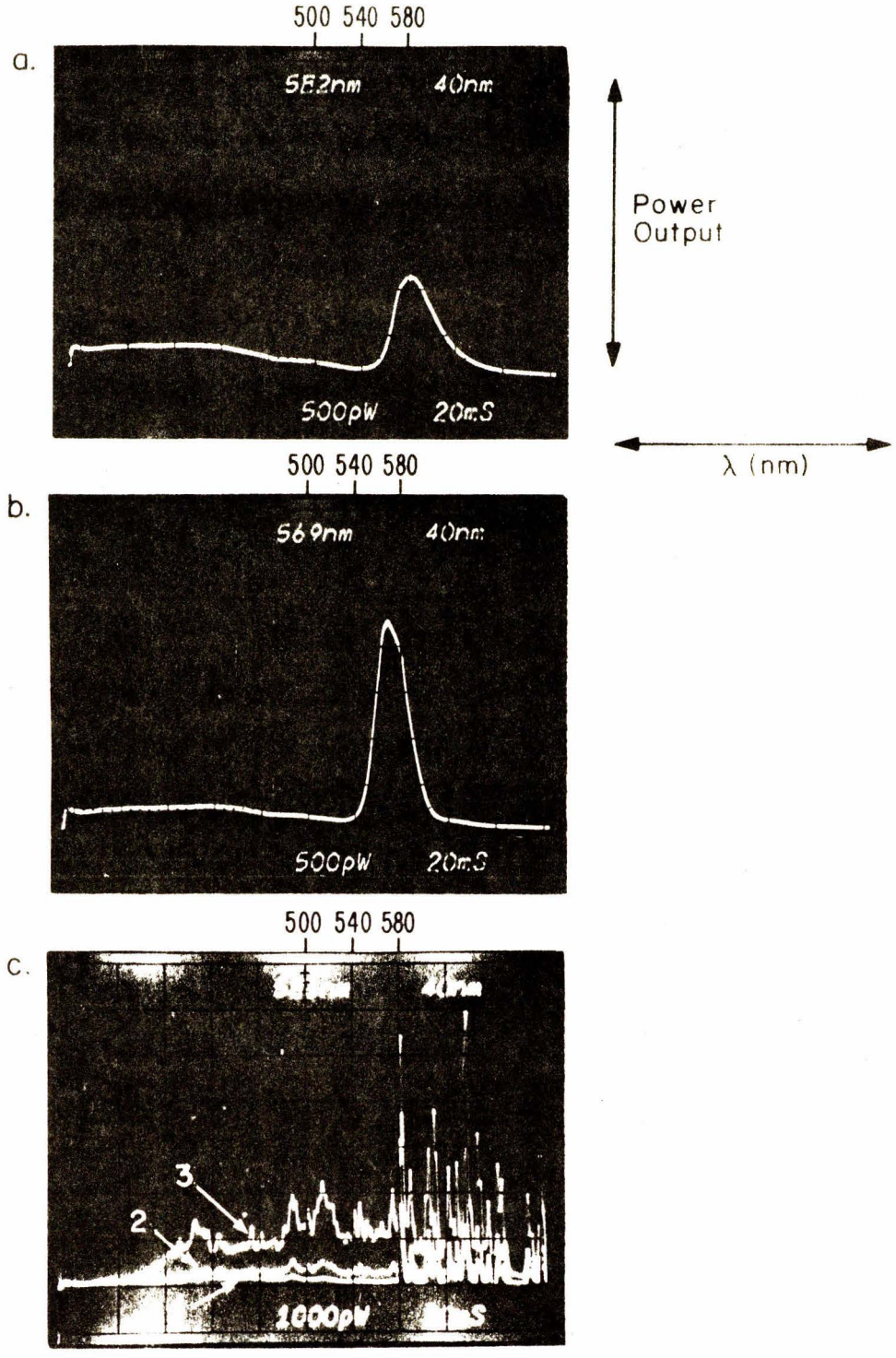

Fig. 2.2.2 Spectral Characteristics of LED and Glow Tube
a) LED at 20 ma; b) LED at 40 ma; c) glow tube at 1) 10 ma 2) 30 ma, 3) 50 ma.

where A_{fiber} and A_{source} are the areas of the fiber core and the LED's emitting surface areas, respectively. Typically, coupling efficiencies of only a few percent are possible (Hudson, 1974). For a fixed choice of LED type and fiber size the only way to increase coupling is by choosing a fiber with as large a numerical aperture as possible.

Despite the poor coupling efficiency, the effectiveness of a LED as a light source is greatly enhanced by choosing one whose nearly monochromatic spectrum (half power bandwidth approximately 30 ηm) matches the region of maximum spectral sensitivity, λ_{max}, of the stimulated visual system's photopigment(s) of interest. Despite the fact that a conventional incandescent source might be capable of generating more total power than can be coupled into an optic fiber, the LED makes up for this by insuring that nearly 100% of its coupled light optimally stimulates the eye. For example, the stimulus package developed in this thesis incorporates yellow GaAsP LEDs (Hewlett Packard #5082-4558) whose peak emitted wavelength, λ_{pk}, is at 583 ηm, thus insuring maximal stimulation of the crayfish's yellow-sensitive retinular cells (see Figure 2.1.3d) and 038, both of which have relative sensitivities of over 95% at 583 ηm. Blue GnN LEDs (λ_{pk} = 428 ηm) (supplied by Dr. J. Pankove of RCA Laboratories) were used to excite the crayfish's blue system.

For the experiments, fibers with core diameters of either 20 or 60 microns were used, but had numerical apertures of .5 for optimizing the coupling efficiency and light-carrying capacity of the fibers. The size of the cone emerging from the fiber and stimulating an ommatidium can be reduced, as suggested by equation 2.2.1, by using a medium such as mineral oil with an index of refraction $n_0 > 1$.

In some assemblies light leaves the fiber at the exit aperture from the cladding. This occurs when light is launched into the cladding when the numerical aperture of the exit beam of the source is greater than the fiber's numerical aperture. These unwanted "cladding modes" can be eliminated by placing a mode stripping liquid between the fiber and the input source. Mineral oil or special fiber coupling epoxies with a refractive index close to that of the cladding can be used to eliminate this problem.

The package for the LED-fiber optic stimulus must provide protection against mechanical damage inflicted by the experimenter or the animal and must provide and maintain the alignment of the optic fiber(s) and LED(s) for optimal coupling. The construction of the stimulus package is described in Section 2.2.2.

Direct fiber-LED coupling allows permanent one alignment adjustment and the ability to individually control the light intensity emanating from each fiber independent of local coupling efficiency, via appropriate gain control and biasing of the LEDs' drive current. This eliminates the periodic realignments required when fibers are coupled to incadescent sources via lens-micromanipulator systems.

2.2.2 The Stimulating System: LED and Fiber Preparation

The Hewlett-Packard diodes are of the edge-emitting variety, mounted within a metallic reflector and covered with a protective epoxy. For these diodes it is necessary to grind through the epoxy and reflector into the diode's edge using SiC (grits 400 and 600) and Al_2O_3 (.3 μm). The diode is polished with serium oxide. All grinding and polishing is

done on a modified lathe system.

A disposable plastic syringe (20 cc, Becton-Dickinson #5661) houses the fiber-LED ensemble. The polished LEDs are mounted by threading their leads through holes drilled into the four walls emanating radially from the syringe's plunger. Four LEDs can be mounted in a single syringe this way. Eight LEDs can be mounted using a tier system. A modified version, with the LEDs mounted on a platform attached to the syringe body, can support 30 LEDs with individual fiber couplings mounted in a field of remaining fibers coupled to a common source (Figure 2.1.4).

The fiber ends are ground and polished for optimal coupling to the LEDs. Several fibers can be prepared simultaneously, using the above procedure, by inserting them in a glass tubing (A. Gover, personal communication). Mishandling during the coupling process occasionally necessitates repairs of broken fiber ends with a diamond knife.

The fibers are cemented together into an array of the desired geometric configuration (Figures 2.1.4, 2.2.4, and insert of 2.3.1) for about one-half of their length. The fibers are inserted, polished ends first, into a syringe through a previously mounted ground hypodermic needle. The polished fiber ends are individually held by tweezers mounted on micromanipulators (Figure 2.2.4) and are carefully brought into contact with the polished diodes. To facilitate coupling, the LEDs are on and a photodiode is connected to a digital voltmeter which monitors the light emitted at the needle tip indicating when maximum coupling is achieved.

The peak drive currents used determine the choice of epoxy. Occasionally peak currents of 80-100 ma are used for high light intensities

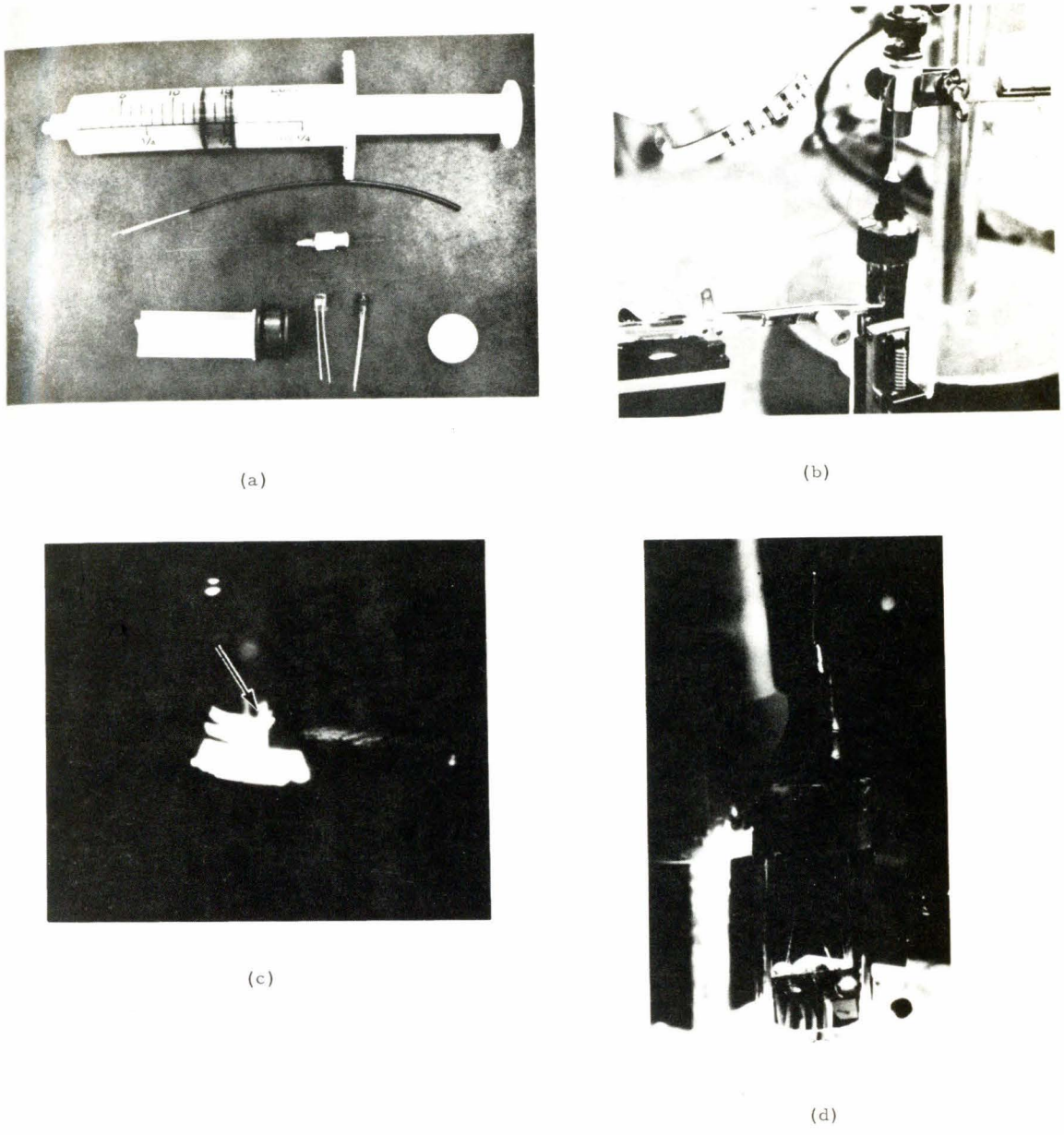

(a) (b) (c) (d)

Fig. 2.2.4 LED-fiber assembly. a) Components used in assembly. b) Coupling optic fibers to LEDs. c) Close-up of fiber (arrow) - LED coupling. d) Partially completed assembly showing four optic fibers coupled to individual LEDs

which produce sufficient heat to melt the epoxy and upset the coupling. This is overcome with a two-step procedure. First, a five-minute clear epoxy (Hysol 608) is used for epoxying an initial coupling. A silicone adhesive (Dow-Corning #3140) is then applied over the fiber-epoxy-LED interfaces, and it is this adhesive, capable of withstanding temperatures to 400°F, that maintains the fiber-diode coupling. One 24-hour curing period is required for the entire fiber-LED ensemble which has otherwise been completed within several hours.

The syringe is sprayed with black paint and is checked for light leaks with all diodes turned on. The fiber ends emanating from the needle shaft are ground and polished to minimize the divergence and irregularities in the beam, due to tiny flaws, at the exit aperture. During grinding, the fibers maintain their geometric configuration because they have been cemented with the silicone adhesive.

The drive currents of each of the LEDs are individually controlled using a 4-channel current modulator built by D. Aranovich of our laboratory. This device permits one to individually set the currents for any combination of output light intensities, equal or otherwise, of the fiber array independent of the differences in the individual fiber-diode coupling efficiencies (Figure 2.2.5). Special purpose white noise and sinusoid signal generators provided the appropriately modulated input signal to the current modulators; oftentimes the signals were generated by a PDP/1145 digital computer (Digital Equipment Co., Maynard, Mass.) which also collected all data in real time (Figure 2.2.6).

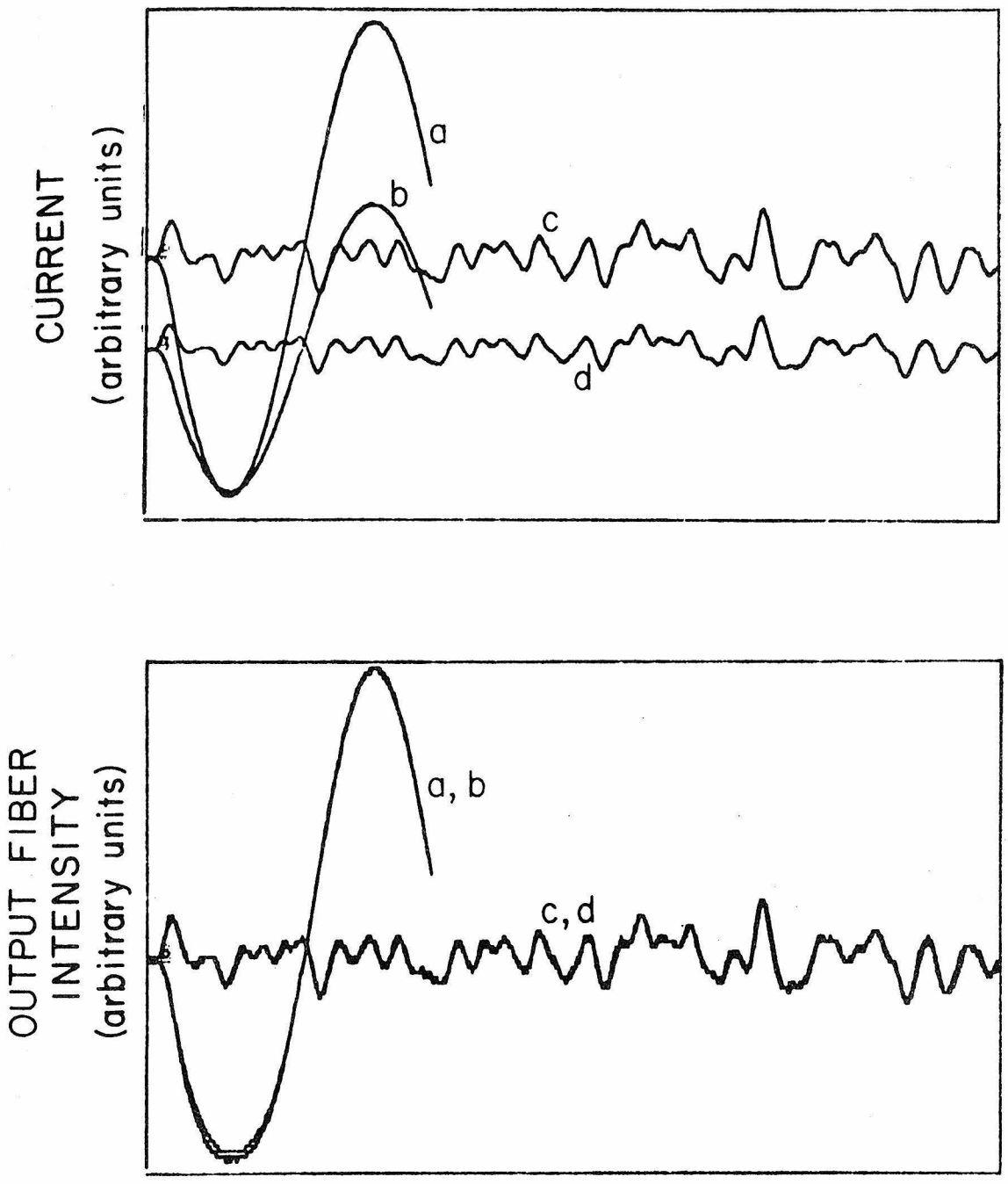

Fig. 2.2.5 Compensation of Unequal LED/Fiber Couplings
Upper: Input drive currents to LEDs a,b,c,d
Lower: Output intensities from fibers a,b,c,d

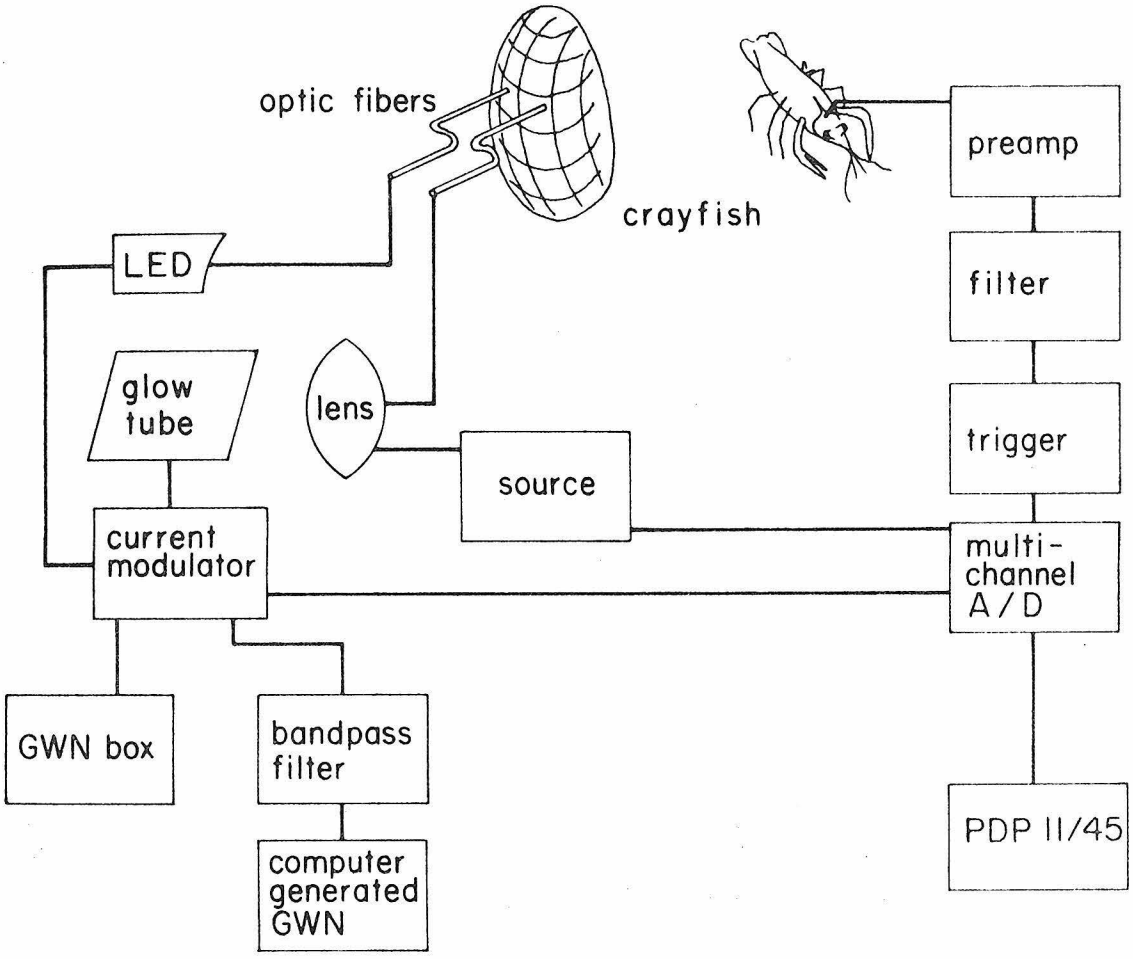

Fig. 2.2.6 Experimental Setup: Stimulus and Data Collection Configuration

2.3 Methods

2.3.1 Electrophysiology

All experiments were performed on intact adult (4" length) specimens of the swamp crayfish Procambarus clarkii (Dahl Co., Berkeley, Ca.). The rostrum was removed at least 24 hours in advance before use to provide access to the animal's optic tract. All animals were kept in an aerated aquarium in a light controlled room with a 12-12 hour (light-dark) cycle. The animals were fed once a week. Since the crayfish is a nocturnal animal (Arechiga, et al, 1973) all experiments were performed between 6 p.m. and 4 a.m. to take advantage of the greater sensitivity of the sustaining fibers at that time (Arechiga, et al, 1973).

Extracellular recording electrodes were etched from stainless steel insect pins (size 000) as described by Wiersma and Yamaguichi (1966). Their insulation procedure, however, was improved. It was found that the synthetic resin polyglycol phthalate was a good insulator that provided excellent protection against mechanical damage to the electrode tip. The polyglycol phthalate is easily liquified, and the electrode is dipped into it. The resin immediately hardens and eliminates the time consuming multiple dippings and dryings required by other metal electrode preparation techniques. The electrode tip diameters were 2-10 microns.

The sustaining fibers are known to have nonvisual inputs which can affect their activity. In particular, they are extremely active when the animal enters an "excited" state. Hence, it is necessary to minimize all nonvisual stimuli (e.g., vibrations) and to keep the animal as immobile as possible. To achieve this the legs and tail were securely tied

together with rubber bands, the animal wrapped with moist tissue paper and securely clamped around the posterior carapace (cf. Chapter 4).

The electrode was then positioned in the optic nerve and moved around until it recorded activity from one or more sustaining fibers. Quite often 038 was obtained as the first identified sustaining fiber, thus assuring us of minimal damage to the visual system.

A sustaining unit was identified as 038 in a three-step procedure. First, with a large plastic optic fiber (250 micron diameter), a flashing light stimulus was presented to the dorso-posterior rim so that the electrode could search for a cell responding to the stimulus. When a cell was found it was next checked for sustaining behavior by presentation of long duration flashes to insure that it did not habituate. Third, the cell's receptive field position was then matched with those mapped and categorized by Wiersma and Yamaguichi (1966). This is the standard method for identifying crayfish sustaining fiber types (e.g., Woodcock & Goldsmith, 1970). After an 038 was found, the electrode was glued in place and the eyestalk was immobilized by gluing it to the carapace with Eastman 910 adhesive.

The signals were fed into a NF1 preamplifier (Bioelectric Instrum. Inc.) in series with another (Tektronix FM1-2). The output from the second preamp was then fed into a broad-band filter (Spencer-Kennedy Laboratories, Model 308A) whose low and high pass characteristics could be adjusted selectively to filter extraneous signals and noise (Figure 2.2.6). Typically the band 600 Hz-5500 Hz proved satisfactory for isolating 038 units with good signal-to-noise ratios. The output from

the filter was then fed into an oscilloscope trigger (Tektronix 2B67) for spike spearation and the resultant trigger signal was sent to a PDP 11/45 computer where its time of occurrence was recorded.

The optic fiber LED stimulus of Section 2.2 was calibrated before each experiment. A sawtooth or sine wave current was fed into each LED that was to be used in an experiment, and the output of its coupled fiber was monitored by a pin diode (United Detector PIN-10, Santa Monica, Ca.), the output of which was fed into a preamplifier (UDT model 101A) and then into an oscilloscope and the PDP 11/45 computer through a special bank of A/D converters used in our laboratory. At the same time the current feeding the LED was fed into the computer and a transfer function relating the input current and output light intensity was run for each LED-fiber configuration. During an experiment the computer-generated white noise (cf. Chapter 3) feeding the LEDs was monitored, but for kernel computations the current was converted into the actual intensity by the transfer function computed for each individual fiber-LED pair. Hence, any artifacts arising from unequal fiber couplings were eliminated. For example, even though the two light intensities from two fibers might be equal, the current necessary to achieve the respective intensity in each LED-fiber pair might be unequal (Figure 2.2.5). If the currents' power levels were unequal and used for computing kernels (cf. Chapter 3) misleading results would occur because the input signals would not be of equal power.

The reference electrode was positioned in a small hole punctured in the anterior lateral carapace of the animal. After a unit was located

and the animal's eyestalks (and the electrode) were glued in place, the experimental eye of interest was aligned in the center point of a goniometer in which the optic fibers are mounted (Figure 2.3.1). This permitted the fibers to be rotated around the eye in great circular sweeps and aligned with the ommatidial axes in 038's field. The choice of 20 μm fibers allows one to build up an array of fibers which can be selectively coupled to permit, for example, every second or every third fiber to be aligned with a distinct ommatidium (Figure 2.1.4).

2.3.2 Optics of the Compound Eye

While the nocturnal nature of the crayfish eye has been utilized advantageously for some experimental procedures, it does cause some inconvenience in others. Shaw (1969) studied the light scattering properties of various compound dyes, using optic fibers. For the crayfish Procambarus, he found that about 12% of the light directed at one ommatidium scattered onto an adjacent ommatidium (i.e., 50% into the nearest four neighbors), and only a small fraction of that excited the retinular cells two ommatidia away.

The scattering results from the physical structure of the eye. Recently it has been demonstrated (Land, 1976) that decapod crustaceans have highly silvered reflective pigments surrounding each ommatidium, which direct entering light into neighboring ommatidia. This phenomenon can be partially minimized by injecting into the crayfish a light adapting hormone which pushes the pigment into a light adapted state, thus absorbing much of the light before it excites neighbors.

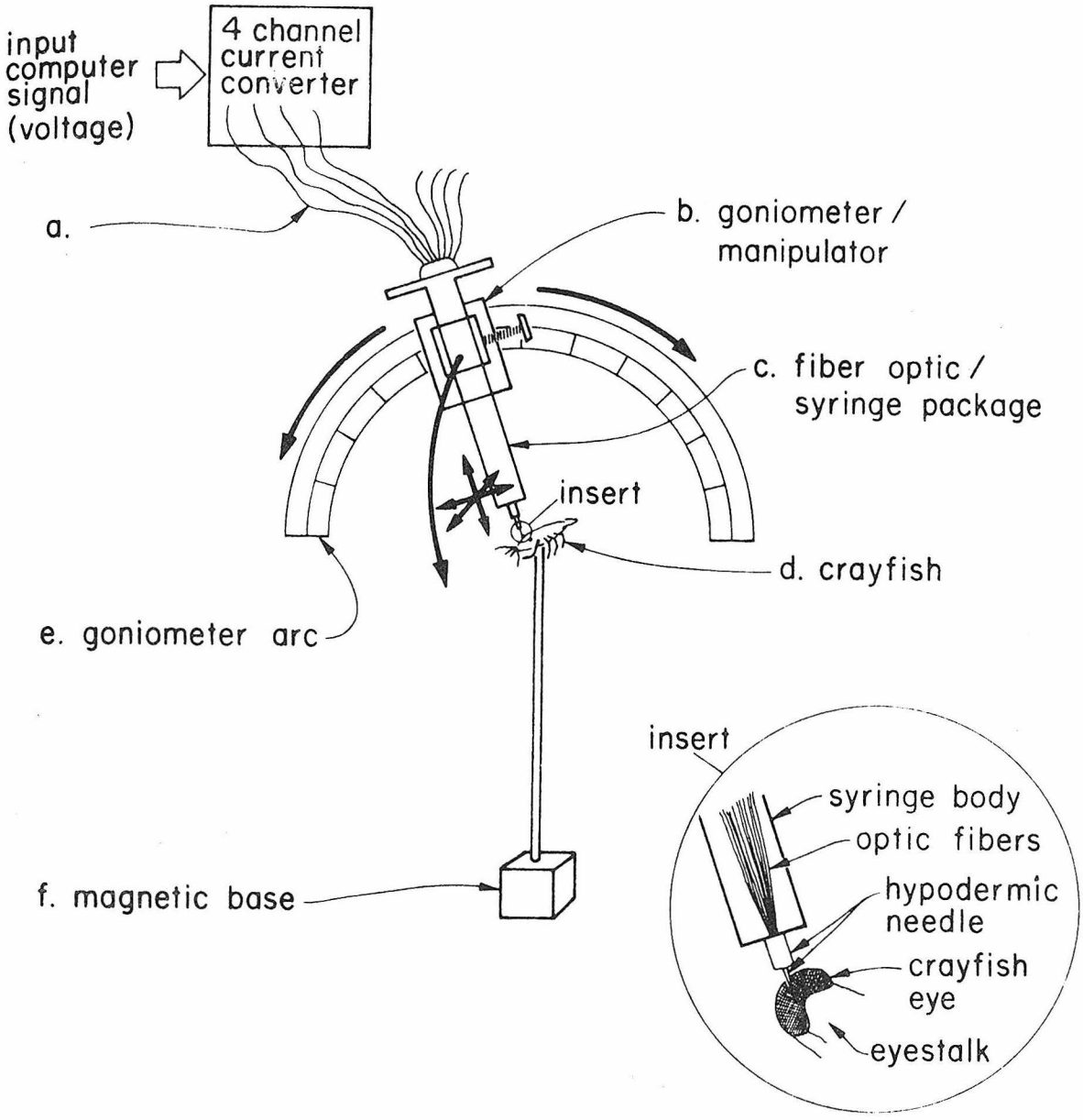

Fig. 2.3.1 Experimental Setup: Alignment of Optic Fibers to Crayfish Eye

Contributing to the light spread was the type of optic fibers that Shaw (1969) used: the unclad variety. In unclad fibers, $n_2 = n_{air} = 1$ and instead of $n_1-n_2 = .001$, $n_1-n_2 = .5$ resulting, as can be seen from equation 2.2.1, in large exit numerical apertures (and diverging light cones). Shaw's use of black paint to coat his fiber only kept visible light from exciting the fiber sides--it would not change the numerical aperture of his fiber if, as is highly probable, air pockets existed between the paint and fiber surfaces.

Attempts were made in this thesis to optically neutralize the effects of the reflective medium by focusing the light directly onto the rhabdoms. The strategy employed here was to melt, with the assistance of Professor N. George, the end of a fiber with a HeNe laser to produce a spherical lens (Paek & Weaver, 1975). Such a lens would be formed on a 85 μm diameter fiber (Figure 2.3.2) which could focus to a spot size of about 10 μm with a focal length of about the diameter of the fiber. While the approach holds great promise, it had to be abandoned, since the lenses were subject to extensive damage during construction of the LED-optic fiber stimulus package (Section 2.2.2). A torch flame could not be well controlled to produce the lenses after the fibers had been mounted in the syringe package.

2.3.3 Field Maps

To be able to compare results obtained from different animals necessitated the development of a technique for recording the identity (i.e., location) of the ommatidia stimulated. Originally each ommatidium

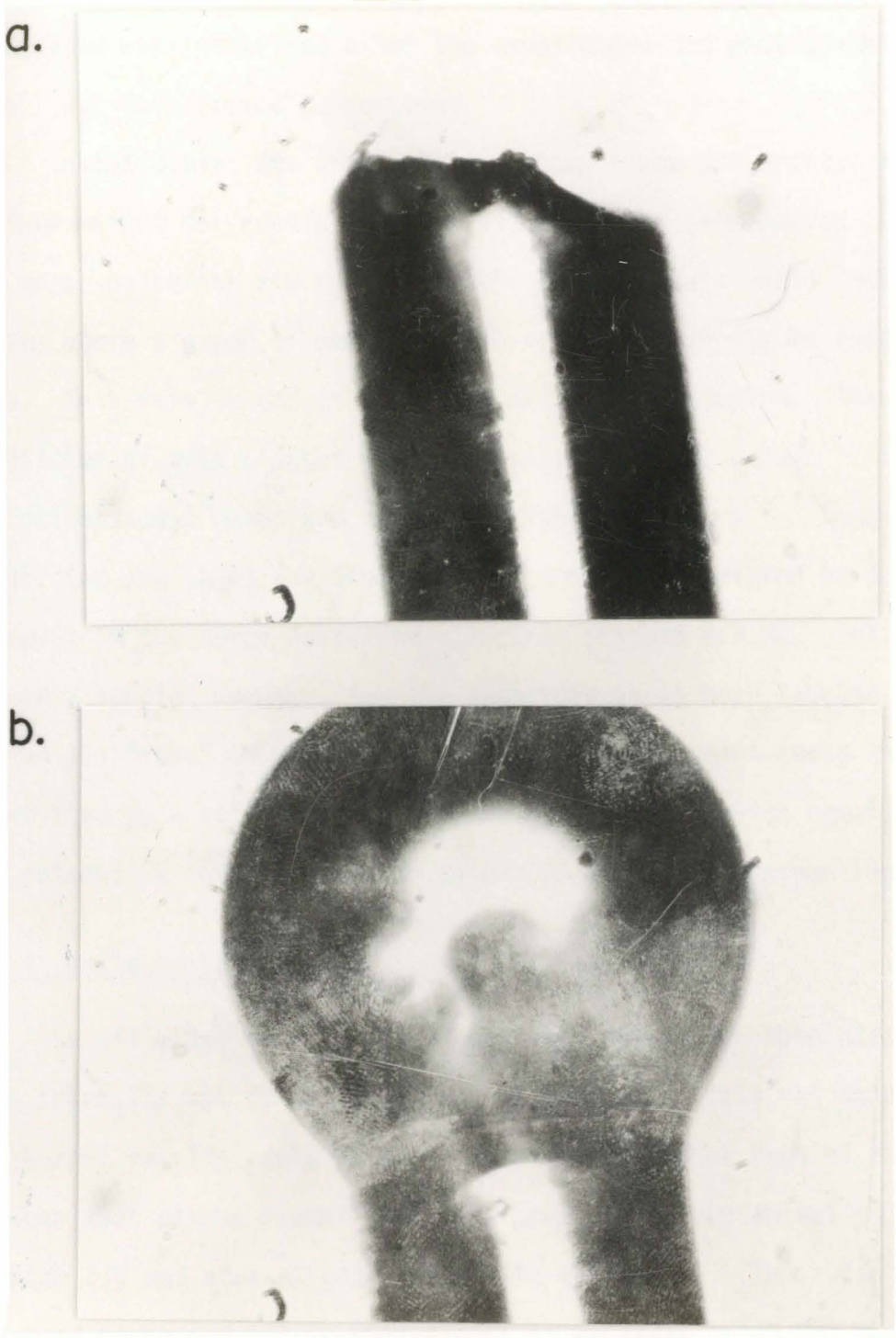

Fig. 2.3.2 Lens Formation on Optic Fiber End
Upper: Unprepared Fiber End
Lower: Spherical Lens Produced

stimulated was identified after the experiment, and photographic records kept. But this proved cumbersome.

Fortuitously, Dr. Donald Rafuse (Loma Linda University) found another method for recording sites of ommatidial stimulation. Along the dorso-posterior rim comprising the edge of 038's field lies only one region where a group of ommatidia (10-15 in number) lie in a straight line. This site is consistent among all animals studied. The central ommatidium of this cluster was designated as row 0, column 1 on the eye and all adjacent ommatidia to it were labeled 2, 3, ···. These numbers identified the label for the column of ommatidia that run perpendicular to row 0 in the dorso posterior direction (Figure 2.3.3). Column 20 served a special purpose, for the ommatidia in it were labeled and identified all "rows" in 038's receptive field. Any point could then be identified by a column row designated by recording which ommatidial rows and columns it intercepted with column 20 and row 0, respectively.

2.3.4 White Noise Stimuli

In all experiments, unless otherwise noted, the absolute output mean intensity was 40 $\mu w/cm^2$ on each fiber used. This was done so that all kernel results could be compared with each other free of the side effects that plague Wiener analyses: power-level contamination (cf. Chapter 3); and adaptational changed in the animal. This also eliminates the need to report all kernel results in absolute units for the type of experiments performed herein: they are only concerned with relative kernel amplitudes and dynamics at a fixed stimulus intensity.

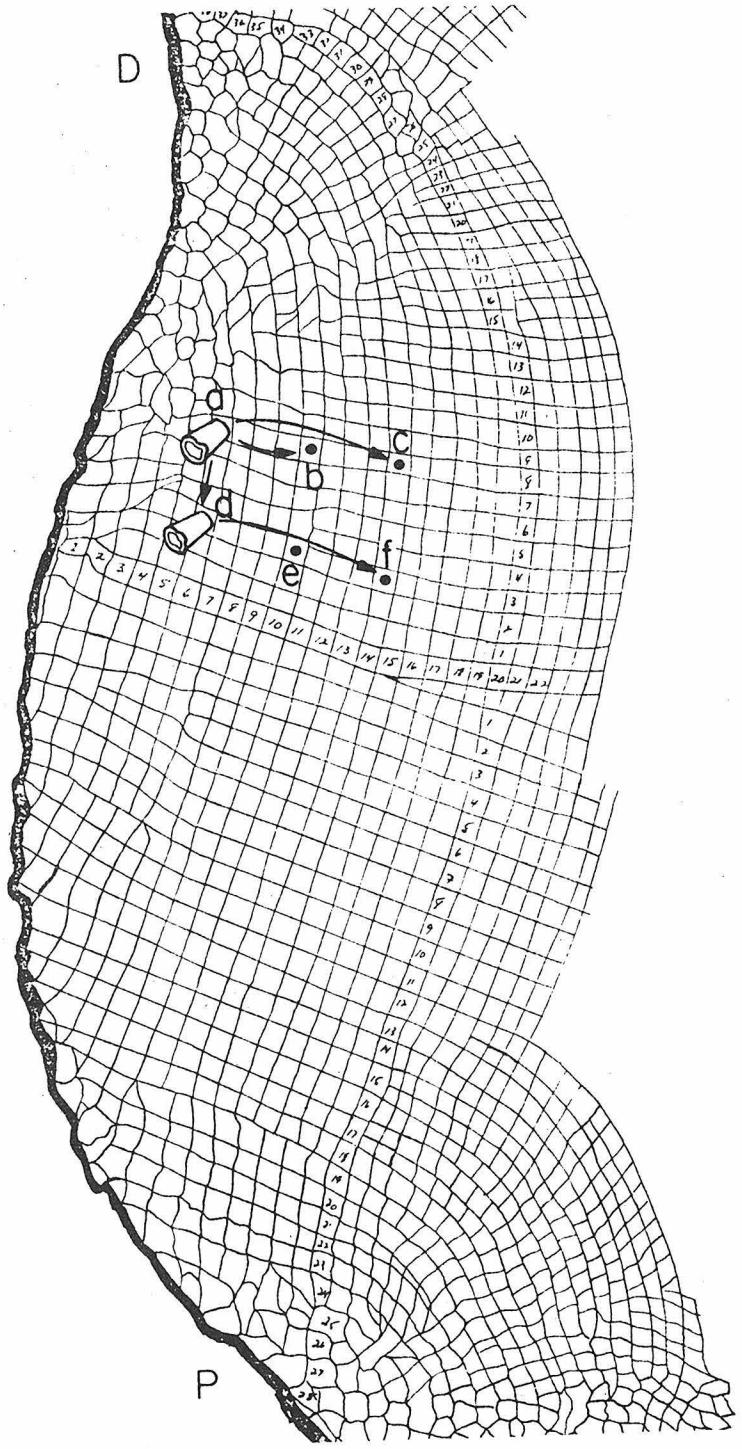

Fig. 2.3.3 Map used to identify ommatidial regions (courtesy of Dr. D. Rafuse, Loma Linda University)

Also, unless stated otherwise, each LED's driving current was a white noise with a bandwidth of .2-25 Hz.

2.4 Dark Adaptation

2.4.1 Systems Analysis and Dark Adaptation

When optic fibers (or other sources) are used to present small spot stimuli to an eye to study its microstructure of (lateral) interactions, an interesting and nontrivial question arises: should these experiments be performed in darkness, presumably so that the animal can "see" and respond to the individual spots of light emanating from the fiber ends, or should the eye be tested with the spots in an environment with a constant background of illumination (i.e., in a light-adapted state?)

McCann, et al (1976) studying temporal responses in fly photoreceptors, present evidence that studies performed on dark-adapted animals reflect complex experimental conditions, since the eye normally operates in a visual environment composed of an average constant background light level. To support this, McCann et al (1976) present data revealing high order nonlinearities (i.e., 31st harmonic) in the response data collected from dark adapted photoreceptor cell responses to sinusoidal light stimulation at 4 Hz; the higher order harmonics were absent in light-adapted eyes. These data are interesting, but the source for this nonlinearity has been difficult to interpret. A possible cause might be localized if responses to sinusoid signals at other frequencies also revealed 31st harmonics. If the 124 Hz component was present at

all other stimulus frequencies then it might arise from a lamina source. While it is true that the dark-adapted state is not the usual operating state for a diurnal animal like the fly, it is less "abnormal" for a nocturnal animal like the crayfish.

The Volterra series for multi-input systems (equation 1.3.3) suggests another possible disadvantage for using a background light level for light adapting an animal. It is quite possible that the illumination of a broad retinal field can set up lateral interactions of p-order 2 or greater, throughout the illuminated region, which can inhibit the cells within this stimulated region and subsequently minimize their mutual interactions with each other. In Limulus such a phenomenon has been thought to be responsible for the discrepancy in the lateral field profiles measured by stimulation of large neighboring retinal regions (Barlow, 1969) versus that found in precision single-ommatidial stimulation (Johnson & Wachtel, 1976).

The differences between the experimental results in light- versus dark-adapted animals (McCann, et al, 1976)are made more urgent to understand when it is realized that some of the nonlinearities detected in dark-adapted animal experiments turn out to be of fundamental importance in modifying conceptions about basic neural processes. For example, Barlow and Lange (1974) using 76 micron diameter optic fibers, stimulated single ommatidia in Limulus and measured the eccentric cell's sensitivity to lateral inhibition arising from a neighboring stimulated region of 4 ommatidia as a function of its own excitation. The result was that the cell's sensitivity was a nonlinear function of its own excitation, thus necessitating the modification of the Hartline-Ratliff equations; in

comparisons of computer simulations of the equations versus actual measurements of Mach Band phenomena it was demonstrated (Barlow & Quarles, 1975) that this nonlinear modification nontrivially improved the predictive power of the Hartline-Ratliff equations.

More important for this present investigation, however, is the fact that background illumination wiped out 038's response to individual fiber stimulation.

Figure 2.3.4 shows the results of having no background, a background equal to the fiber in total flux, a background flux one-half that of the fiber's 40 $\mu w/cm^2$, and a background greater than 40 $\mu w/cm^2$.

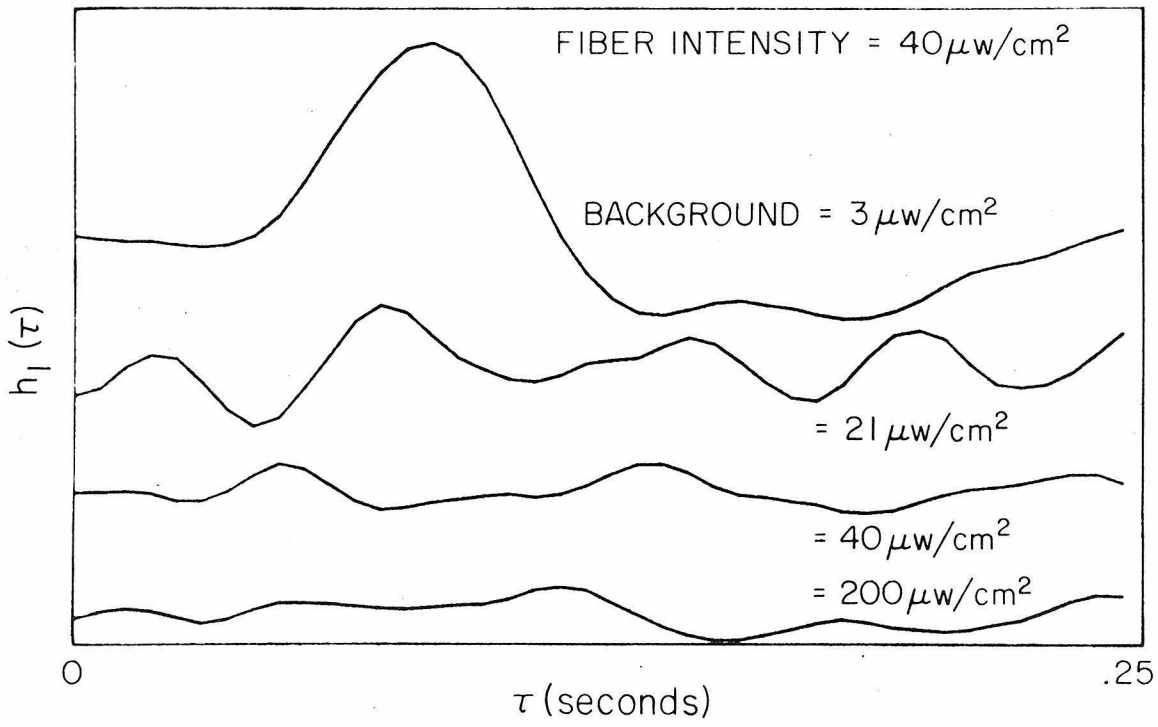

Fig. 2.3.4 Response of 038 to Fixed Fiber Intensity as Function of Background

Chapter 3

VOLTERRA AND WIENER KERNELS, AND NEUROPHYSIOLOGICAL SPIKE DATA

3.1 Volterra and Wiener Kernels

The Volterra series expansion for multi-input single-output systems was introduced in Chapter 1 as a convenient mechanism for classifying the different types of functional interactions that might exist within receptive fields. It, and the better known expansion for single-input systems, are generalizations of a power series expansion, in that they provide for handling memory in nonlinear systems.

The Volterra kernels are canonic descriptors of a nonlinear system: knowledge of them yields the system's response to any arbitrary input signal $x(t)$. Two systems, G and F, with Volterra kernels $g_n(\tau_1,\ldots\tau_n)$ and $f_n(\tau_1,\ldots,\tau_n)$, respectively, are functionally equivalent if $g_i = f_i$ for all i (Parente, 1970). Unfortunately, the biological systems studied do not have known analytic forms: they are true "black boxes" whose dynamics are to be identified. At present no general method exists for determining the Volterra kernels of a completely unknown system unless restrictive simplifying assumptions are made about the system's structure.

Not all systems are susceptible to analysis by Volterra kernels (cf. Yasui, in preparation;) if a system has a Volterra series expansion there is no guarantee that the series will converge (Yasui, in preparation). Such questions are fortuitously bypassed by the necessity to view the Volterra kernels of neural systems through a set of related

kernels developed by Wiener (1958), which exist for even the hardest nonlinearities (Yasui, in preparation).

As part of his general studies on Brownian motion, Wiener (1958) studied the response of a nonlinear device excited by a Gaussian white noise, and introduced the Volterra series expansion for characterizing nonlinear systems. Wiener's use of Gaussian white noise as an ideal stimulus for studying nonlinear systems was motivated by two considerations: 1) the signal's "whiteness" would assure that the device (system) would be equally excited by all frequencies within the bandwidth of the stimulus, and 2) the Gaussian nature of the signal provided (with finite probability), that the device would be excited by segments of input signal comprising all possible wave shapes (Nisio, 1958). Wiener (1958) reasoned that with such a rich stimulus, much information should be contained in the system's response about the nonlinearities comprising it. To study them, Wiener reformulated the Volterra series expansion in equation 1.3.1 into a new series of functionals of the form

$$y(t) = \sum_{n=0}^{\infty} G_n[h_n;x(t)] \qquad (3.1.1)$$

where the G_n and h_n are the Wiener G-functionals and Wiener kernels, respectively, and $x(t)$ is a Gaussian white noise input with power level P, i.e.,

$$\overline{x(t)\ x\ (t-\tau)} = P\delta(t-\tau) \qquad (3.1.2)$$

where the superbar denotes time average.

The Wiener functionals are orthogonal to each other, in that the time averages of products of two functionals of different order are zero (Wiener, 1958), i.e.,

$$\overline{G_m G_n} = 0 \quad \text{for } m \neq n \tag{3.1.3}$$

Wiener developed the functionals from a straightforward application of the Gram-Schmidt orthogonalization procedure: The first functional G_0 (of zero-order) is a constant, h_0, representing the average (i.e., dc) component of the system response y(t), i.e.,

$$G_0 = h_0 = \overline{y(t)} \tag{3.1.4}$$

The first order functional is of the general form

$$G_1[h_1;x(t)] = \int_{-\infty}^{\infty} h_1(\tau)x(t-\tau)d\tau + K_0 \tag{3.1.5}$$

where K_0 must be determined so that

$$\overline{G_1 G_0} = 0 \tag{3.1.6}$$

That condition is satisfied when K_0 is zero, hence

$$G_1[h_1;x(t)] = \int_{-\infty}^{\infty} h_1(\tau)\, x(t-\tau)d\tau \tag{3.1.7}$$

The second order functional is of the general form (Wiener, 1958)

$$G_2[h_2;x(t)] = \int_{-\infty}^{\infty}\int h_2(\tau_1,\tau_2)\, x(t-\tau_1)\, x(t-\tau_2)d\tau_1 d\tau_2$$

$$+ \int_{-\infty}^{\infty} K_1(\tau)\, x(t-\tau)d\tau + K_o^* \qquad (3.1.8)$$

where K_1 and K_o^* must be determined so that

$$\overline{G_o G_2} = 0 \qquad (3.1.9a)$$

and

$$\overline{G_1 G_2} = 0 \qquad (3.1.9b)$$

The second order Wiener G-functional becomes

$$G_2[h_2;x(t)] = \int_{-\infty}^{\infty}\int h_2(\tau_1,\tau_2)\, x(t-\tau_1)\, x(t-\tau_2)\, d\tau_1 d\tau_2 - P\int_{-\infty}^{\infty} h_2(\tau,\tau)d\tau \qquad (3.1.10)$$

where P is the white noise stimulus' power level as previously defined. Wiener (1958) developed an unwieldy scheme for determining his kernels in terms of a set of Laguerre orthogonal functions. Lee and Schetzen (1965) developed a greatly simplified cross-correlation scheme for determining the Wiener kernels, i.e.,

$$h_n(\tau_1,\ldots,\tau_n) = \frac{1}{n!p^n} E[(y(t) - \sum_{m=0}^{n-1} G_m[h_m;x(t)])x(t-\tau_1)\ldots x(t-\tau_n)] \tag{3.1.11}$$

where E denotes expectation.

Wiener's G-functionals and Lee and Schetzen's cross-correlation algorithm have been extended to multi-input systems by P. Marmarelis (Marmarelis & McCann, 1973; Marmarelis and Naka, 1973, 1974). For a single output system with two independent power spectral densities P_x and P_u, respectively, P. Marmarelis expanded the system response, y(t), by a series of Wiener G-functionals with the form

$$y(t) = \sum_{n=0}^{\infty} G_n[h_n;x(t),u(t)] \tag{3.1.12}$$

where the first three functionals are

$$G_0[h_0;x(t),u(t)] = h_0 \tag{3.1.13a}$$

$$G_1[h_1;x(t);u(t)] = \int_{-\infty}^{\infty} h_{1x}(\tau)\, x(t-\tau)\, d\tau + \int_{-\infty}^{\infty} h_{1u}(\tau)u(t-\tau)\, d\tau \tag{3.1.13b}$$

$$\begin{aligned} G_2[h_2,x(t);u(t)] = {} & \iint_{-\infty}^{\infty} h_{2xx}(\tau_1,\tau_2)\, x(t-\tau_1)x(t-\tau_2)\, d\tau_1\, d\tau_2 \\ & + \iint_{-\infty}^{\infty} h_{2uu}(\tau_1,\tau_2)\, u(t-\tau_1)\, u(t-\tau_2)d\tau_1 d\tau_2 \qquad - P_u \int_{-\infty}^{\infty} h_{2uu}(\tau,\tau)d\tau \\ & + \iint_{-\infty}^{\infty} h_{2xu}(\tau_1,\tau_2)\, x(t-\tau_1)\, u(t-\tau_2)\, d\tau,d\tau_2 - P_x \int_{-\infty}^{\infty} h_{2xx}(\tau,\tau)d\tau \end{aligned} \tag{3.1.13c}$$

where h_{1j} and h_{2jj} are the first and second order Wiener kernels, respectively, of the channel whose input is j (see Section 3.3 for a slightly different notation to identify these kernels from those computed for the one-input case). h_{2jj} is symmetric, but the cross kernel h_{2xu} describing the interactions between 2 channels is, in general, asymmetric, although Koblasz (1976) has described some interesting cases where it is not. Direct analog of Lee and Schatzen's cross-correlation algorithm exist (cf. P. Marmarelis & Naka, 1973) for computing the kernels resulting from multi-input experiments, for example

$$h_{2xu}(\tau_1,\tau_2) = \frac{1}{P_x P_u} E[y(t)x(t-\tau_1)u(t-\tau_2)]$$

A "multi-input" experiment stimulates a system's channels with independent Gaussian white noise stimuli (Figure 3.1.1) and identifies self kernels of all orders (for all channels) as well as all inter-channel "cross-talk" terms, thus greatly reducing and simplifying the experimental effort otherwise required to study such interaction phenomena. Care, however, must be exercised in interpreting the self kernels from such experiments; the reason for that is explored in Section 3.3.

3.2 Relationship of Wiener and Volterra Kernels

The n^{th} order Volterra and Wiener kernels, g_n and h_n, of a nonlinear system are, in general, not identical (Yasui, in preparation),

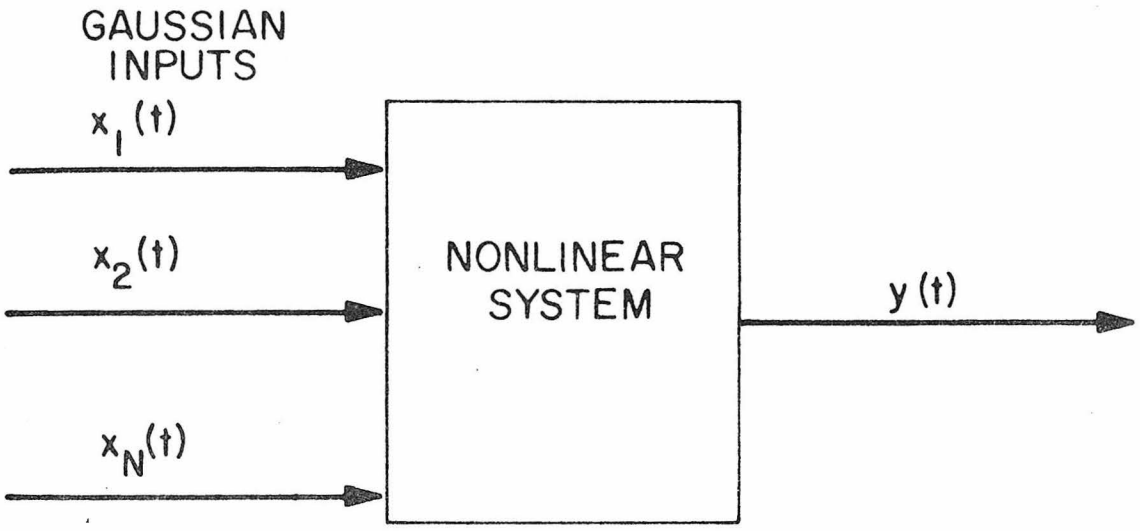

MULTI-INPUT NONLINEAR SYSTEM

Fig. 3.1.1 N independent Gaussian signals probing for system channel interactions

i.e.,

$$g_n(\tau_1,\ldots,\tau_n) \neq h_n(\tau_1,\ldots,\tau_n) \tag{3.2.1}$$

For example, consider a third-order, single-input nonlinear system whose output, y(t), has a Volterra expansion of the form

$$y(t)= \sum_{n=1}^{3} \int_{-\infty}^{\infty}\ldots\int g_n(\tau_1,\ldots,\tau_n) \prod_{j=1}^{n} x(t-\tau_j)d\tau_1\ldots d\tau_n \tag{3.2.2}$$

The first order Wiener kernel is computed by the Lee-Schetzen algorithm:

$$h_1(\tau) = \frac{1}{P} E\ ((y(t) - G_0)\ x(t-\tau)) \tag{3.2.3}$$

Substituting y(t) of 3.2.2 into (3.1.11) and recognizing that

$$G_0 = \int_{-\infty}^{\infty} g_2(\tau,\tau)d\tau \tag{3.2.4}$$

yields

$$h_1(\tau) = g_1(\tau) + 3P \int_{-\infty}^{\infty} g_3(\tau,\sigma,\sigma)d\sigma \tag{3.2.5}$$

Yasui (in preparation) was the first to realize the nonequivalence between Wiener and Volterra kernels of identical order and to establish their interdependence relationship:

$$h_n(\tau_1,\ldots,\tau_n) = \sum_{i=0}^{\infty} (-1)^{i+1} \frac{P^i(n+2i)!}{2^i n!\, i!} \underbrace{\int_{-\infty}^{\infty}\cdots\int}_{i \text{ times}} g_{n+2i}$$

$$(\tau_1,\ldots,\tau_n,\sigma_1,\sigma_1,\sigma_2,\sigma_2,\ldots,\sigma_i,\sigma_i)\, d\sigma_1\ldots d\sigma_i \qquad (3.2.6)$$

Prior to Yasui's work, there was no realization of the differences between these two kernel types (e.g., Schetzen, 1974, p. 597; Goldman, 1973). These results have had important implications in re-evaluating the utility and interpretation of results obtained from Wiener kernel analyses. Equation (3.2.6) reveals how any n^{th} order Wiener kernel contains power level-dependent contamination from higher order Volterra kernels. By exciting a system with stimuli of different power levels, and comparing the shapes and amplitudes of the resultant first order kernels, the presence of higher order nonlinearities can be detected. But this same phenomenon impedes the ability to examine the effects of adaptation on a visual system's response without seeing kernel artifacts arising from different stimulus power levels (Naka, 1975).

3.3 Wiener Kernels and Lateral Interactions

Experimental results (reported in Chapter 5) suggested a need to re-evaluate (with the assistance of Dr. V. Marmarelis) the correctness of the notion that the Wiener self kernels obtained from multi-input experiments are identical to the self kernels extracted from single input experiments (cf. P. Marmarelis & Naka, 1973; 1974).

Consider, for example, a system S with: linear channels A and B with first order Volterra kernels g_{1A} and g_{1B}, respectively; and a third order interaction term between A and B of the form g_{3AAB}. Hence, S's output, y(t), is described by the Volterra series:

$$y(t) = \int_0^\infty g_{1A}(\tau)x_A(t-\tau)d\tau + \int_0^\infty g_{1B}(\tau)x_B(t-\tau)d\tau$$

$$+ \int\int\int_0^\infty g_{3AAB}(\tau_1,\tau_2,\tau_3)x_A(t-\tau_1)x_A(t-\tau_2)x_B(t-\tau_3)d\tau_1 d\tau_2 d\tau_3 \qquad (3.3.1)$$

where x_A and x_B are the input signals into channels A and B, respectively. Let h_{1A} be the first-order Wiener kernel identified for S when only A is excited by a Gaussian white noise x_A ; h_{1B} is the Wiener kernel when only B is excited by noise x_B. When S is excited by the independent noises x_A and x_B simultaneously, then the resultant first order Wiener kernels are $h_{1A(B)}$ and $h_{1B(A)}$ for channels A and B, respectively.

It has been widely assumed that the conditions

$$h_{1A(B)}(\tau) = h_{1A}(\tau) \qquad (3.3.2a)$$

and

$$h_{1B(A)}(\tau) = h_{1B}(\tau) \qquad (3.3.2b)$$

are always true. Chapter 5's data, however, showed the above not to be true in the crayfish's eye. The mechanism that explains the experimental finding, for example, that

$$h_{1A(B)}(\tau) \neq h_{1A}(\tau) \qquad (3.3.3)$$

derives from the Volterra interaction terms (i.e., cross kernels) of order 3 (or greater (cf. Section 1.3) which can affect lower-order self Wiener kernels in a manner analogous to that described in Section 3.2.

If only channel A is excited (by x_A in a single-input experiment) then g_{1A} is the sole contributor to $y(t)$, and

$$h_{1A}(\tau) = g_{1A}(\tau) \qquad 3.3.4)$$

However, when channels A and B are simultaneously excited in a two-input experiment, g_{3AAB} is "activated" and contributes to $y(t)$, yielding

$$h_{1A(B)}(\tau) = g_{1A}(\tau) + Q$$

where

$$Q = P_A\left(\int_0^\infty g_{3AAB}(\sigma,\sigma,\tau)d\sigma + \int_0^\infty g_{3AAB}(\sigma,\tau,\sigma)d\sigma + \int_0^\infty g_{3AAB}(\tau,\sigma,\sigma)d\sigma\right) \qquad (3.3.5)$$

and P_A is the power spectral density of the Gaussian white noise stimulus $x_A(t)$. Q could be simplified in form if g_{3AAB} were symmetric in its arguments; also, g_{3AAB} is not equivalent to the term g_{3BBA} (if it exists). Clearly then, the inequality of (3.3.3) exists and in general all odd (even) order Wiener self kernels, identified from multi-input experiments, are contaminated by all higher order odd (even) Volterra cross kernels, in a manner similar to the single-channel Volterra-Wiener kernel relationship defined by Yasui. This, however, has the benefit of revealing (vaguely and indirectly) the presence of such higher order interaction terms without resorting to lengthy computations to identify them.

3.4 Volterra and Wiener Kernels for Cascaded Systems

Consider two networks, F and G, cascaded with output signals, y(t) and z(t), which can be expressed in Volterra series of the form

$$y(t) = \sum_{n=1}^{\infty} \int_0^{\infty} \cdots \int f_n(\tau_1,..,\tau_n) \prod_{j=1}^{n} x(t-\tau_j)\, d\tau_1 \ldots d\tau_n \qquad (3.4.1a)$$

and

$$z(t) = \sum_{n=1}^{\infty} \int_0^{\infty} \cdots \int g_n(\tau_1,\ldots,\tau_n) \prod_{j=1}^{n} y(t-\tau_j)\, d\tau_1 \ldots d\tau_n \qquad (3.4.1b)$$

respectively. The first two kernels of the cascaded system K=F*G are:

$$k_1(\tau) = \int_0^\infty g_1(v) f_1(\tau - v)\, dv$$

and

$$k_2(\tau_1,\tau_2) = \int_0^\infty\int g_2(v_1,v_2) f_1(\tau_1 - v_1) f_1(\tau_2 - v_2)\, dv_1 dv_2 + \int_0^\infty g_1(v_1) f_2(\tau_1 - v_1, \tau_2 - v_1)\, dv_1 \qquad (3.4.1c)$$

From equation (3.4.1c) we see that even if both F and G contain quadratic nonlinearities (i.e., first and second order Volterra kernels), then the cascaded system K will have a cubic Volterra term capable of contaminating its first order Wiener kernel.

3.5 Spike Data and Wiener Kernels--An Introduction

Some of the most important visual neurons are those which transmit their processed signals over long distances through trains of action potentials (i.e., spikes, pulses), p(t), of the form

$$p(t) = \sum_k P(t - t_k) \qquad (3.5.1)$$

where P(t) is the shape of an action potential and t_k is the time of occurrence of the k^{th} spike. Typical of such systems are the vertebrate retina's ganglion cells and the crayfish's sustaining fibers. Neurophysiologists generally agree, however, that the shape, amplitude, and

(brief) duration of P(t) does not change with time or the neuron's input signal, thus making these parameters unlikely candidates for encoding and transmitting information. The only available parameter for encoding appears to be t_k. Consequently the standard procedure for collecting neurophysiological spike data for analysis obliterates all spike parameters but t_k; P(t) is replaced by the Dirac delta function, $\delta(t)$, in representations of p(t), i.e.,

$$p(t) = \sum_k \delta(t-t_k) \qquad (3.5.2)$$

Such systems, however, present several problems not found in continuous output systems when attempts are made to analyze them by Wiener functionals. For example, to overcome questions of existence and convergence of the functionals, the spike tarin p(t) must be converted into a smooth signal p*(t) via a transformation T that will, hopefully, preserve in p*(t) the information of p(t). A correct choice for T precludes a knowledge about the encoding schemes employed by the neural system which often is a matter of speculation (cf. Perkel & Bullock, 1968, for a discussion of various neural codes thought to underlie various systems).

Fortunately, the choices for T are limited by the fact that neurophysiological spike trains fall within the realm of point processes (i.e., collections of times (t_k) with the property that $t_k < t_{k+1}$) whose properties fall within two categories only: 1) counting properties which involve the number of points (spikes), $N(t,\tau)$; and 2) interval statis-

tics which concern the relative spacing between points, i.e., $t_k = t_k - t_{k-1}$. In neurophysiology two popular choices have evolved for T, reflective of each of the above properties: spike density $N(t,\tau)$; and instantaneous frequency, the reciprocal of the interval between successive pulses, i.e., $f(t_k) = 1/t_k$. (Algorithms exist for smoothing instantaneous frequency onto a continuous function of time, $f(t)$ (cf. Shapley, 1971)).

The choice of transformation determines what the subsequently computed Wiener kernels will predict: either the distributions of the spike density or the intervals between spikes. The two properties of a spike train are not identical (Jowett & Vere-Jones, 1972). Consider for example a point process whose points are Poisson distributed in time with parameter, β. Then the probability of having exactly m spikes in the interval $(t,t+\tau)$ is also Poisson-distributed, i.e.,

$$\text{prob}(N(t,t+\tau) = m) = \frac{e^{\beta\tau}(\beta\tau)^m}{m!}$$

The interval distribution between pulses, however, is not Poisson, but is of the form (Coggshall, 1973):

$$C_n(\tau) = \frac{\beta(\beta\tau)^{n-1}e^{-\beta\tau}}{(n-1)!}$$

where $C_n(\tau)$ is the distribution function for the length of n successive intervals, and for the first order (n=1) the interval distribution is

exponential. From $C_1(t)$ the probability distribution for the instantaneous frequency is, in turn, $\beta\exp(-\beta/f)f^{-2}$, where f denotes instantaneous frequency. Real spike trains are rarely Poisson, and have counting and interval statistics that differ in more complex manners. In general it is not simple to derive counting statistics from interval statistics or vice versa: typically, all the moments of an interval property will require knowledge of all the distributions of the counting properties (Daley & Vere-Jones, 1972). Furthermore, stationarity is usually defined in terms of counting statistics, since interval statistics rarely are stationary (Daley & Vere-Jones, 1972).

Furthermore, the Volterra kernels for the two transformations are unequal. Spike density can be extracted by a simple zero-order hold device which only has a first-order Volterra kernel. Instantaneous frequency requires a second-order kernel to examine the interval between spike pairs. Bode plots of the two transformations (McKean, et al,1970), as a function of a pulse train's average firing rate, reveal differences too. The gain for spike density is constant with no phase shift; the gain and phase relations for instantaneous frequency depend on the average spike rate.

Hence, the Wiener kernels computed for a spiking neuron are for the neuron cascaded with an additional signal processing stage T. Furthermore, the neuron itself may be thought of as a cascaded network F*G, where G is the spike generating mechanism, and F represents all the neural processing stages (of the cell and/or presynaptic inputs to the cell) preceding spike initiation.

Several interesting and nontrivial questions now arise about the interpretation of kernels computed for spiking neural systems which in fact represent the cascade F*G*T;

1) How well do the kernels for F*G*T reflect the dynamics of the system F so that spike data can be compared with kernels for continuous output systems?

2) Experience has consistently demonstrated higher mean square errors associated with kernels computed from spike data than those computed from analog data. Is that due to higher-order nonlinearities associated with the spike generating mechanism, G, (or data conversion step, T) insufficiently handled by low-order models, or does it result from noise inherent in spike data?

3) Are there differences in the resultant models computed from different choices for T? Can this lead to confusion if different investigators, studying identical systems, process spike data differently?

3.6 Computer Simulations

To answer some of the questions raised about spike trains and Wiener kernels, it was decided to analyze some basic properties of spike data derived from a noise-free environment, i.e., a computer simulation of a known spike generating mechanism cascaded with a nonlinear network of known characteristics.

The spike generating network had to have some physiological basis--a criterion that could not be absolutely satisfied, since the mechanisms of spike generation are still a matter of continued study and contro-

versy. For simplicity, the simple integrate and fire spike encoder (also known as the integral pulse frequency modulator, IPFM) was chosen (see Figure 3.6.1). It consists of three basic parts: an integrator which integrates an input signal, z(t), to produce an output signal, A(t), a comparator and pulsing circuit which examines the value of A(t) against a threshold value, θ. When A(t) equals θ at time t_k, a pulse is produced and a feedback loop resets the integrator's integrand to zero.

The integrate and fire model has been used extensively as a model of spike encoding in Limulus eccentric cells (Knight, 1969,1972) and other neural systems (e.g., Gordon, 1975). The integrate and fire model is an extremely simple model, but it has interesting characteristics. The rate of generation of nerve impulses will be directly proportional to the average value of z(t). This model behaves linearly for all deterministic time varying input signals as long as the input, z(t), produces a monotonically increasing integrator output A(t). A decrease in A(t) cannot generate pulses, hence it demonstrates characteristics of a rectifier. Despite the IPFM's simplicity, an analytical analysis of the model is extremely difficult in all cases except where the input, z(t), is a sinusoid with a low depth of modulation, m.

V. Marmarelis and McCann (1975) briefly examined the last question as a byproduct in their study of ways to minimize the mean square errors in their sustaining fiber 038. They found that only minor differences existed between the kernels computed for 038 when its spike data were converted into spike density or instantaneous frequency. Furthermore,

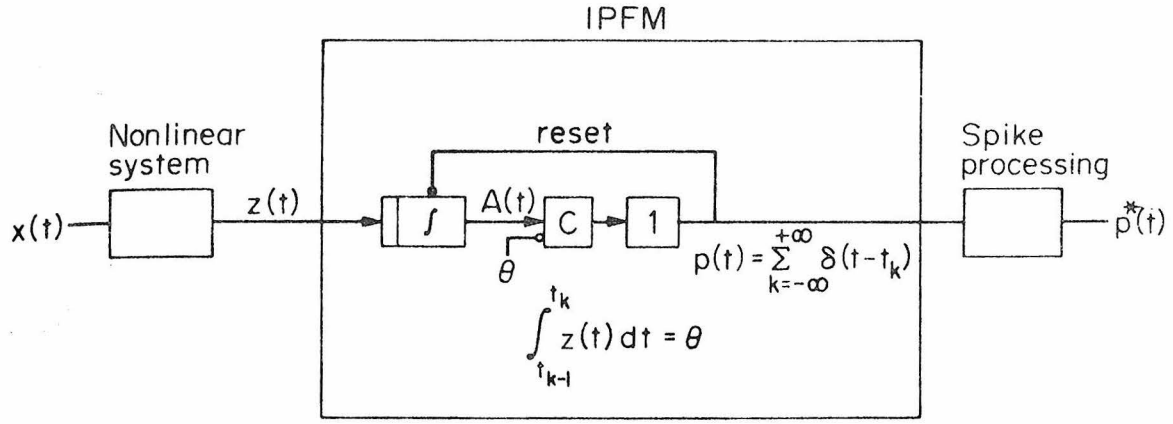

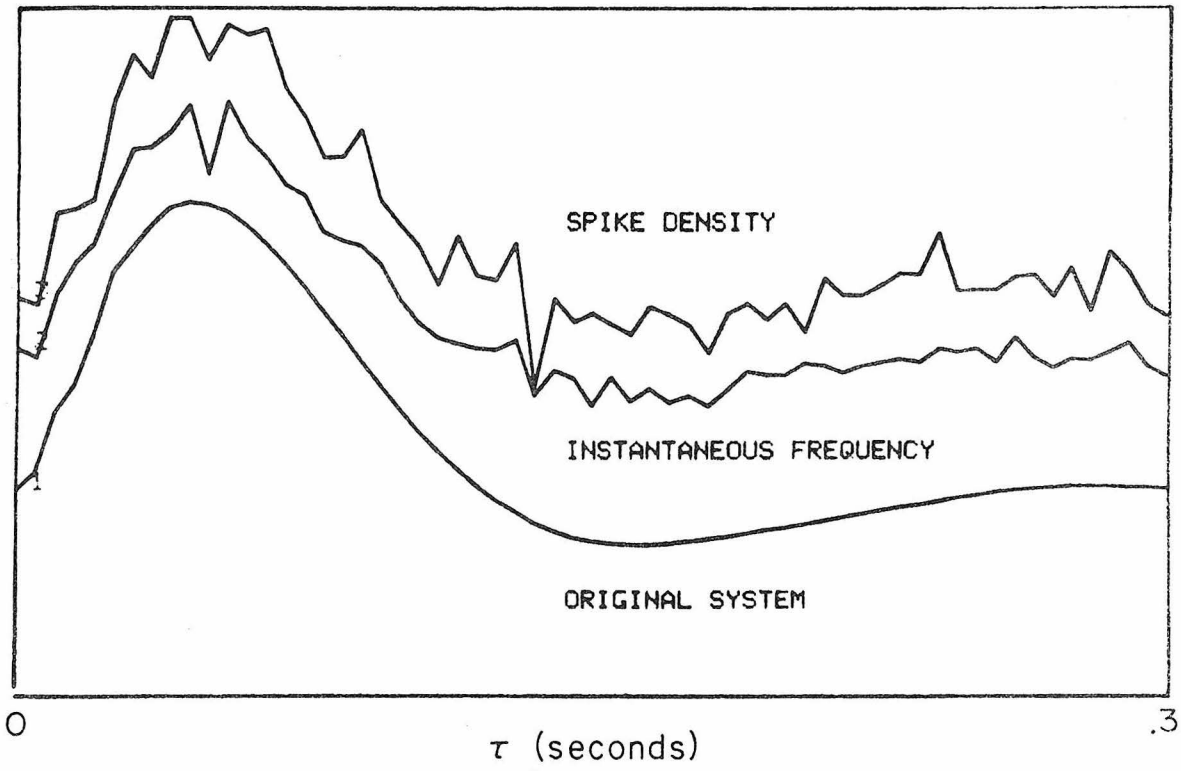

Fig. 3.6.1 Spike Generating Network (IPFM) Cascaded with Nonlinear System. a) System configuration; b) Computed kernels (see text)

both transformations yielded nearly identical mean square errors when an "optimal" bin size of 0.04 sec was used: 34.91% for the former, 34.05% for the latter. These results come as a surprise in view of the previous discussions.

Question 1 could be answered if a spike generating neuron could be excited intracellularly with an appropriate noise source, and the resultant spike train recorded to determine the kernels for G. Bryant and Segundo (1975,1976) have incorporated this technique on abdominal ganglion cells of Aplysia, but the technique is not, at present, easily applicable to 038, due to a protective sheath around the fiber which prevents microelectrode penetrations (D. Rafuse, personal communication). Bryant and Segundo's (1975,1976) analyses have been limited to identifying first-order Wiener kernels, thus making their interpretation limited. The fact that higher order nonlinearities exist (Bryant & Segundo, 1975,1976) means that their first order kernels are contaminated by higher order Volterra kernels. This might explain why the kernels appear to be so sluggish, i.e., slow in their peak rise time (about 40 msec) although Aplysia is known to produce long duration action potentials (i.e., 20 msec). Also, there is no reason to expect that Alypsia abdominal ganglion cells need replicate the mechanisms or dynamics of visual neurons of more evolved animals with different information-handling requirements.

The family of simulated nonlinear systems consisted of a linear system, L (with impulse response $g(\tau)$) cascaded with a squarer. The squarer's output, $z(t)$, defined by

$$z(t) = \int_0^\infty\int g(\tau_1)\, g(\tau_2)\, x(t-\tau_1)\, x(t-\tau_2)\, d\tau_1\, d\tau_2 \qquad (3.6.1)$$

fed into an IPFM to produce a spike train, p(t), which, in turn, was converted to $p_d^*(t)$ or $p_f^*(t)$ by either a spike density or an instantaneous frequency transformation, respectively.

In the simulations the input signal to L, x(t), consisted of a 100 second presentation of bandlimited (.2-50 Hz) Gaussian white noise, whose mean and standard deviation could be modified to produce desired characteristics in p(t)'s average firing rate.

Because the simulations were not intended to become an independent study of IPFM's, only those results relevant to kernel interpretation vis-a-vis spike data will be presented here.

Consider the system defined by L:

$$a_3 z''' + a_2 z'' + a_1 z' + a_0 z = x \qquad (3.6.2)$$

where $a_1 = 1.44\text{x}10^{-4}$, $a_2 = 3.29\text{x}10^{-2}$, $a_3 = 1583$, and $a_0 = 60$, such that

$$g(\tau) = 0.2652(\exp(-180t) - \exp(-24t)(\cos(41.58t) - 3.753 \sin(41.58t))) \qquad (3.6.3)$$

Other system parameters are $\overline{x(t)} = 12.5$ (arbitrary units), $\overline{p(t)} = 25$ spikes/sec, and $\theta = .5$ (arbitrary units).

Second order Wiener kernels were computed from

$$h_{2z}(\tau_1,\tau_2) = E(z(t)x(t-\tau_1)x(t-\tau_2)) \qquad (3.6.4)$$

$$h_{2d}(\tau_1,\tau_2) = E(p_d^*(t)x(t-\tau_1)x(t-\tau_2))$$

$$h_{2f}(\tau_1,\tau_2) = E(p_f^*(t)x(t-\tau_1)x(t-\tau_2))$$

These kernels, depicted in Figure 3.6.2, all appear remarkably similar (except that h_{2d}, the spike density kernel, is a bit noisier). Longer simulations would have yielded smoother kernels without affecting the upcoming results; those conclusions, however, would not have been readily extendable to the data reported in later chapters that were derived from experimentally necessitated short duration white noise runs. In an unrelated study on Wiener kernels, featuring a diode-RC filter-IPFM cascade, French (1976) presents second order kernels (his Figures 2 and 5) supporting the observation in Figure 3.6.2 that spike generating and conversion mechanisms minimally mask the dynamics of a (neural) system's pre-spike stages in the Wiener kernels computed for the total system cascade. Furthermore, the two different spike-to-analog conversion schemes do not appear to result in significantly different kernels for the total cascade despite their different Volterra kernel decompositions. Interestingly, Marmarelis and McCann (1975) observed a similar equivalence in kernels computed for 038 when its spike train was processed spike density or instantaneous frequency transformations.

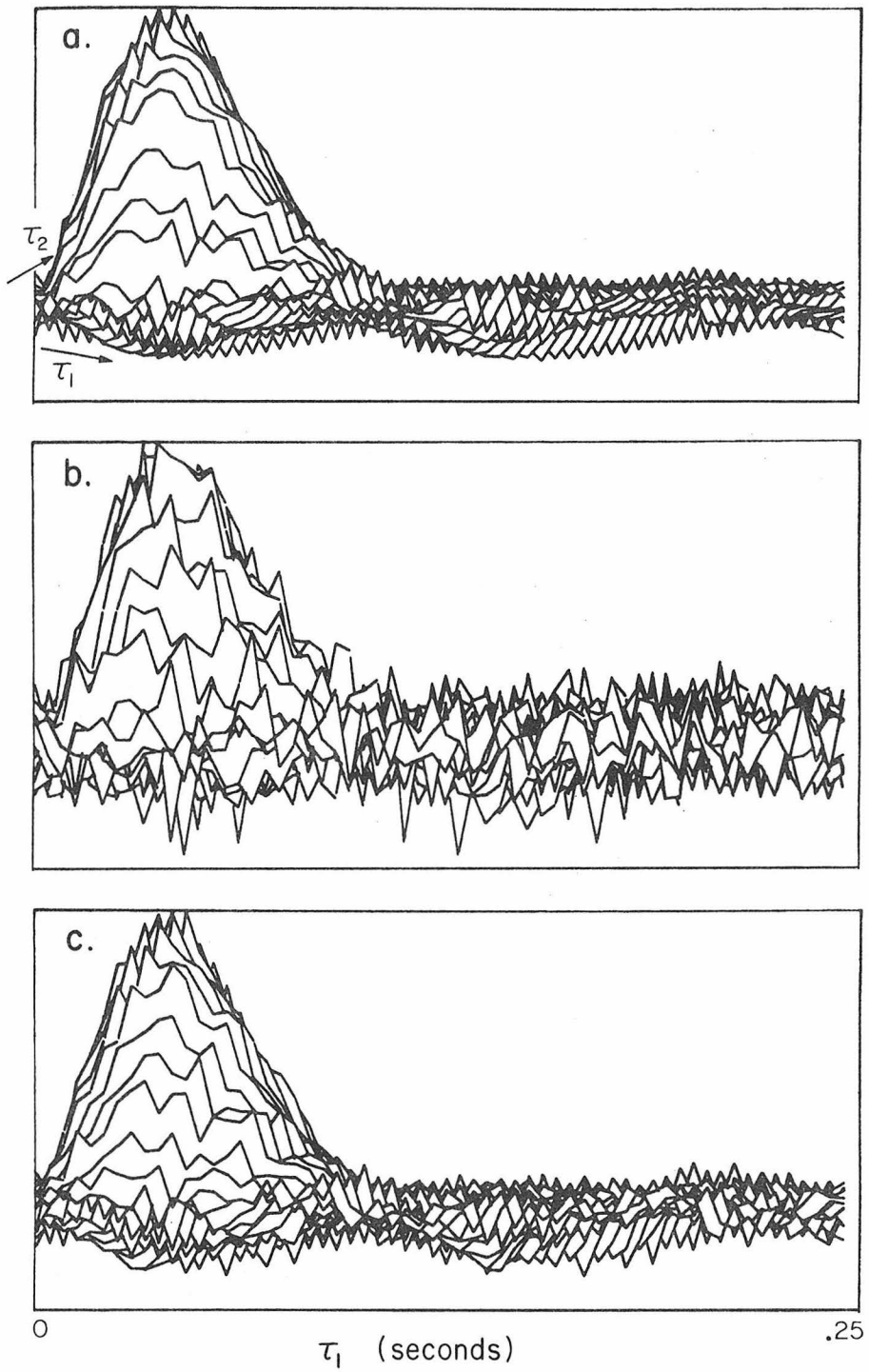

Fig. 3.6.2 Second-Order Kernels for a Nonlinear System (a) - IPFM Cascade Using: b) Spike Density; c) Instantaneous Frequency

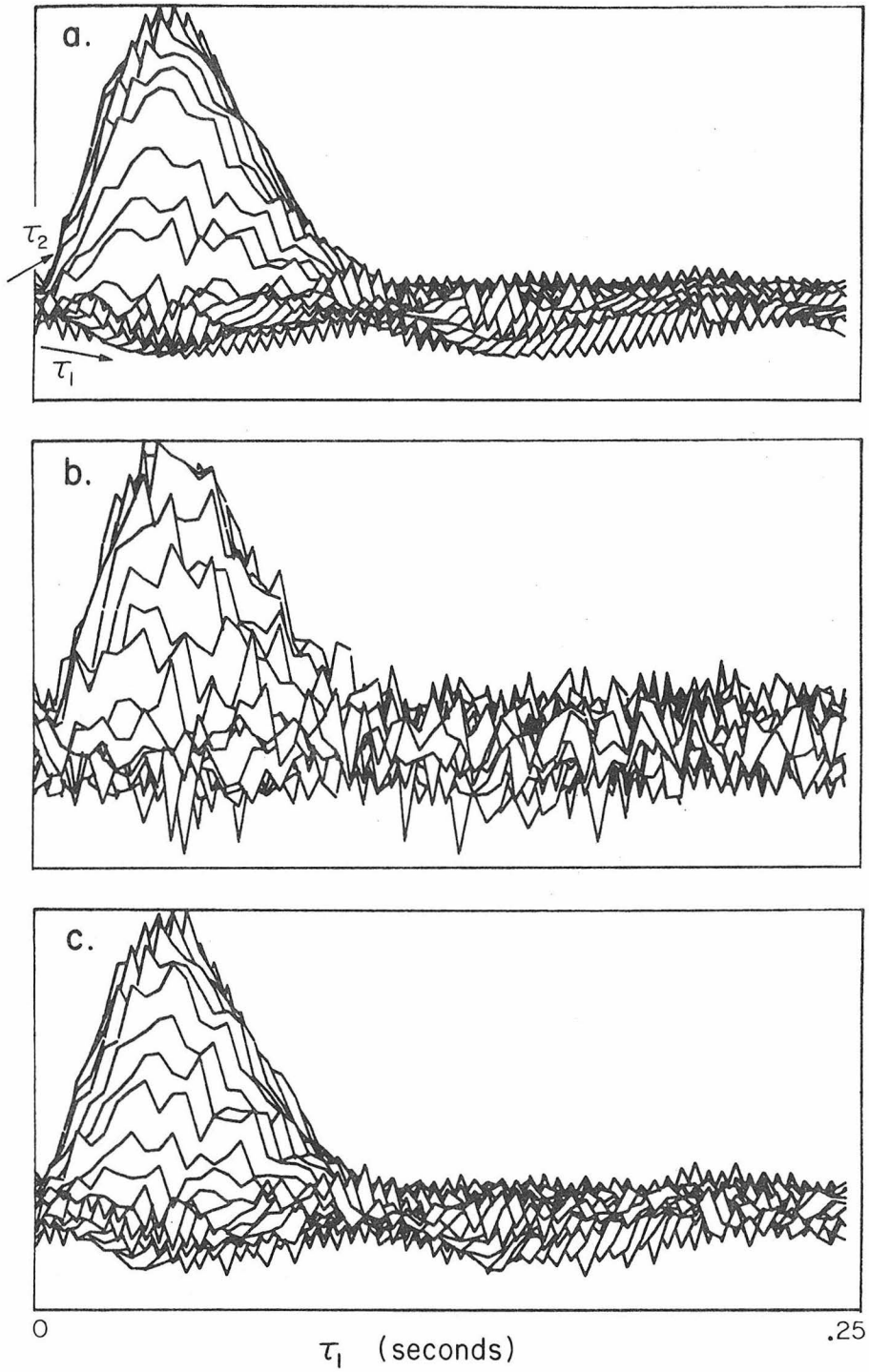

Fig. 3.6.2 Second-Order Kernels for a Nonlinear System (a) - IPFM Cascade Using: b) Spike Density; c) Instantaneous Frequency

The accuracies of h_{2d} and h_{2f} as system descriptors are reflected by the mses' of their model predictions outlined in Table 3.6.1. The kernel h_{2f} results in a lower mse (16.83%) than does h_{2d} (65.45%). This is due in part to h_{2d}'s noisier nature, but horizontal cuts along the kernels (Figure 3.6.1) shows that h_{2f} is noisy too. Other causes, then, must contribute to the poor "modeling" performance of h_{2d}, the most probable being the use of mse as an error measurement.

The error criterion used to evaluate the effectiveness or accuracy of a Wiener kernel model is the mean square of the difference between the model's predicted output ($y_{pred}(t)$) versus the output of the actual neuron ($y(t)$) for the same input signal, $x(t)$. The error, $e(t)$, is then defined as

$$e(t) = (y(t) - y_{pred}(t))^2 \quad \text{where } y_{pred}(t) = \sum_{m=0}^{n} G_n \qquad (3.6.5)$$

The spiking neuron's output is a train of delta functions, and the predicted response $y_{pred}(t)$ is a continuous, smoothed signal. When comparing $y(t)$ (in spike train) to the continuous signal $y(t)$, a serious weakness becomes apparent in the mean square error criterion. It is sensitive to "isolated noises", i.e., data points which deviate from the majority by large amounts. For most t, $y(t)$ will consist of no signal, but $y_{pred}(t)$ will always have some value. Hence, any (small) number of bad data points, with large errors, are made larger by squaring and can contribute much more than any number of good data points, since the area of the good spike signal $y(t)$ usually will not cancel the

Table 3.6.1

Bin Size	Rebinned .005 sec Model Responses*		Re-computed Kernels at New Bin Size **	
	Spike Density Model (new mse)	Inst.Freq Model (New mse)	Spike Density	Instan.Freq.
.005	65.45	16.83		
.010	55.93	12.59	272/75	321/53
.015	40.45	22.15	789/68	930/57
.020	37.55	12.40	1700/67	1748/57
.025	35.44	29.62	5500/6674	7564/58
.030	52.14	12.93		4775/57
.035	54.50	12.72		5917/56
.04	57.63	17.45		9514/55
.045	37.88	48.61		17,000/55
.05	89.68	16.66		13,000/53

* mse's are absolute

** mean square errors are absolute/scaled

large area of $y_{pred}(t)$. Hence, to minimize the error it is necessary to decrement the portion of y(t) with zero signal. That is why, in part, it is advantageous for Wiener kernel analysis to increment bin-width of the signals used for computing mean square errors.

Marmarelis and McCann (1975) noted that one way to decrease the mse of the kernel models was to re-bin the kernel model responses (computed from fine temporal resolution kernels) and to recompute their mean square errors against appropriately re-binned spike data. (New kernels were not computed at these new bin sizes: if they would be, no improvements in the mse's would be seen--cf. Table 3.6.1).For their data a bin size of 0.04 seconds was found to result in nearly identical minimal mean square errors for h_{2d}'s and h_{2f}'s model responses (34.91% and 34.05%, respectively). When the data underlying Table 3.6.1 were re-binned, the mse's of Table 3.6.1 were found. In general, Table 3.6.1's data generally followed the expectations set by Marmarelis and McCann (1975), but dual mse minima for each of the spike conversion schemes were found at different bin sizes which did not bear obvious relationships with the mean interspike interval (0.041 sec) of the unprocessed raw spike data. Table 3.6.1 reveals similar results taken from 038 data. That an optimal (data smoothing) bin size can be found is certain, but it does not appear to manifest itself in a consistent manner. In any event, the improved mean square errors for the kernel model responses do not increase the information already contained in the fine resolution kernels.

These data can now supply answers to the previously posed question:

1) (Conjecture) The kernels computed from spike data very closely reflect the dynamics of the neural system just prior to its spike generation stage.

2) High mean square errors for kernel models developed from/for spike data result from two sources: a) the inappropriate use of mse as an error measurement between spike data and the smooth output of kernel models; and b) an inherent noisiness in kernels computed from sparse spike data.

3) (Surprisingly, and as yet inexplicably) Instantaneous frequency and spike density transformations result in kernels with almost identical dynamics.

These results have important implications for the experiments described in the following chapters in which many regions on a retina have to be tested within a short time (thus eliminating the luxury of long duration tests for low mse kernel models). The above results suggest that (for spike data) poor mean-square-error kernel models do not mean that the identified kernels are "worthless"; instead, much relative information about the system's dynamics can still be extracted from them.

Chapter 4

SINGLE INPUT EXPERIMENTS

4.1 Double Pulse Experiments

The invocation of any form of the single- or multiple-input Volterra series expansion to study a system presumes the presence of nonlinearities whose characteristics cannot be examined by linear systems theory. A similar rationale applies to the crayfish. Hence, one must first test for a superposition principle, or lack of one, in the crayfish sustaining fibers single input channels response to brief pulses of light intensity to determine if the system is worthy of nonlinear analysis.

The nearly instantaneous rise time of the LEDs permits arbitrarily brief duration light pulses to be presented to the crayfish eye. By averaging, for example, 038's response to fifty or one hundred 1-millisecond pulses (with an interpulse interval of 5 seconds) an "average impulse response" function for 038 can be extracted. With this average response 038's linearity or nonlinearity can be examined by a two-fold procedure. First, superposition is assumed, and predictions are made of 038's response to two identical pulses separated in time by τ seconds. This is achieved by a simple algebraic summation of 038's average impulse response with a time-delayed version of itself. That prediction is then compared with results obtained from an actual two-impulse experiment. If the predicted responses coincide with the experimental results, then 038's behavior is linear and no need would exist to proceed with Wiener kernel analyses of it. If, however, linear summation does not predict actual experimental data, then, as discussed in Chapter 1, one is

confronted with a nonlinearity whose source and nature must be determined. Figure 4.1.1 presents the results of such a comparison between simulation and experiment.

Figure 4.1.1a shows the actual impulse response function. It is, as often described, characterized by an initial high frequency burst of spikes with a frequency of 200-500 impulses per second, which decays in approximately 40 milliseconds to a steady state discharge of approximately 20-100 spikes per second. The transient response usually consists of approximately 10 closely spaced spikes separated by about 2 millisecond intervals, followed by a variable number of spikes in the steady state dependent on the stimulus intensity and duration. The latency of response varies from 45 to 65 milliseconds, depending on the stimulus intensity.

Figure 4.1.1b compares predicted (superposition responses) linear summation responses with actual 038 response to two 1 millisecond pulses separated by 5 milliseconds. The figure shows that the predicted response and actual response are dramatically different from each other. As will be noted from Figures 4.1.1b, c, and d, the real experimentally obtained data demonstrate a higher initial spike frequency than predicted by simple superposition. This result disposes of the proverbial two birds with one stone, by establishing that: 1) superposition does not hold; and 2) a spike compression mechanism has not been confronted. The 5 millisecond pulse separation reveals two interesting aspects of the second order interaction in 038: 1) there is an initial excitatory phase (reflected in the experimental data's higher spike rate than that of the

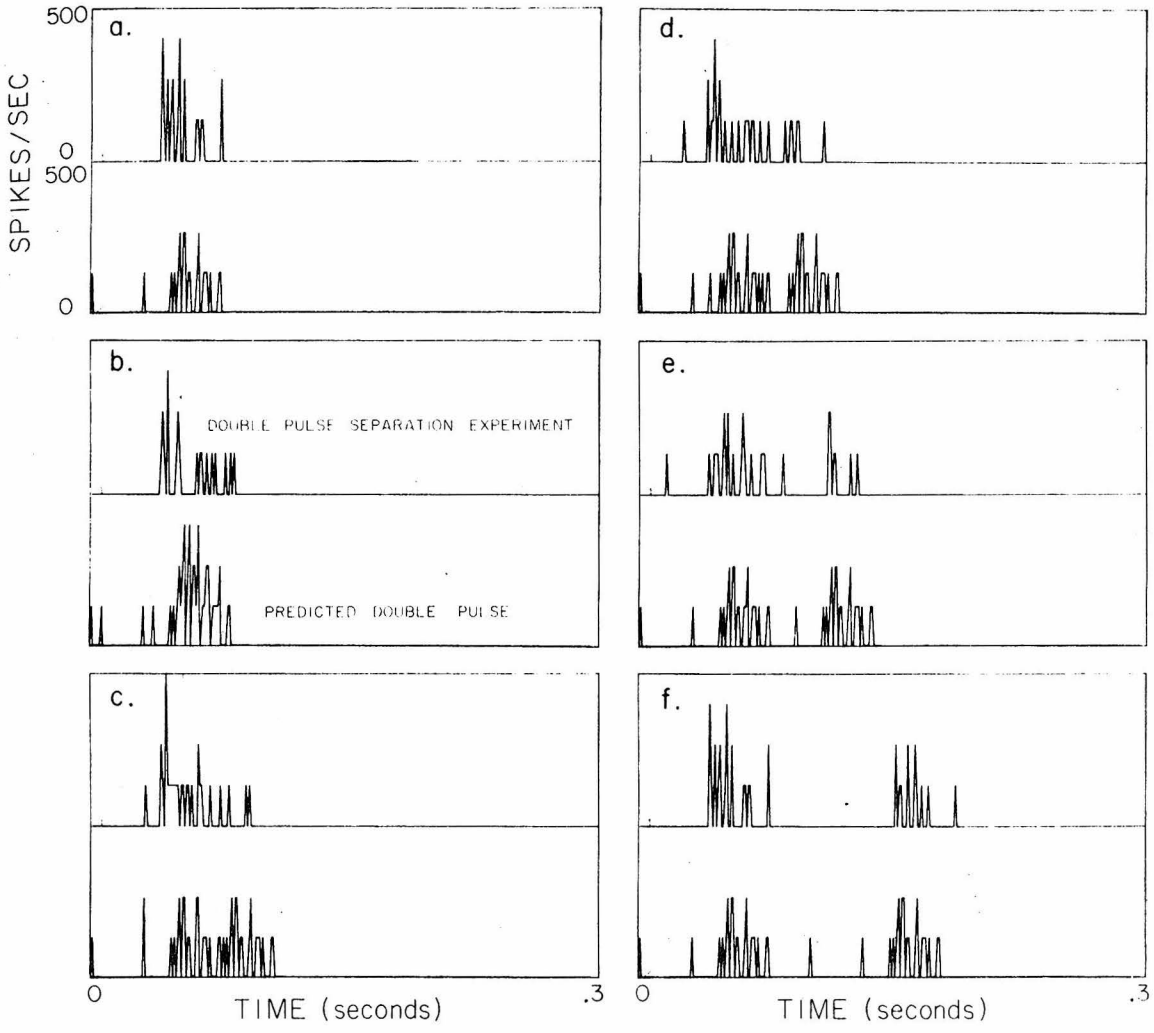

Fig. 4.1.1 Double - (1 msec) Pulse Experiments with: b) 5; c) 30; d) 40; e) 60; and f) 100 msec Separations.
Upper Responses: 038's Actual Response
Lower: Predict Response from Single Pulse (a)

predicted response); 2) followed by an inhibitory phase, reflected by the observation that the steady state rate of the experimental data is well below that predicted by superposition. Pulse separations of 30 and 40 milliseconds reflect similar phenomena. The 60 millisecond pulse separation data mark a start of the experimental data to begin to follow the predicted response: 100 millisecond pulse separation suggests that the memory of the system has just about faded, but it is still in the midst of an inhibitory phase (Figure 4.1.1f).

From the data presented in Figure 4.1.1 and the above discussion, we may conclude that:

1. The 038 system is nonlinear, independent of any spike compression mechanisms (Figure 4.1.1b);
2. The nonlinearity is at least second order and is characterized by an initial excitatory phase followed by an inhibitory phase, the nature of which is examined in Section 4.3;
3. The memory of the 038 system is at least 100 milliseconds;
4. The latency of the 038 system is at least 40 milliseconds;
5. The initial excitatory phase lasts for at least 60 milliseconds (Figure 4.1.1e).

4.2 Single Channel Sine Wave Excitation

To efficiently test 038 with white noise, in the next section it is necessary to determine the bandwidth of temporal frequencies that 038 responds to. This is accomplished by recording 038 response (i.e., total spike production) to sinusoidal variations of light intensity.

Table 4.2.1 shows the averaged normalized response of ten 038 fibers at different stimulus frequencies with respect to the number of spikes produced at one hertz. (The normalized response for a single fiber is shown in Figure 4.2.1.) Peak sensitivity is localized around 1-2 hertz and falls off rapidly after 5 hertz. The almost constant response between 8 and 15 hertz reflects phase locking phenomena which makes computation of phase angles meaningless (cf. Gordon, 1975).

Figure 4.2.2 shows a basic difference in the response pattern of 038 to stimuli above and below 1 hertz: for 3 and 5 hertz (Figure 4.2.2) 038's response is characterized by spikes occurring at one particular point in the stimulus cycle. For 1 hertz and below the spikes produced by 038 have a broader distribution throughout the stimulus cycle. This phenomenon was first observed by Gordon (1975) who classified .2-1 hertz as 038's linear range: between 2-3 hertz, 038 begins to take on the characteristics of a half-wave rectifier.

Figure 4.2.2 also shows a phenomenon first observed by Gordon (1975): 038 appears to fire on the rising slope of the sine wave. From the data contained in Table 4.2.1 we can conclude that white noise with a frequency of 20 hertz will sufficiently cover the major operating range of 038.

4.3 White Noise Experiments

The double-pulse experiments of Section 4.1 established the presence, and some minimal characteristics, of (at least) second-order nonlinearities within 038's excitatory field. Wiener kernels, reflecting structure underlying these dynamics are readily computed from 038's

Table 4.2.1

RELATIVE FREQUENCY RESPONSE OF 038 (NORMALIZED AT 1 Hz)

Hz	Relative Response (Total Spikes in 1 Cycle of Stimulus)
1	1.0
2	.84
3	.58
4	.54
5	.40
6	.40
7	.29
8	.25
9	.25
10	.20
11	.21
12	.20
15	.11
20	.07
25	.04
30	.04

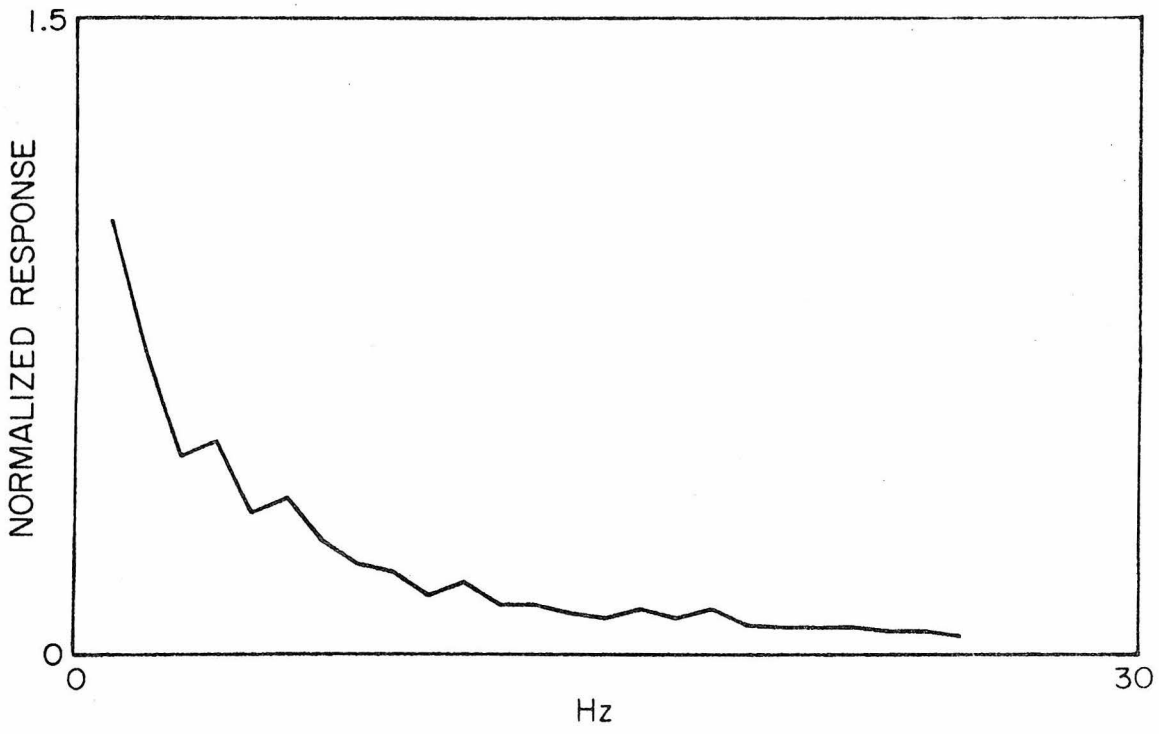

Fig. 4.2.1 Normalized 038 Response to Sine Waves

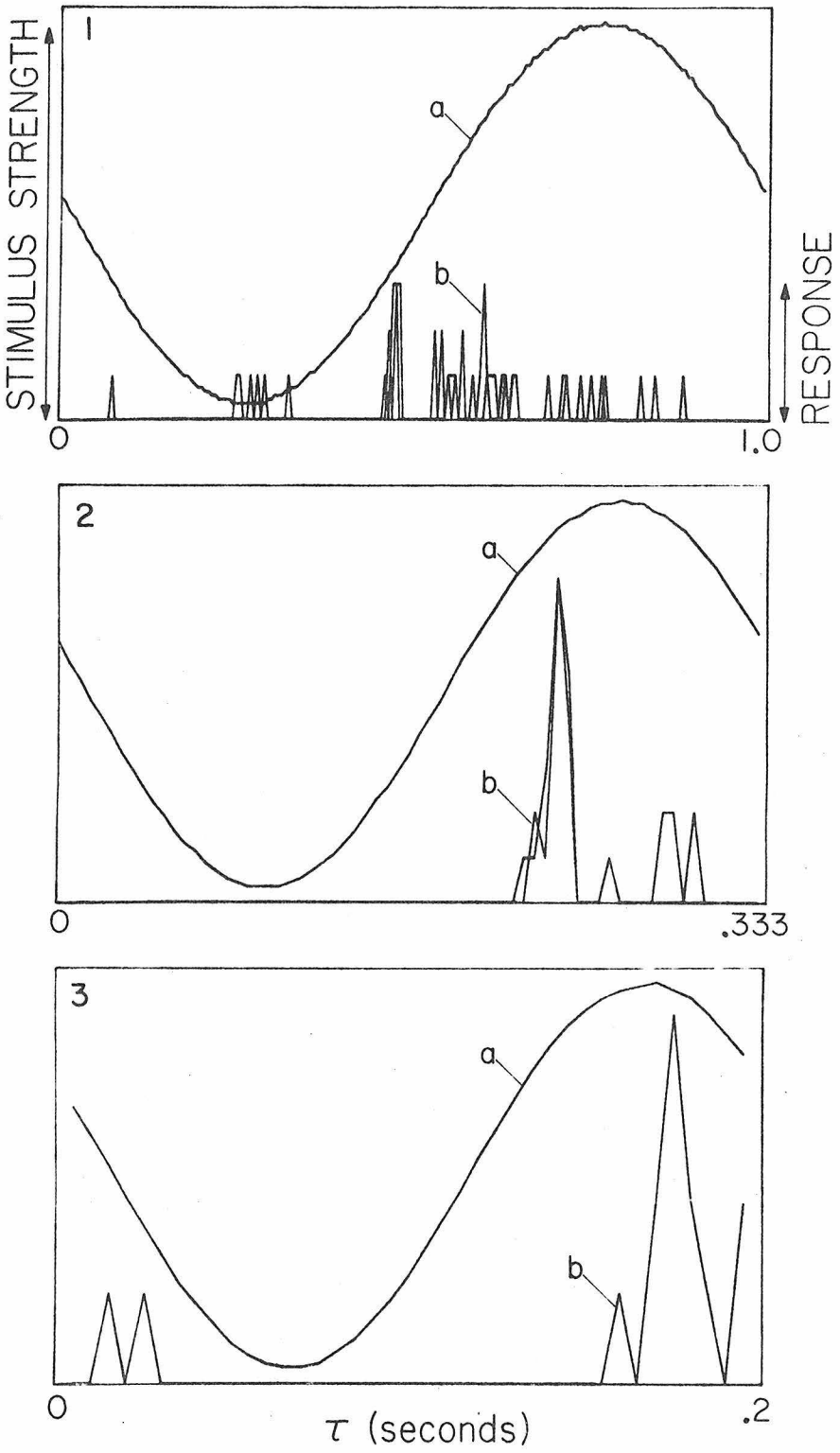

Fig. 4.2.2 038's Response, b, to sine waves, a.
1) 1 Hz; 2) 3 Hz; 3) 5 Hz

response to appropriate stimulus regimes of the type and with the procedures described in Chapters 2 and 3. The sinusoid response data of Section 4.2 revealed 038's low-frequency operating range as sufficiently narrow to be effectively excited by a bandlimited noise of .2-25 hertz.

A typical set of "daytime" first- and second-order Wiener kernels (h_1 and h_2), computed for 038 from spike-density transformed data, are shown in Figure 4.3.1. The accuracy and effectiveness of these kernels as descriptors of 038's behavior are measured by the mse between h_1 and h_2's combined predicted, and 038's actual response to an identical stimulus: Figure 4.3.2 shows a segment of Figure 4.3.1's kernels' (i.e., h_0, h_1, and h_2) predicted response compared with a corresponding segment of (spike-density) processed 038 data. The mse between the two responses is 63.8%.

The high mse may be suspected, from Chapter 3, as a premature detractor of these kernels' reliability as 038 descriptors. Examination on a finer time scale (Figure 4.3.3) of the model responses (decomposed as h_0+h_1 and $h_0+h_1+h_2$ combinations), and 038's unprocessed spike train reveals the zeal with which the kernels follow the dynamics of 038's spike train. (The h_0+h_1 combination yields an mse of 93.2%.)

A third order kernel, h_3, was computed for 038 for which the τ_3 = .050 sec cut is shown in Figure 4.3.1e, but which contributes a negligible 2% to the total model response (61.9%). The third order self-kernel does not appear to be a significant entity in 038. Figure 4.3.4 shows the result of stimulating 038 in one animal, with white noise of different power levels (cf. Section 3.2). The maximum amplitude of h_1

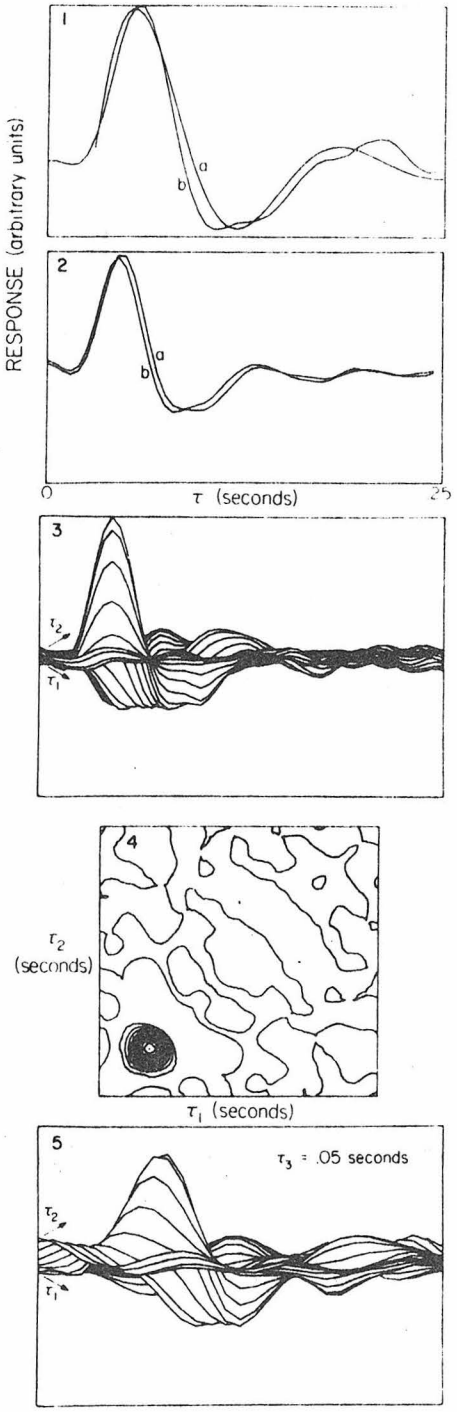

Fig. 4.3.1 038's "day kernels". 1) h_1 vs $e^{-15t}\sin 48.38t$; 2) h_1 vs h_2 cut; 3) h_2; 4) h_2 contour; 5) two-dimensional collapse of h_3

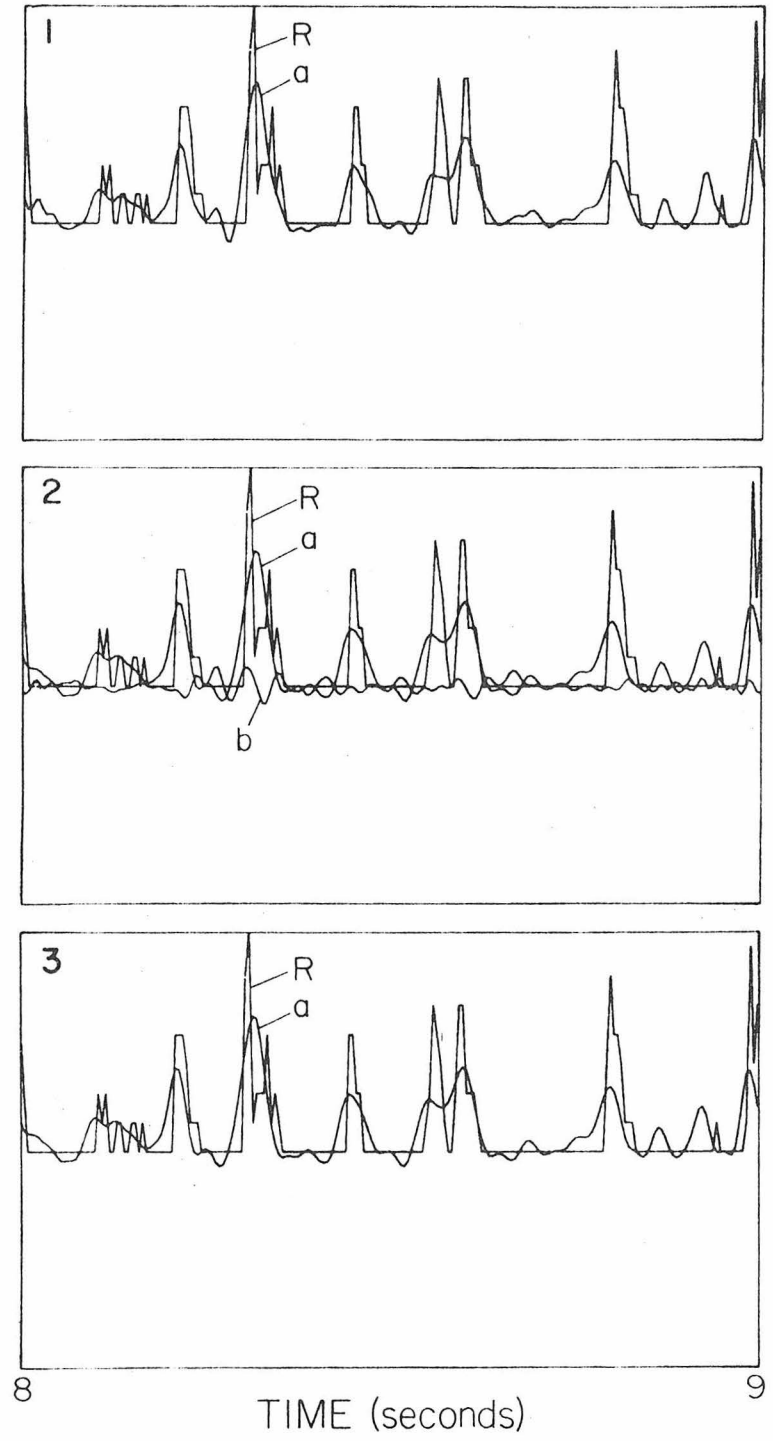

Fig. 4.3.2 038's response R vs kernel predictions, a.
1) $a = h_1+h_2$, 2) $a = h_1+h_2$, $b = h_3$; 3) $a = h_1+h_2+h_3$

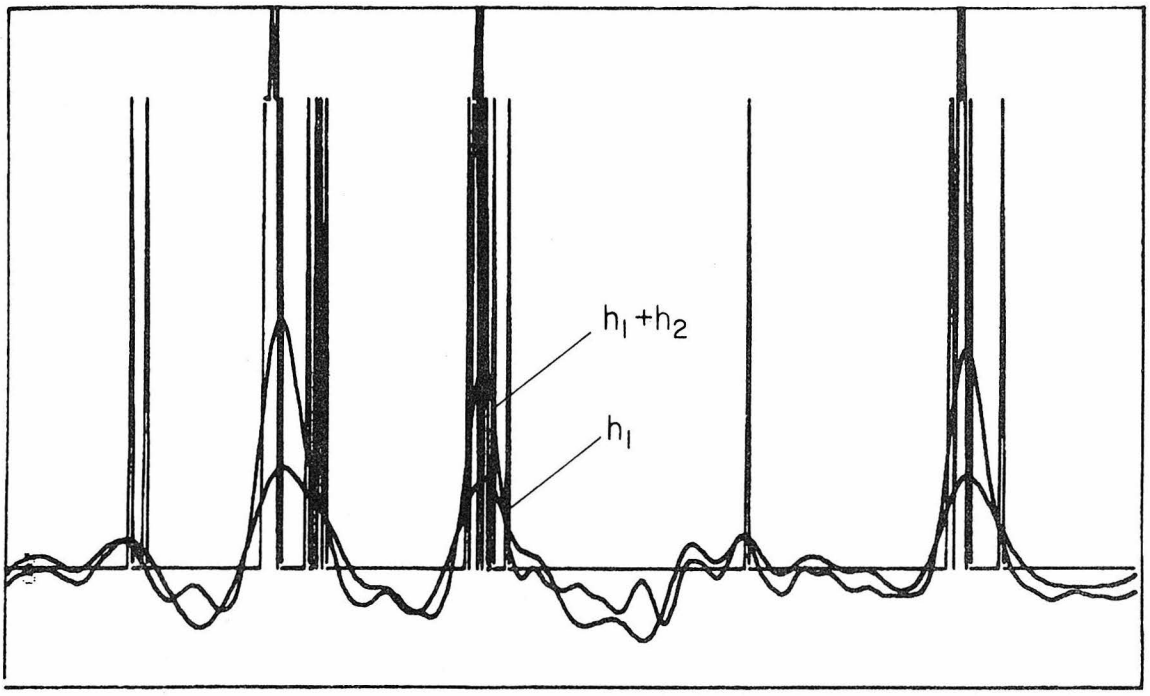

Fig. 4.3.3 Fine Detail of 038's Response vs h_1 and $h_1 + h_2$ Model Responses

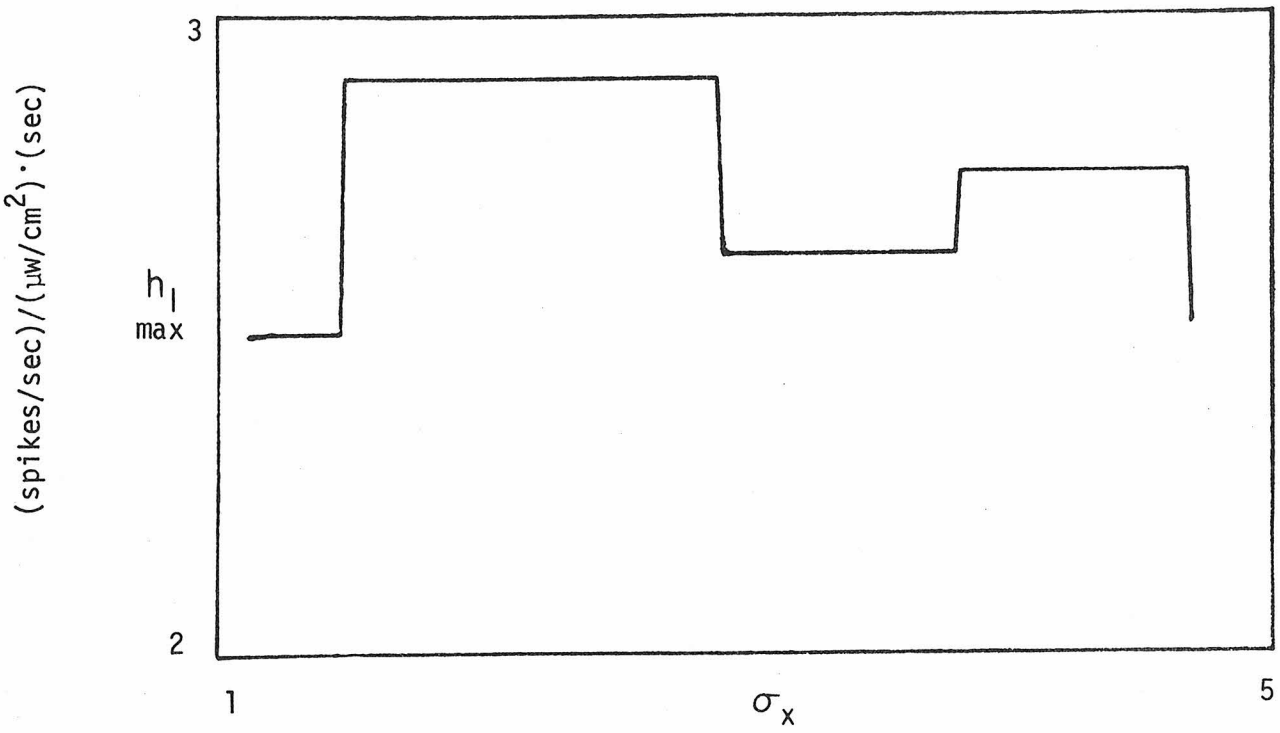

Fig. 4.3.4 $|h_1(\tau)|$ vs σ_{noise}

undergoes an excursion of about 13% for the range $\sigma_x = 1$ through $\sigma_x = 5$. (More often than not, however, the results of such an experiment were not that clear). Hence, it appears that 038 is adequately described by a set of first- and second-order Wiener kernels despite mean square errors indicating otherwise. (Note: P. Marmarelis (1972) obtained 20% mse's for spike data that had been low-pass filtered after it had been spike-density transformed.)

From h_1 and h_2 some global aspects of 038's functional organization begin to materialize. First, a scaled horizontal cut of h_2 (at $\tau_2 = .05$ seconds) overlaid on h_1 (scaled) reveals identical dynamics in the two kernels (Figure 4.3.1). This suggests that single channels within 038's excitatory field can be conceptualized initially as being composed of a linear system (described by h_1), followed by some form of zero-memory nonlinearity (ZNL; cf. Figure 4.3.5) (Caughey, 1975; McCann, et al, 1976). Similar results and conclusions were reached by McCann and Wiersma (unpublished) from kernels computed from full field excitation of 038.

The time course of h_1 (Figure 4.3.1) appears to follow that of a damped sinusoid of the form $e^{-at} \sin bt$. The period of h_1 can be directly measured from the spacing between its zero crossings (approximately 65 msec), yielding 7.7 hertz; fitting by eye yields a = 15, so that h_1 may be approximated by the function

$$h_1^*(t) = e^{-15t} \sin(48.38t) \qquad (4.3.1)$$

Figure 4.3.1 shows h* overlaid on h_1 (but shifted 20 msec to compensate

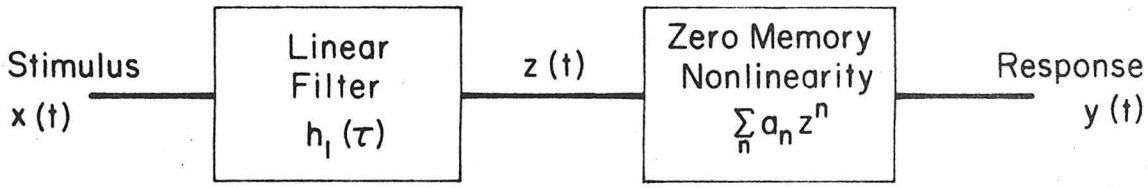

Fig. 4.3.5 Linear System - Zero Memory Nonlinearity (ZNL) Cascade

for the latter's latency). That, however, is for a kernel computed for an experiment performed at 12:00 hours. Kernels computed for experiments performed between 20:00 and 04:00 hours in the midst of the animal's active period are faster and less damped with approximations of the form

$$h_1^*(t) = e^{-35t} \sin(69.81t) \qquad (4.3.2)$$

Figure 4.3.6 shows h_1 and horizontal and vertical cuts of h_2. These kernels are highly reproducible as the kernels of Figures 4.3.6 reflecting experiments performed at one month intervals attest (although the relative amplitudes between kernels may vary, indicating individual differences in sensitivity among the animals).

These Wiener kernels can now be used to predict 038's response to sine wave data: Figure 4.3.7 shows the (h_1+h_2) model response to a 3 hertz signal compared against 10 superimposed responses of 038's actual spike response to such data. Obviously a half-wave rectifier is being simulated at 3 hertz. Interestingly, when a 1 hertz signal is passed through the kernels, the predicted output is nearly a sine wave, flattened sufficiently to show an effect by h_2. The important point is that the kernel accurately mimics the broad (nearly) linear response of 038 at 1 hertz.

The output of 038's kernel models can be passed into an IPFM whose threshold can be adjusted so that a spike train output is produced with the same general timing characteristics of 038's. The 3 hertz data passed through an IPFM are shown in Figure 4.3.7.

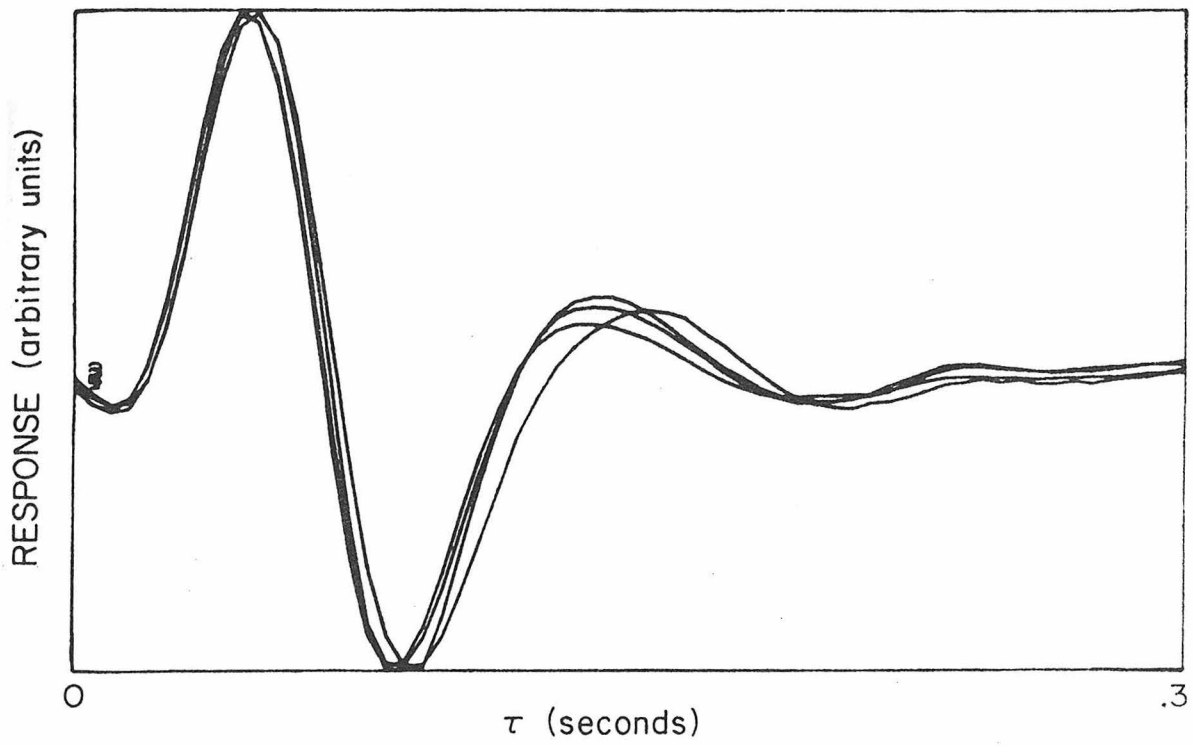

Fig. 4.3.6 038's (Night Kernels) - see text.

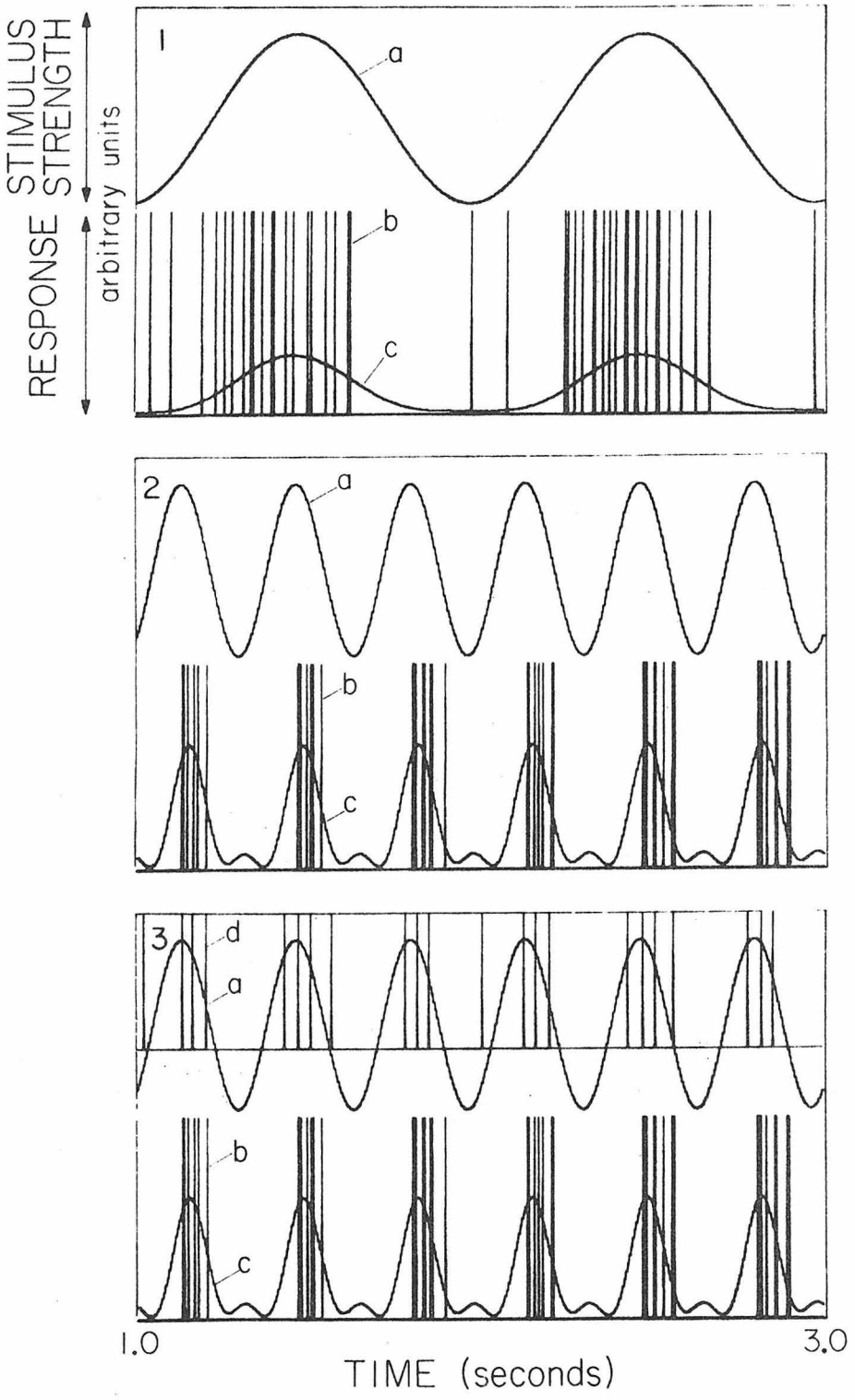

Fig. 4.3.7 Sine Waves: 038's response, b, and (h_1+h_2) kernel predictions, c. 1) a = 1 Hz; 2) a = 3 Hz; 3) a = 3 Hz, d = output of IPFM fed by kernel prediction, c.

These kernels confirm the conjectures developed in Section 4.1:

1) nonlinear, frequency dependent, behavior in 038;
2) significant second-order kernels exist--both h_1 and h_2 have initial excitatory dynamics followed by inhibitory dynamics;
3) the kernels' dynamics die after approximately 200 msec;
4) the peak response in the first order kernel occurs between 54 and 70 msec;
5) the inhibitory phase begins at about 86 milliseconds.

4.4 038 Field Plots

For the multi-spot experiments in later chapters it will be necessary to stimulate 038 in regions of equisensitivity for the reasons outlined in Section 1.2.

Equisensitivity curves for 038's field are "easily", if laboriously, compiled from the maximum amplitude of first-order kernels computed at various locations within 038's receptive field. For each of 20 animals, approximately 30 points were stimulated along horizontal and vertical axes of 038's field. Each set of kernels was normalized with respect to the maximum value of h_1 (found in that experimental sequence) which invariably was located at an ommatidium 2 to 3 columns (i.e., ommatidia) away from the rim (Figure 4.4.1). This is seen in Figure 4.4.1 as the long vertical strip running along 038's rim boundary. Sensitivity, as measured by $\max_{\tau}|h_1(\tau)|$ fell by about 20% every 2-3 ommatidia cuts for points A and B on Figure 4.4.2. 038's hot spot fan may be identified from dorso-posterior cuts along Figure 4.4.2 (i.e., max sensitivity = 1).

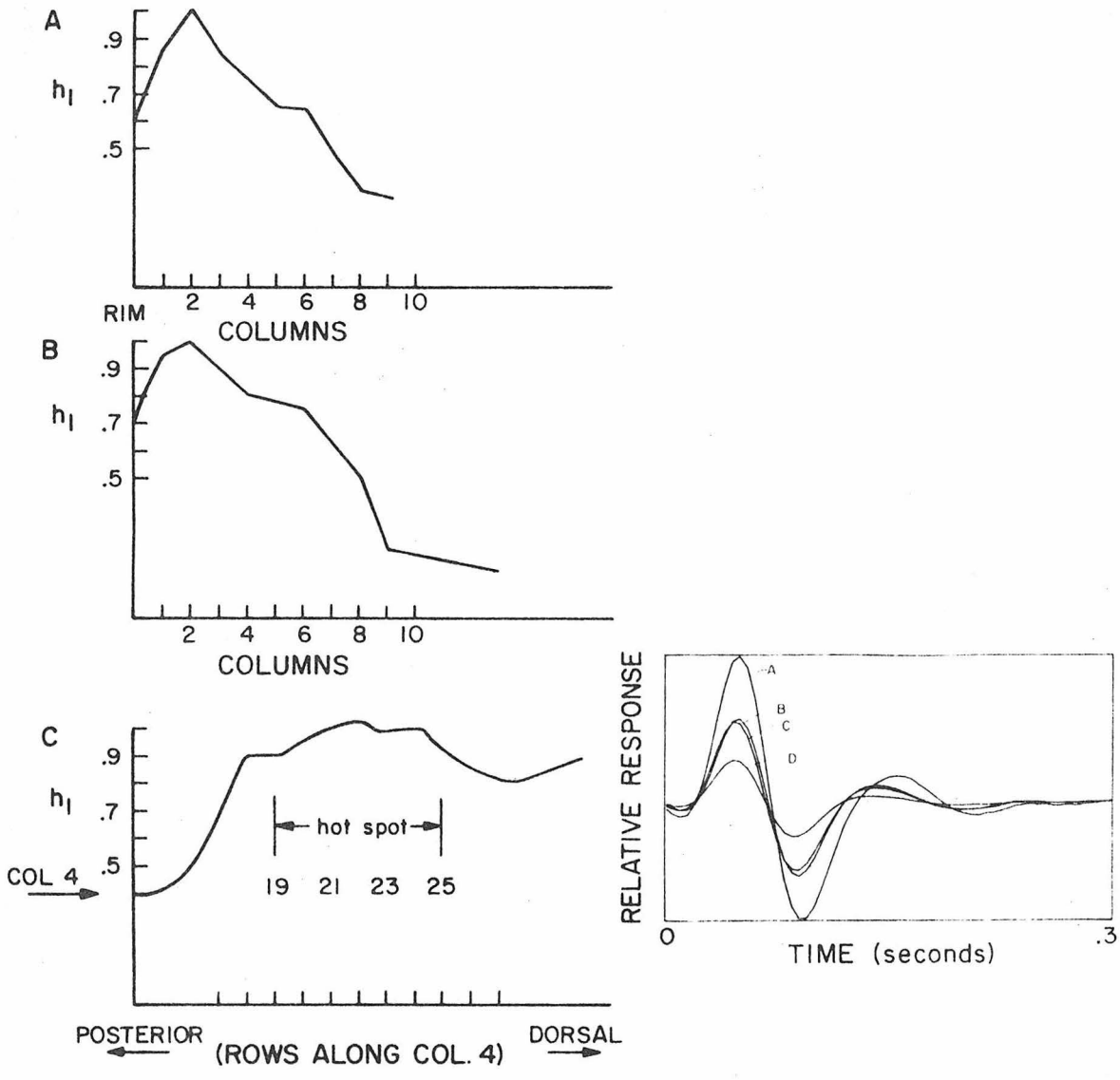

Fig. 4.4.1 038 Field Plots. A) Through row 16; B) through row 6; C) through hot spot along column 4.
Insert: h_1 for row 6, column 2(A), 6(B), 8(C), 16(D).

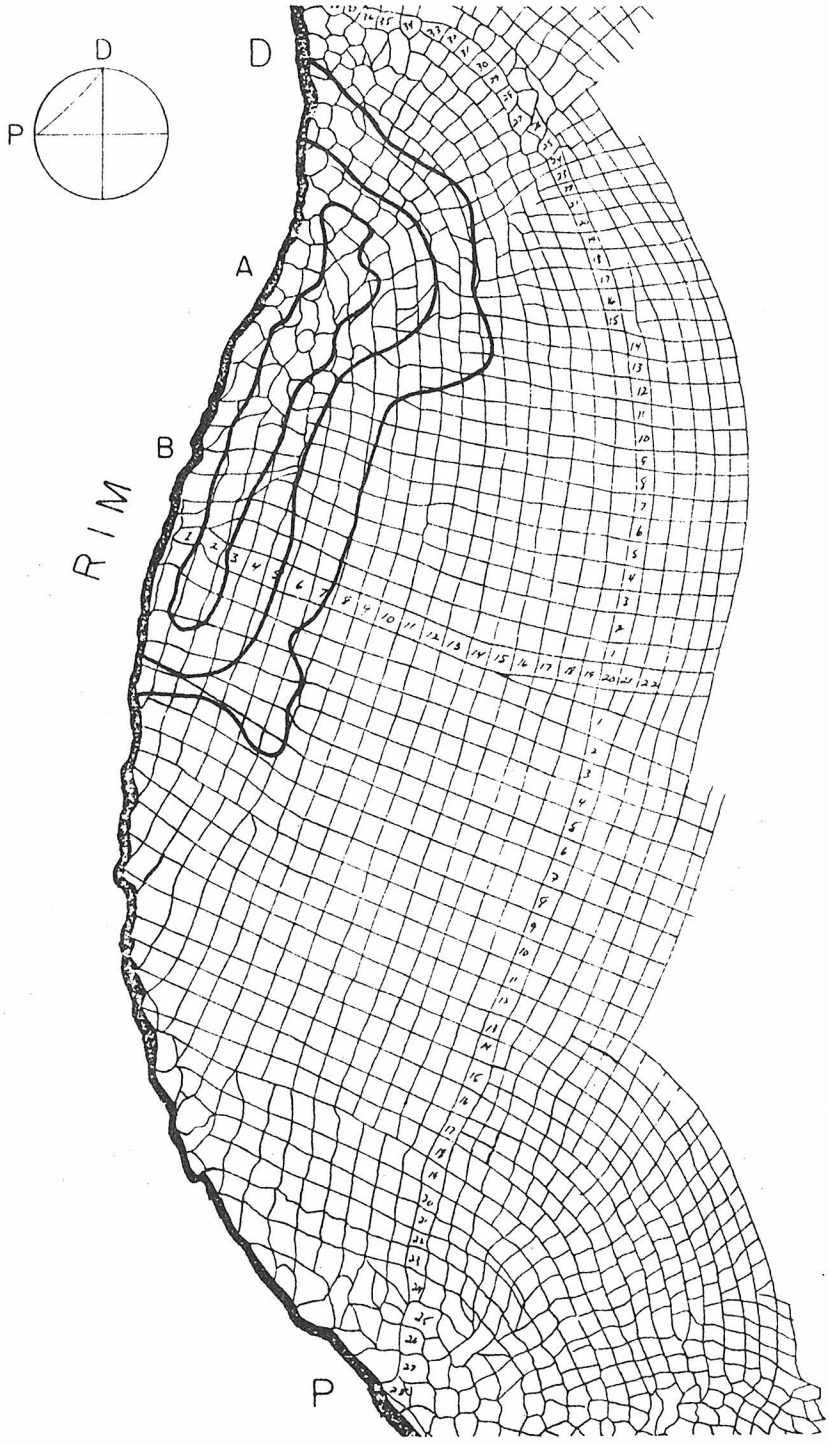

Fig. 4.4.2 Field Map of 038

This appears near the indentation which is the famous landmark for 038. The hot spot consists of approximately 10-15 ommatidia and is used by experimentalists to identify 038. The dorso-posterior cut along column 4 (see Chapter 2 for notation) identifies the hot spot as being located at approximately column 4, rows 19-23. From Figure 4.4.1 we can identify an area of maximum equisensitivity for 038 (.9-1.0) as being columns 3-5, rows 19-25 (approximately 21 ommatidia), or if we define it as 0.8-1.0, then the area becomes columns 1-4, rows 19-25 (i.e., about 30 ommatidia). The inset in Figure 4.4.1 shows typical kernels computed for column 4, rows 18(A), 8(B), 4(C), and -2(D) (taken from Sheby & McCann, 1976).

The general contours of dorso-posterior and rim-to-center-of-eye cuts reveal profiles very similar to those found by Woodcock and Goldsmith (1973) in their study of spectral sensitivities in sustaining fibers.

4.5 Models of 038's Dynamics

Despite the fact that 038 has been directly studied in nearly every investigation of crayfish sustaining fibers, few models of the mechanisms underlying its temporal dynamics have evolved. Most studies have been satisfied with substantiating Wiersma and Yamaguichi's (1967, 1968) observations of 038's exponentially decaying response to step functions of light, and the inhibitory interactions between points lying outside and inside of 038's excitatory field (e.g., Arechiga & Yanagisawa, 1973). Along the latter's lines, Yamaguichi and Ohtsuka (1973) have presented a model of a connectivity scheme to explain their

observations of mutual antagonistic interactions between sustaining and dimming fibers, but have not attempted to model any of the system's dynamics.

Glantz (1971) simultaneously recorded the responses of a sustaining fiber and a retinular cell to a 20-second stimulus, and concluded that the two systems were ac-coupled as a result of the former's faster peak rise time and subsequent decay (to one-half peak value) compared with the latter's. As a result of this observation, and the sustaining fibers' "preferred directional" response to sinusoidal stimuli (Section 4.2; Gordon, 1975), Gordon (1975) developed a "nonlinear" model of the "general to time-varying light intensity within its excitatory field." Gordon's model is depicted in Figure 4.5.1. It consists of two summed input channels. Channel 1, containing a differentiator and an integrator, collectively referred to as $H_1(s)$ (cf. Figure 4.5.1) extracts information proportional to changes in the input stimulus. Channel 2 extracts information about the present level of illumination. The outputs of both channels sum into a common linear element, $H_2(s)$, whose output feeds into a half-wave rectifier (with breakpoint X_θ), which in turn is cascaded with an IPFM. The output of the IPFM is converted into instantaneous frequency.

Gordon's motivation in constructing the model was to formulate a network capable of: 1) compensating for the "slower" photoreceptor dynamics reported by Glantz (1971); and 2) responding to the instantaneous value of illumination (or photoreceptor activity). By appropriate manipulation of the parameters τ_1, τ_2, G_1 and G_2 in the collective linear

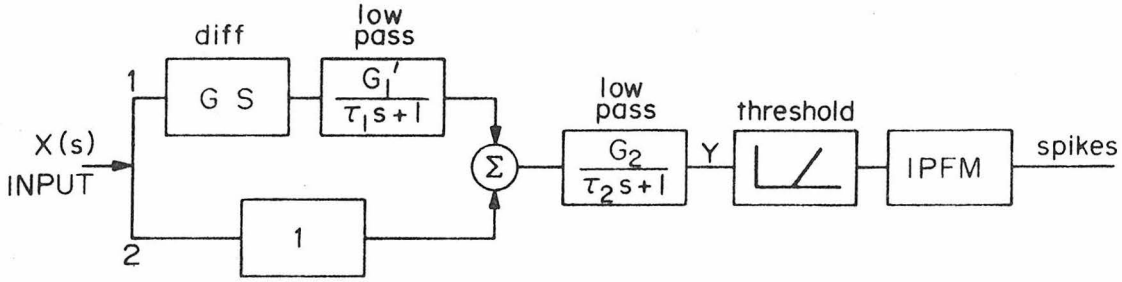

$$Y(s) = G_2\left[\frac{(G_1+\tau_1)\ s+1}{(\tau_1 s+1)(\tau_2 s+1)}\right]\left[X(s)\right]$$

$$G_1 \equiv G_o G_i$$

$$Y(s) = H(s)\ X(s)$$

GORDON'S (1975) MODEL FOR THE CRAYFISH SUSTAINING FIBERS

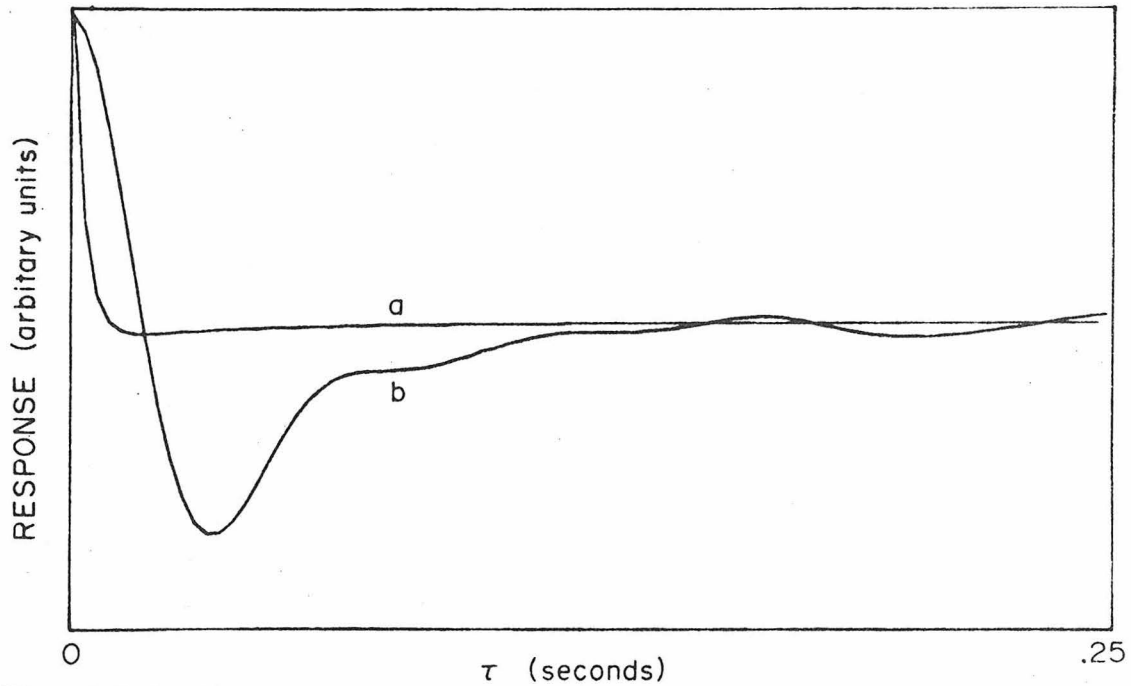

Fig. 4.5.1 (Upper) Gordon's (1975) Model for the Crayfish's Sustaining Fibers. (Lower:) Impulse Response (a) for G_1=.29,G_2=.33,τ_1=.003,τ_2=.04 (see text);(b) h_1 for the System.

filter H(s) (cf. Figure 4.5.1), Gordon was able to match his model's responses to the sustaining fibers' response to step changes and sinusoidal variations in intensity in the range .1-15 Hz. Each change in stimulus, however, required a change in parameter values capable of best fitting the sustaining fibers' actual responses; Gordon (1975) admitted that some undefined sustaining fiber dynamics had not been incorporated into his model. Gordon (1975) did not test the crayfish sustaining fibers with double pulse experiments, hence the only nonlinearity that he concerned himself with was the half-wave rectifier to extract the appropriately rectified responses to sinusoidal inputs.

Since Gordon's model is the only extensive analysis of the crayfish sustaining fiber 038 (and 014) outside of this work, a Volterra-Wiener kernel analysis of his model was performed to compare its behavior with the results of Section 4.3.

4.5.1 Gordon's Model

Two approaches were used to examine the properties of Gordon's model: The Volterra kernels of his model were computed directly; and a simulation of his model was compared with experimental results obtained from crayfish sustaining fibers.

H(s) in Figure 4.5.1 can be simplified to the form

$$H(s) = G(s+a)/(s^2+ \alpha s + \beta) \qquad (4.5.1)$$

which can be inverted directly (Roberts & Kaufman, 1966, p. 200) to yield an impulse response function of the form

$$h(t) = (G(a-r_1)\, e^{-r_1 t} - (a-r_2)\, e^{-r_L t})/(r_2-r_1) \qquad (4.5.2)$$

where $-r_1$ and $-r_2$ are roots of $s^2 + \alpha s + \beta = 0$, and

$$\begin{aligned} G &= G_2(G_1 + \tau_1)/(\tau_1\tau_2) \\ a &= 1/(G_1 + \tau_1) \\ \alpha &= (\tau_1 + \tau_2)/(\tau_1\tau_2) \\ \beta &= (\tau_1\tau_2)^{-1} \end{aligned} \qquad (4.5.3)$$

Incorporation of typical values for the various parameters (e.g., $G_1 = .29$, $G_2 = .33$, $\tau_1 = .003$, $\tau_2 = .04$: Gordon, 1975, p. 106) reduces $h(t)$ to

$$h(t) = 2.613(-.07\, e^{-25t} + 1.07\, e^{-333.33t}) \qquad (4.5.4)$$

which is plotted in Figure 4.5.1 (curve a). The characteristics of $h(t)$, determined primarily by the $e^{-r_1 t}$ term, resembles a delta function near the origin.

The parameters used in the threshold device were not explicitly stated, but from Figure 4.5.1 we may assume it to be of the form

$$\begin{aligned} f(x) &= x - x_\theta && x \geq x_\theta \\ &= 0 && x < x_\theta \end{aligned} \qquad (4.5.5)$$

in which case the Volterra kernels for $f(x)$ can be found by expanding in some interval $[-b,b]$ $(b > x_\theta)$ into a power series expansion of any degree. i.e.,

$$f(x) = \sum_{n=0}^{N} a_n x^n \qquad (4.5.6)$$

Then f(x) will have Volterra kernels $f_n(\tau_1,\cdots,\tau_n)$ of the form (Bedrosian & Rice, 1973)

$$f_n(\tau_1,\cdots,\tau_n) = a_n\ \delta(\tau_1)\cdots\delta(\tau_n)$$

Cascading the threshold device (which is a zero memory nonlinearity) with h(t) yields an amplitude scaled version of h(t) as the first order kernel of the cascaded system (Smith, 1966, p. 22).

Probing H(s) with the band-limited white noise used in crayfish experiments is equivalent to cascading a low pass filter in front of Gordon's model: the first order Volterra kernel for such a cascaded system will have greater memory than that of h(t). Direct cross-correlation of input with output yields the first-order kernel shown in Figure 4.5.1 (curve b).

These two tests demonstrate that the theoretical and computed first-order kernel for Gordon's model do not match those experimentally extracted for 038 in Section 4.3, nor do they match any of the requirements set by the double pulse experiments.

If h(t) was of the form described by equation 4.5.4, then the Wiener technique would have detected it; such systems have been identified in spike generating networks (in the guitarfish semicircular canal) by O'Leary and Honrubia (1976). Hence, it appears that Gordon's network has not modeled the full range of dynamics of the sustaining fiber's system. More will be said about Gordon's model in Chapter 8.

4.6 Conclusion

The first- and second-order kernels identified in Section 4.3 accurately model the dynamics of the individual channels comprising 038's field. These channels' dynamics appear to be homogenous throughout the field (Figure 4.4.1) but their gains are different.

Although Gordon's model for 038 does not reveal the dynamics and nonlinearities identified in this chapter, his idea, based on Glantz's (1971) data, of 038 as ac-coupled to the retinula cells is very interesting. McCann, et al (1976) have already described (insect) retinula cells as linear-ZNL cascades which operate in a much higher frequency band than does 038. Perhaps, then, something else is cascaded between the retinula cells and 038, but the details of this will be deferred until Chapter 8, where a model for 038's functional microstructure is presented.

Chapter 5

TWO-INPUT WHITE NOISE TESTS

5.1 Introduction

5.1.1 Limitation of Conventional Stimuli for Studying Lateral Interactions in Visual Systems

Chapters 1 and 3 discussed the use and identification of cross kernels used for classifying lateral interactions within visual systems. But misinterpretations can arise about the characteristics of a cross kernel of a lateral interaction when conventional stimuli consisting of pulses or steps of illumination are employed to extract information about lateral interactions.

If lateral interaction phenomena could be simply described by scalar coefficients, K_{ij}, of the type used by Hartline and Ratliff (1961) for describing the relative strength of interactions between channels i and j in a system, then pulse and step stimuli would be able to identify the interaction's characteristics. Barlow and Lange (1974), however, demonstrated that in Limulus each channel's susceptibility to interaction from another channel was a function of its own activity. To describe such a mechanism requires at least a second order cross kernel. The complete identification of the kernel would not be possible by simultaneous presentations of pulses to both channels; only the main diagonal of the kernel would be extracted. Full identification would require presentations of pulses on both channels separated in time by τ seconds (for all $\tau = \tau_1 - \tau_2$ and $\tau = \tau_2 - \tau_1$, since in general $h_{ij} \neq h_{ji}$) to identify the diagonals. Stimulating both channels $h_{ij}(\tau_1, \tau_2)$ with a constant

illumination k would result in an interaction phenomenon of the form

$$k^2 \int_0^\infty \int h_{ij}(\tau_1, \tau_2) d\tau_1 d\tau_2 \qquad (5.1.1)$$

Equation 5.1.1 clearly shows that different manifestations of the kernel can arise depending on the stimulus used.

5.1.2 The Lateral Interactions Subserving 038's Excitatory Field

Two types of lateral interaction appear to subserve the sustaining fibers of the crayfish. The first is an inhibitory interaction that any eye region outside of a fiber's excitatory field appears to exert on the excitatory field. For example, 038's response to a (.6 mm diameter) spot of light positioned within its excitatory field can be inhibited by a second spot positioned at the opposite (i.e., ventral-anterior) pole of the eye (Wiersma & Yamaguichi, 1967).

The second form of interaction appears to be excitatory and manifests itself when two 200 micron spots are simultaneously presented to the excitatory field. In that case, for example, 038's response is an "excitatory summation" (Wiersma & Yamaguichi, 1967) of the two stimulated areas. However, when one of the stimuli is ceased, the sustaining fiber experiences a brief inhibition in its response to the remaining stimulus (Wiersma & Yamaguichi, 1967).

Glantz (1973) has raised the possibility that lateral inhibitory interactions may subserve the sustaining fibers' excitatory fields. Glantz (1973) compared the relative response of large field sustaining fibers (e.g., 01 and 022) to small diameter stimuli (i.e., 1.85°, 3.9°,

6.9°, 9.4°, and 11.9°: an ommatidium's diameter = 1.85° (Glantz, 1973)) as a function of stimulus intensity. Different R-log I curves were found for the very small diameter stimuli: however, the curves for the 8.6° and 14° stimuli superimposed on each other. Glantz (1973) suggested that this phenomenon was arising from either a lateral inhibitory interaction within the excitatory field; or from the 14.6° stimulus exceeding the diameter of the sustaining fiber's most sensitive region in the field. Glantz discounted the latter because of the large field sizes of the sustaining units used. He postulated that a lateral inhibitory network within the sustaining fiber's excitatory field was responsible for his observations.

Additional support for this hypothesis was provided by summation-response experiments of the type described in Section 1.2 in which Glantz (1973) found an inhibitory effect (i.e., $\Delta < 0$) whenever $R_1 + R_2$ was less than 40 spikes/second.

Recently Glantz (Glantz & Nudelman, 1976; Nudelman & Glantz, 1977) has invoked some very indirect evidence for lateral inhibition within the sustaining fibers (including 038's) excitatory field. In the presence of high intensity illumination (i.e., 10^2-10^3 times threshold (.3-4 mw/cm^2) the crayfish's sustaining fibers rhythmically discharge (burst) independent of the light's intensity and the fiber's mean firing rate (Glantz & Nudelman, 1976). By examining the autocorrelation of single and cross correlation between simultaneously recorded pairs of rhythmically bursting sustaining fibers, Glantz and Nudelman (1976) have noticed that the burst cycle among all studied sustaining fibers is

approximately the same (within 2%) with an average natural frequency (for 14 sustaining fibers) of 7.35 Hz; and that the sustaining fibers burst in approximate synchrony. From these observations Glantz and Nudelman (1976) concluded that the entire population of sustaining fibers are driven by a common presynaptic inhibitory network. To explain the bursting phenomena and to support their hypothesis they invoked the theoretical work of Coleman and Renninger (1974) which predicted the ability of a recurrent network of lateral inhibition (of the type found among Limulus' eccentric cells) to support, in the presence of steady high illumination, cycles of stable bursting and alternating quiescent periods of activity. Nudelman and Glantz (1977) envisioned the crayfish sustaining fibers as being driven by such a recurrent lateral inhibitory network.

According to the Coleman-Renninger (1974) model, the burst duration of Limulus' eccentric cells should equal the system's inhibitory delay. These parameters were measured in the crayfish and found to be 10-15 msec and 6-17 msec, respectively (Glantz & Nudelman, 1976). The close agreement of times was interpreted as indirect evidence for the correctness of the inhibitory network hypothesis.

If such lateral interactions do exist, then their effect (inhibitory or otherwise) should be captured by the cross kernels computed from multi-input white noise experiments.

5.2 Two-Input White Noise Tests: Lateral Excitation in 038's Excitatory Field

Figure 5.2.1.1 shows segments of the two independent Gaussian (25 hertz band limited) "white" noise used to excite two ommatidia within

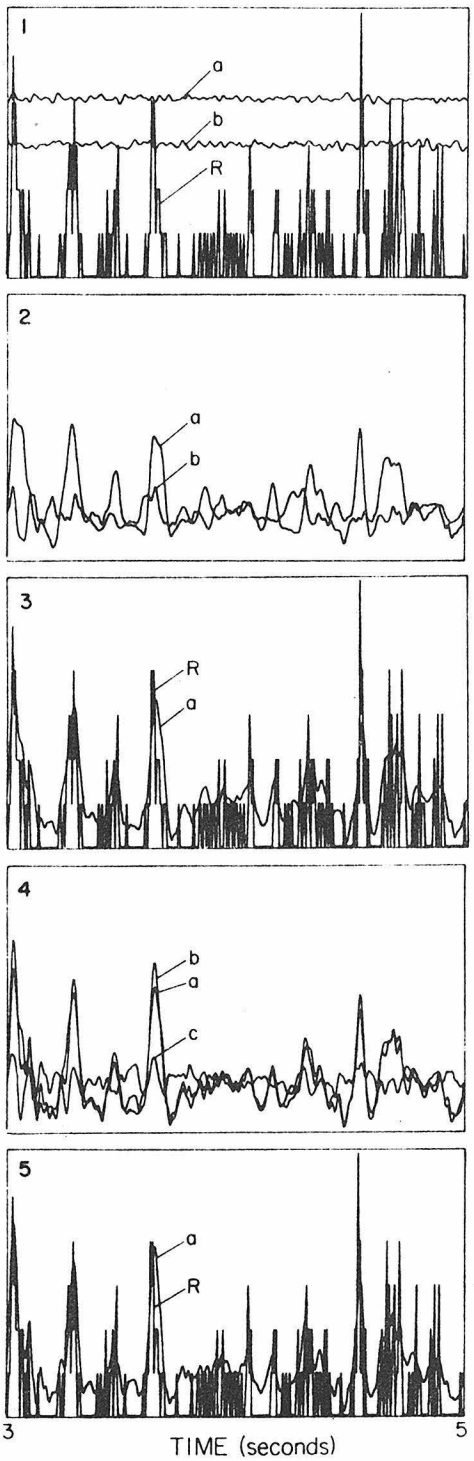

Fig. 5.2.1 Two-Input White Noise Test.
1) 038's Response,R, to stimuli a and b;2)combined 1st-,and 2nd-,order Model Responsees for Stimuli a and b; 3) 038 (R) vs. sum of a and b in (2); 4) a as in (3), c= 2nd order cross term contribution, b=a+c; 5) a=combined first and second order models for two channels + cross term. (See Text.)

038's excitatory field (column 4, rows 21 and 25 and 038's binned response to the simultaneous presentation of the two stimuli.

For each of the ommatidial channels (denoted as i and j) first- and second-order self Wiener kernels were computed (i.e., $h_{1j}(i)$, $h_{2j}(i)$, $h_{1i}(j)$, $h_{2i}(j)$). The self kernels resembled those of Chapter 4, depending on the time of the experiment. In addition, the cross kernel h_{2ij} was computed.

For each of the channels a combined first- and second-order model response was computed from its kernels; the two predicted responses are shown in Figure 5.2.1.2. Comparison with 038's response reveals that neither model matches 038's response completely, although at times one or the other of the channels appears to be the major contributor to 038's response.

To predict 038's response to both stimuli, however, dictates that the model responses of both combined first- and second-order channel models have to be summed to get a complete (self kernel) model of 038. The result of that summation is shown in Figure 5.2.1.3 in which the model's excellent prediction of 038's actual response is immediately seen. The mean square error of the model at this point is 57.3%; individually each channel model had a mean square error of approximately 82.7%.

The two-input model is, however, incomplete without the contribution from the cross kernel h_{2ij}. Figure 5.2.2 shows a contour of h_{2ij} and immediately it is noticed how symmetric the kernel is. The symmetric cross kernel implies that the two points within 038's excitatory field

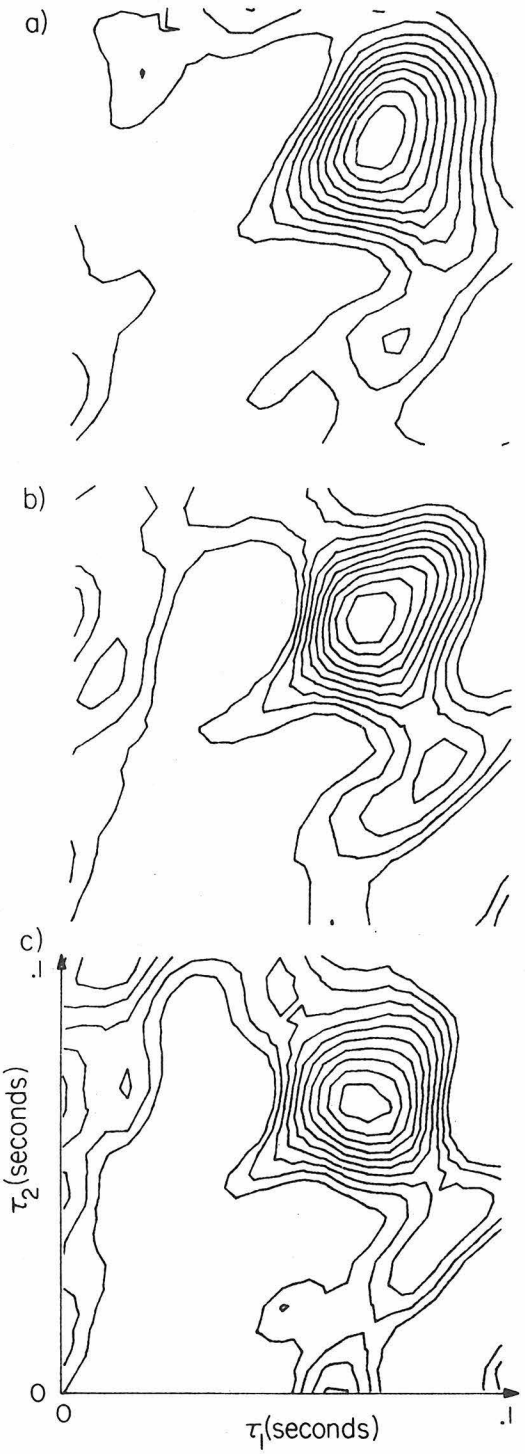

Fig. 5.2.2 "Hotspot" Cross Kernels as a Function of Inter-Ommatidial Distance: a) 150 Microns; b) 400 Microns; c) 600 Microns

act on each other with mutual strength and dynamics. There is, for example, no preferred direction of motion sensitivity in this part of the receptive field.

A cut through this cross kernel reflects another interesting property: it overlays the dynamics of h_1 and those of h_2 (see Chapter 8).

The computed model response for h_{2ij} is shown in Figure 5.3.1.4c Adding this to the modal response of Figure 5.2.1.3 yields the total second order model shown in Figure 5.2.1.5 with a mean square error of 51.1%, thus increasing the accuracy by about 3%.

Comparisons of Figures 5.2.1.3 and 5.2.1.5 show that the primary contribution of the cross kernel is an excitatory effect at the points of peak responses in 038's actual spike train and self kernel model. Little hint of a lateral inhibitory phenomenon is manifested in the contribution of h_{2ij}; this is not to say that lateral inhibition does not reside within 038's excitatory field, but that it is not manifested in the behavior of h_{2ij}.

5.3 The Extent of Lateral Interactions within 038's Excitatory Field

The strength and extent of lateral interactions underlying 038's behavior can easily be identified by varying the position and distance between the optic fibers introducing white noise stimuli onto 038's excitatory field. "Strength" of the interaction can easily be extracted by simply observing the maximum amplitude of h_{2ij} as a function of interommatidial distance. Such a field diagram for 038's hot spot is depicted in Figure 5.3.1. However, the advantage of computing h_{2ij} is

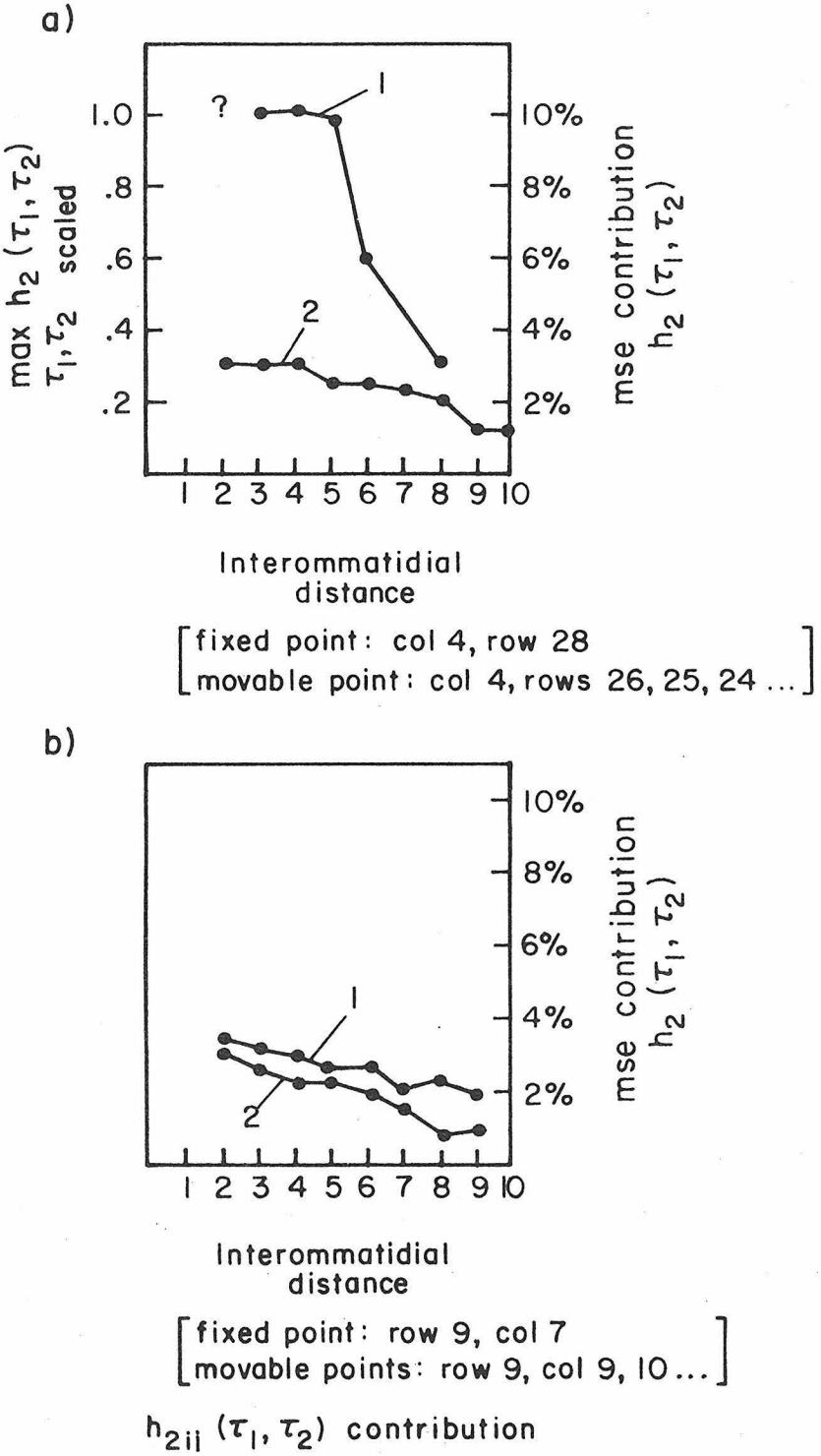

Fig. 5.3.1 Field Strength of 038's Lateral (2nd-Order) Interactions

that one can "see" the dynamics of h_{2ij} as the interommatidial distance changes. Figure 5.2.2 displays such kernel contours and reveals a surprising consistency in the kernels' dynamics for 500 microns. At 650 microns the amplitude of the kernel appears to be diminished. The functional utility of these kernels can also be computed as a function of interommatidial distance by simply computing h_{2ij}'s relative mean square error for the appropriate kernel's models. Figure 5.3.1 shows the averaged mean square errors for the "hot spots" of 10 different 038 units--over 7 ommatidia the relative contribution of h_{2ij} appears to be approximately 2-3%.

Outside 038's "hot spot" the cross kernels become markedly asymmetric. Figure 5.3.2 shows a set of kernels taken through a horizontal cut across 038's excitatory field (i.e., row 4, columns 3-10); Figure 5.3.3 shows a similar result taken across a vertical slice of the field (column 15, rows 1-21). For such asymmetric kernels a maximum amplitude may not occur at the same point in time. Hence, only mean square error can be used to measure the functionality (i.e., strength) of these cross kernels. Figure 5.3.1 shows that in both directions these cross kernels also contribute about 3% to a 2-input white noise test.

For stimuli presented within two ommatidia of each other, the resulting cross kernels take on an extremely symmetrical characteristic. This is probably due to light scattering of the type described by Shaw (1969). Because these (3 ommatidial distant) cross kernels are contaminated with each channel's second order kernels (cf. Chapter 5 of Koblasz (1976)), their maximum amplitude and mean square error are not compared with other cross kernels of Figure 5.3.1.

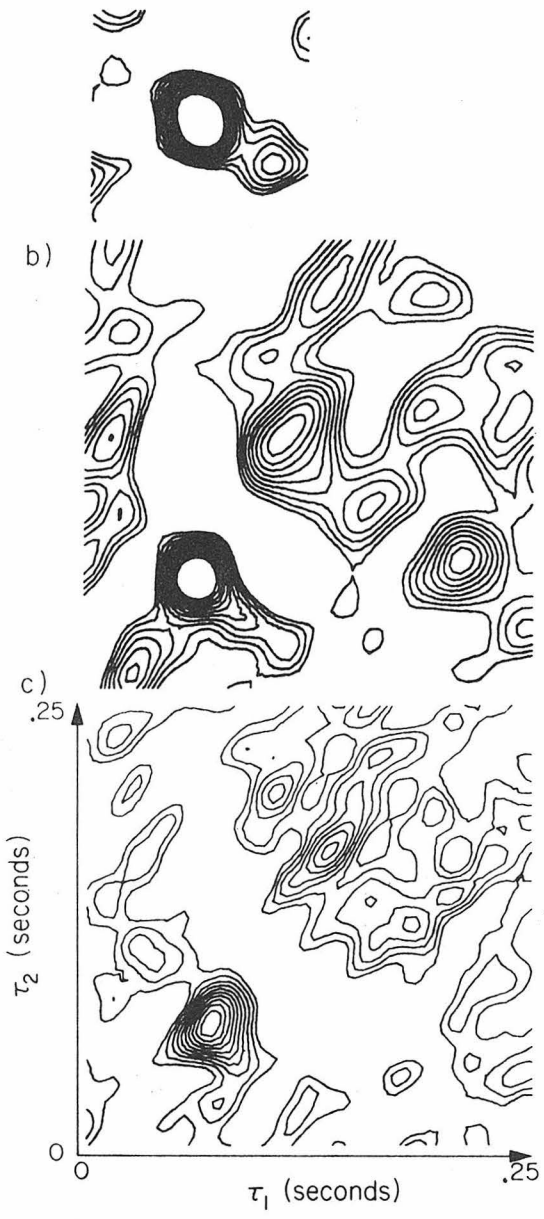

Fig. 5.3.2 Cross Kernels (See Text)

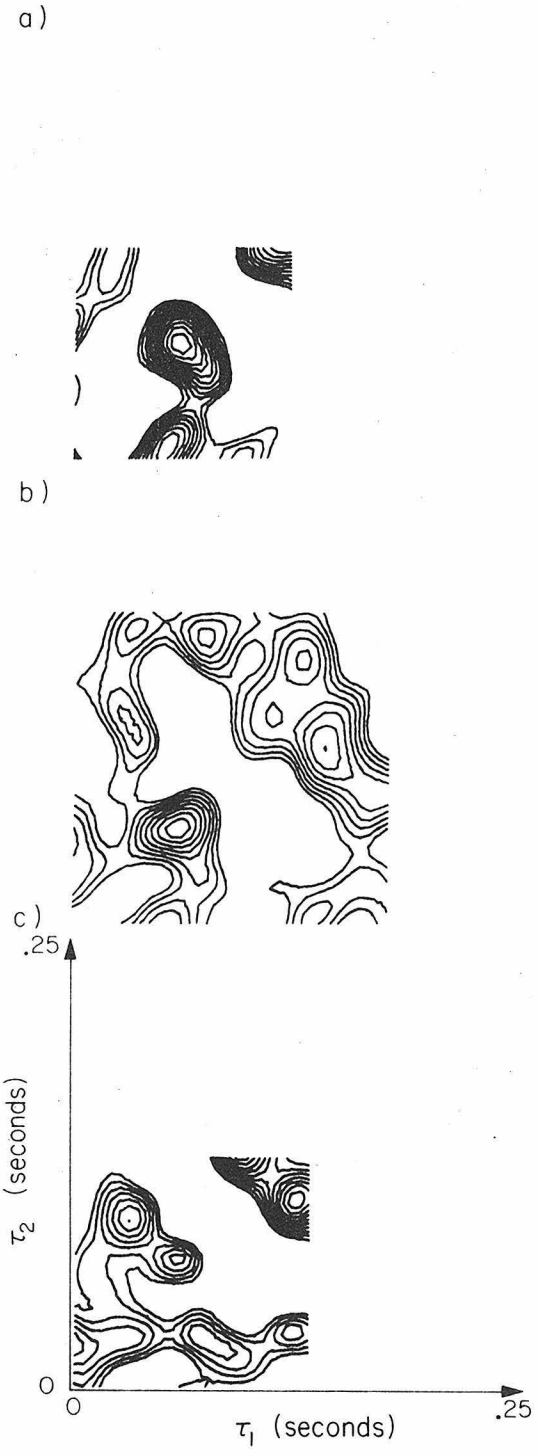

Fig. 5.3.3 Cross Kernels (See Text)

5.4 Higher-Order Lateral Interactions within 038's Excitatory Field?

Although the above results do not negate the presence of lateral inhibition within 038's excitatory field, they appear to eliminate its appearance in second cross kernels.

An interesting phenomenon does occur in the 2-spot tests that suggests that higher order Volterra kernels, e.g., g_{iij} or g_{jji} may exist within 038's excitatory field which might possibly subserve a lateral inhibitory interaction mechanism: the first order kernels $h_{1i(j)}$ and $h_{1j(i)}$ consistently are of smaller amplitude than are the first order kernels computed for the channels in one input tests (Figure 5.4.1). As discussed in Chapter 3, this result can only originate from underlying higher order (odd) interaction processes: increases in light flux increase first order kernel amplitude--not decrease it (Figure 5.4.1).

5.5 Conclusions

Definitive conclusions for this chapter will be postponed until the results of Chapter 7's multi-spot experiments are presented.

Chapter 6

BLUE CHANNELS AND 038

6.1 Introduction

That the crayfish visual system has two photopigments makes it a candidate for possessing color vision. Optokinetic experiments recording the crayfish eye's tracking of red and blue stripes in a rotating drum have been interpreted to suggest a color discrimination ability (Olivo, et al, 1975). Color vision, in turn, would suggest a more active role for blue channels in crayfish than has been documented to date, although the neural circuitry for it need not manifest itself in the sustaining fibers.

That a blue channel into 038 may exist has not been disputed; but its functional significance is a matter of continued concern for understanding the sustaining fiber's field microstructure considering its predominant yellow sensitivity. This is particularly so in view of Woodcock and Goldsmith's (1973) puzzling finding of a greater, however slight, blue sensitivity in dorsal eye regions because of 038's field location along the dorso-posterior rim. While past studies have examined 038's response to either blue or red light alone (cf. Section 2.1), none have looked for interactions that might exist between two color channels leading into it.

Such interactions can be studied with two independently (Gaussian white noise) modulated monochromatic light sources directed onto 038's field. A duel channel incandescent/xenon arc lamp configuration (Figure

6.1.1) (described by McCann, et al (1976)) was used to produce (parallel) beams of monochromatic blue (463 nm) and red (600 nm) light, respectively, onto a common 1 cm^2 circular region. A crayfish was positioned in this field so that 038's field intercepted the beams; all but a narrow rim region of the studied eye (columns 10 and beyond, intact rows 5-33) was blackened to prevent excitation of 038's inhibitory field, and to facilitate comparisons with optic fiber tests. The entire contralateral eye was also blackened. Both beams were independently calibrated to have mean intensities of $.3 \times 10^{-6}$ watts/cm^2. 600 nm was chosen to minimally excite any blue channels (cf. Figure 5 in Wald (1968)); excitation of the "yellow channels" by 463 nm is unavoidable due to the photoreceptors' sensitivity (cf. Section 2.1).

6.2 Two-Color Input Tests

6.2.1 Single Pulse Responses

As a first step in identifying the characteristics of any blue channel into 038, a regime of one hundred 1-millisecond duration pulses of 463 nm wavelength light (with peak intensities of .3 $\mu w/cm^2$), with 5-sec interpulse intervals, was presented to five different eyes that had been dark-adapted for 3-4 hours. After the 463 nm presentation, the eyes were dark adapted for 30 minutes, and an identical regime of 600 nm pulses was presented to the same eye region. Figure 6.2.1a shows a typical averaged response of 038 to each of the stimulus regimes.

The immediately noticed difference in the two responses is the longer latency secondary smaller background spike train present in the

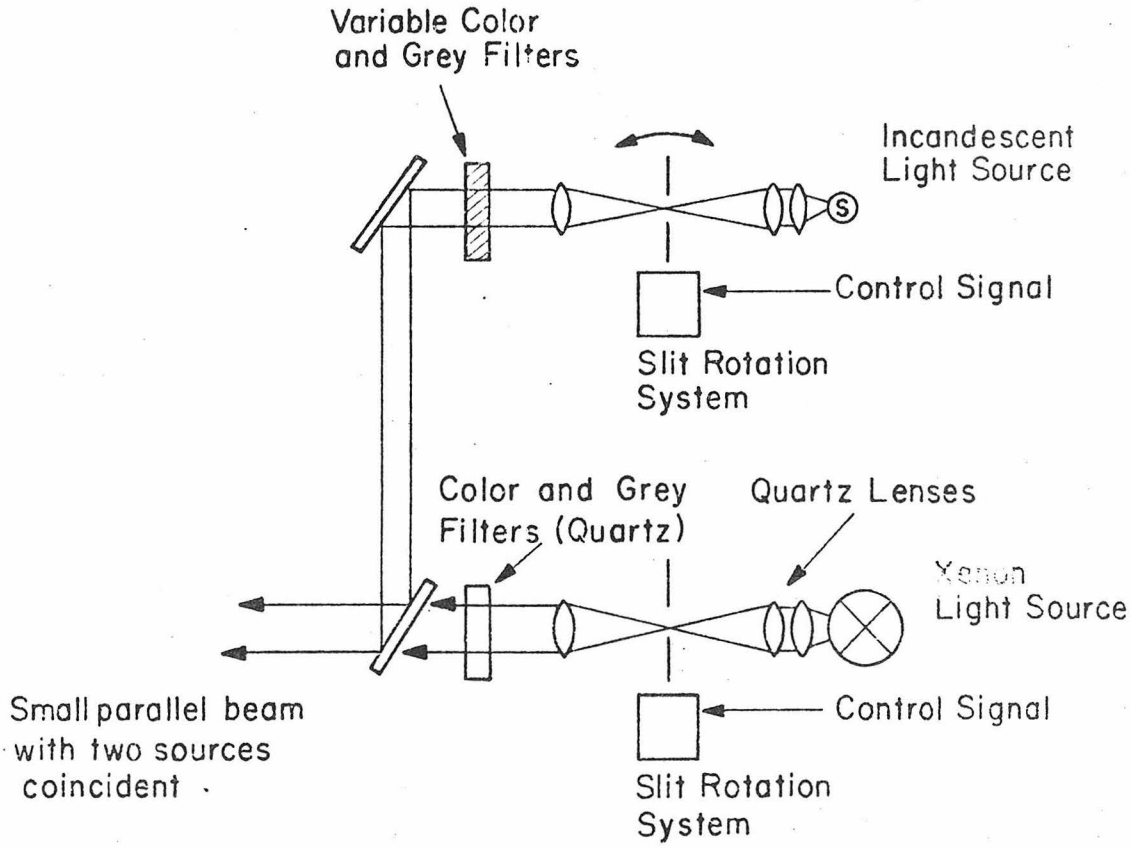

Fig. 6.1.1 Stimulus Configuration for Full Field Two-Color Tests.

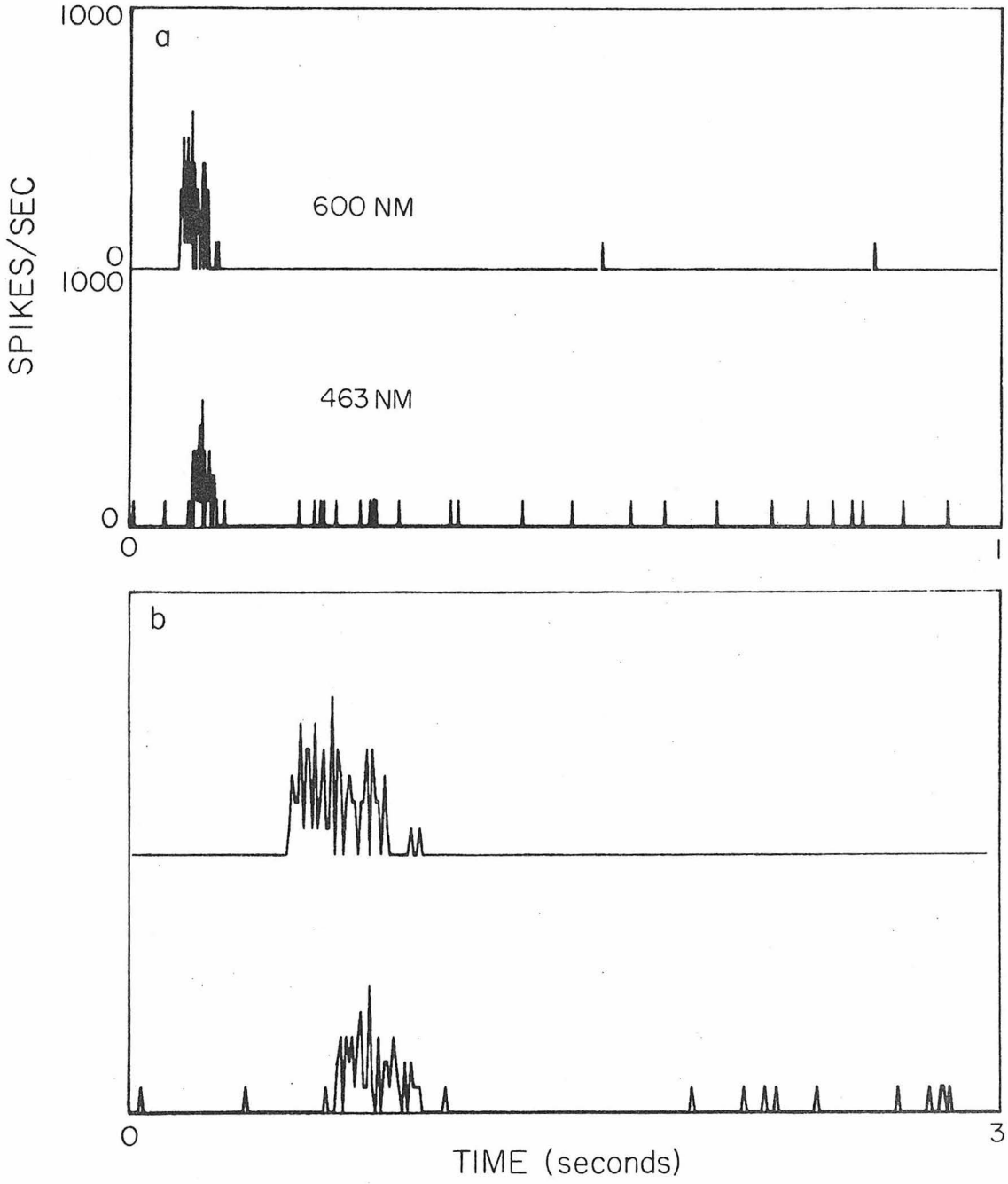

Fig. 6.2.1 038's Averaged Response to 100 1 msec. Presentations of 600 nm and 463 nm Light. Upper Scale : 1 second. Lower Scale: .3 seconds.

blue response, but absent in 038's red response. Figure 6.2.1b reveals the finer structure of the two responses.

The latency of the 463 nm response is 70.5 msec and the secondary response begins another 70 msec after that. The 600 nm response has a latency of 50 msec and is about 20% greater in amplitude (i.e., spike count) than the blue response. Other than the blue response's longer latency there appear to be no major discernible differences in the dynamics of the two impulse responses.

No differences of the type observed by Trevino and Larimer (1970, their Figure 1;cf. Chapter 2) could be seen in responses obtained from identical pulse regimes presented to several eyes that had been (selectively) chromatically adapted (for 1 hour) to 463 nm or 600 nm light. This may be due to an insufficient strength of the adaptation stimulus: Trevino and Larimer's (1970) adapting stimuli (e.g., 660 nm at 3.2×10^{-3} w/cm^2) were approximately 4 log units more intense than the maximum used here (3×10^{-7} w/cm^2).

If functional differences exist between blue and yellow channels feeding into 038, they should, hopefully, be detected in Wiener kernels computed from 1- and 2-color input "white" noise experiments.

6.2.2 Wiener Kernels: 1- and 2-Color Inputs (Whole Field Tests)

For comparison with the pulse results, the same animals of the preceding section's tests were again dark adapted for 1 hour, after which time the yellow channel was tested with the 600 nm source, driven by the noise sources of Chapter 2. First and second order kernels h_{1r}

and h_{2r} were computed from 038's response to the 600 ηm noise excitation. 038's presumed "blue" input channel was then excited with the 463 ηm source alone, driven by another, but independent, noise signal, and kernels h_{1b} and h_{2b} were computed from the response.

038's response to simultaneous presentation of independently modulated 463 ηm and 600 ηm sources resulted in kernel pairs $h_{1r(b)}$ and $h_{2r(b)}$, and $h_{1b(r)}$ and $h_{2b(r)}$, computed for the "channels" underlying 038's yellow and blue related responses, respectively.

Figure 6.2.2 compares the kernels h_{1r} (curve 1) and h_{1b} (curve 2). Two differences are immediately noticeable: h_{1r}'s greater amplitude and h_{1b}'s greater latency. Slight differences also appear to exist in the kernels' envelopes.

Figure 6.2.3 presents the results of the 2-color input test: there is a distinct kernel $h_{1r(b)}$ indicative of a red (i.e., yellow) channel, but the blue-dependent $h_{1b(r)}$ appears to have disappeared! Initially, it appears as if 038 has responded only to the 600 ηm stimulus; the blue stimulus appears to have had no input into (i.e., effect on) 038.

To check the effectiveness of the various kernels, the model responses for $h_{1r(b)}$, $h_{2r(b)}$, $h_{1b(r)}$, and $h_{2b(r)}$, and the cross term h_{2rb} (indicative of any red-blue interchannel interactions) were computed with and without the dc response, h_0. Table 6.2.1 contains typical percent mean square errors computed for the various kernel models against 038's actual response.

Table 6.2.1 reveals that 038 is functionally responsive to two-color stimulation, but only to the red signal. The figure compares

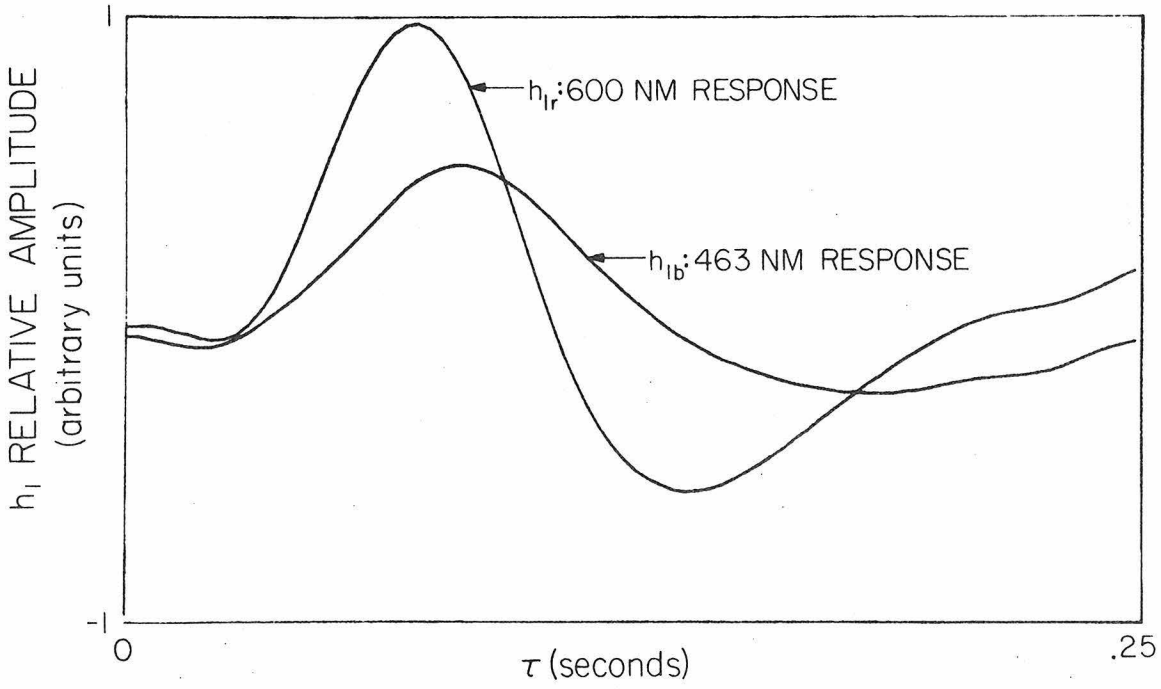

Fig. 6.2.2 h_1 for 038's Response to Monochromatic light: 600 nm; 463 nm

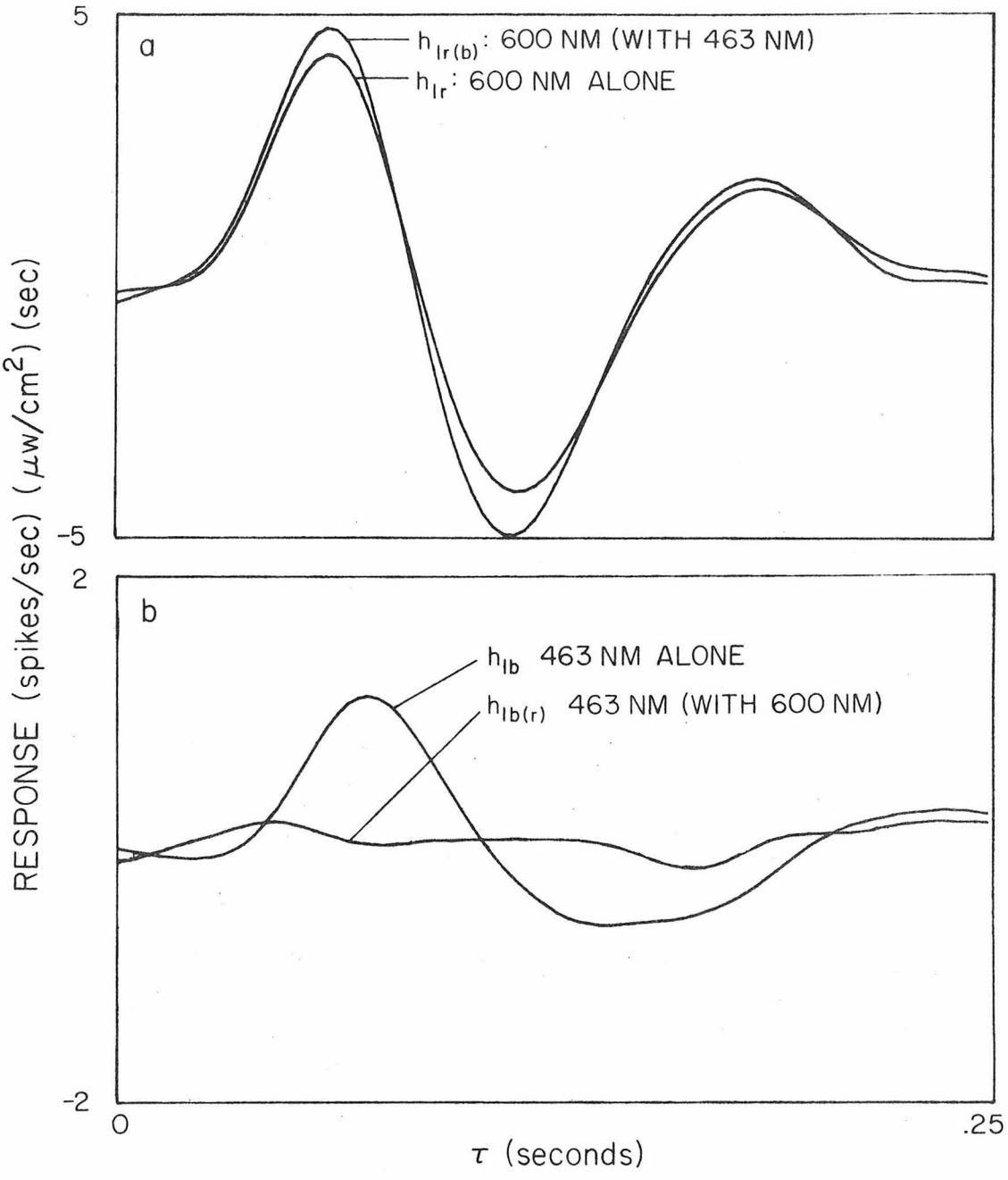

Fig. 6.2.3 First-Order Kernels for Two-Color Input Tests [Full Field].

Table 6.2.1

	Term	% mse
	$h_{1R(B)}$	97%
Ia:	$h_{1R(B)} + h_0$	88%
Ib:	$h_{2R(B)} + Ia$	69%
	$h_{1B(R)}$	98%
	$h_{1B(R)} + h_0$	98%
II:	$h_{2B(R)} + h_{1B(R)} + h_0$	97%
III:	$Ib + II - h_0$	74.2%
	h_{2RB}	93%
	$III + h_{2RB}$	76%

models Ib (yellow response) and II (blue response) (from Table 6.2.1) with 038's actual response. One or two possible interpretations are available for the data at this point: 1) that blue inputs to 038 are inhibited in the presence of yellow-channel excitation; or 2) that a strictly "red" response derived from the majority of yellow-sensitive receptors is "swamping" any blue contribution (Olivo, personal communication).

6.2.3 Wiener Kernels: 1- and 2-Color Inputs (Small Field Tests)

A variant of the above experiment was performed to take advantage of results in Chapter 5 to assist in discriminating between explanations for Section 6.2.2's results. Instead of simultaneous red and blue light excitation of the whole (excitatory) field, Chapter 5's optic fibers were used to bring independent blue and yellow light sources directly onto two ommatidia (separated by three ommatidia). Hence these experiments (5 animals) are identical in format to some of those of Chapter 5, except that one yellow LED (λ_{pk} = 583 nm) has been replaced by a GaN blue LED (λ_{pk} = 423 nm) (the mean intensity out of each fiber 30 $\mu w/cm^2$). As in the previous section, kernels were computed for: single-channel (i.e., ommatidium) yellow input, single-channel blue input, and combined 2-input (i.e., yellow and blue) excitation.

Figure 6.2.4 displays the resultant kernels; they match the results of the preceding section except for the minor differences that the dynamics of the two channels appear identical.

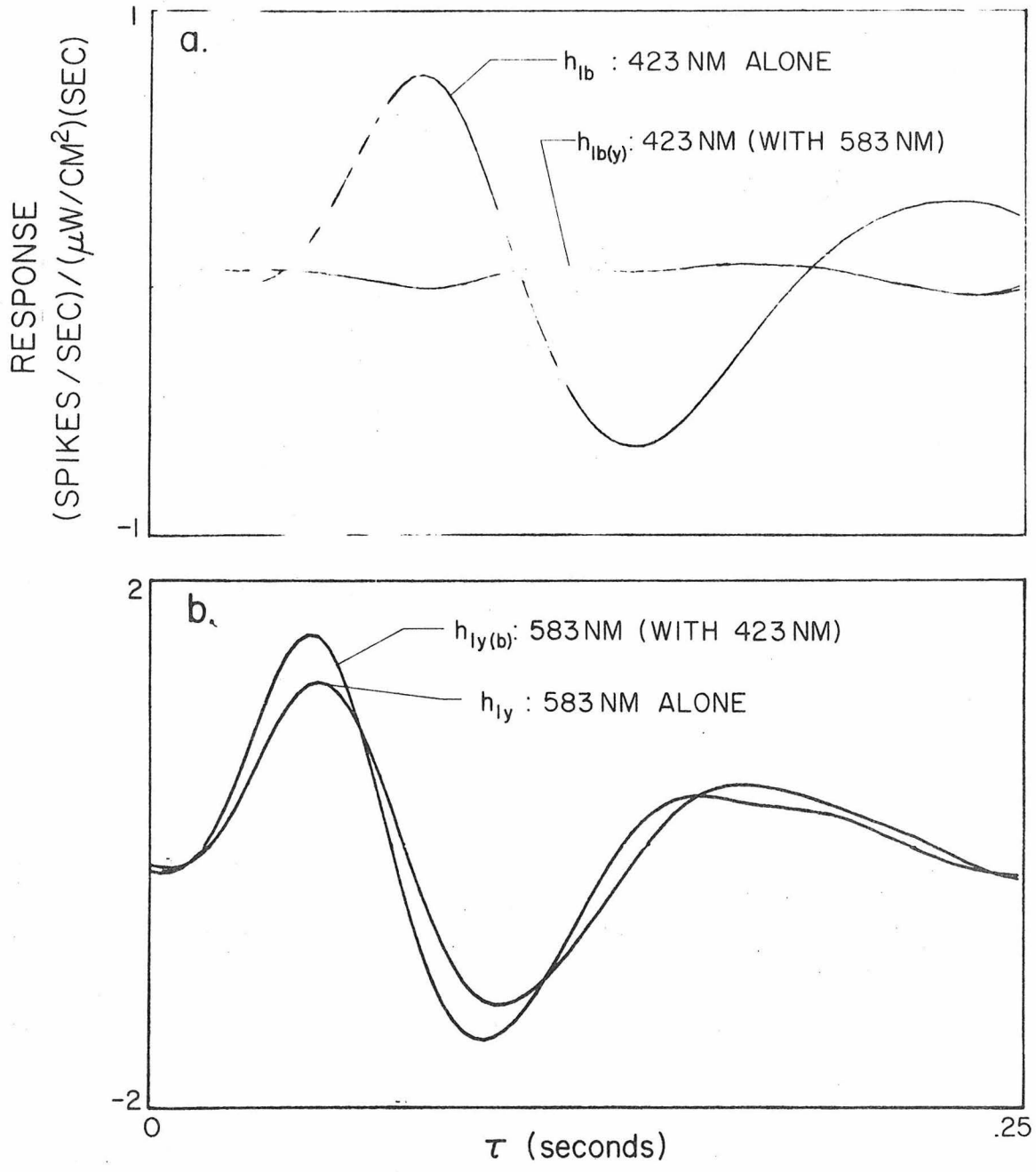

Fig. 6.2.4 Two-Color Input Tests (LEDs/Fiber Optics) 038's Response to 423 nm/583 nm Lights

6.3 Data Analyses

6.3.1 The "Swamping" Hypothesis

As a first step in interpreting the above results, assume that a "swamping" phenomenon is at work. Intuitively this would suggest that the (dark-adapted) system's response to excitation by monochromatic red or blue light should reflect the properties of the dominant majority yellow-sensitive photoreceptor population (which is sensitive to both "red" and "blue" wavelengths). Simultaneous excitation by red and blue light should, again, reflect only the overwhelming activity of the yellow receptors "swamping" any blue-channel response.

Such a conclusion, however, is inconsistent with the analytic prediction(s) of this model; to understand why, consider the system physiology depicted in Figure 6.3.1. A system S, composed of two populations of photoreceptors (yellow-sensitive [system Y] and blue-sensitive [system B]) pool their outputs into a simple summing point (038). System Y, the dominant system in the dark adapted eye (Wald, 1968) is sensitive to both 600 (or 583) nm light ($x_Y(t)$) and 463 (or 423) nm ($x_B(t)$) with relative sensitivities of a and b, respectively. (B's sensitivity coefficient to 463 nm, k, is extractable, for example, from Wald's (1968) Figure 5). Y has Volterra kernels h_{1Y} (and h_{2Y}); B's kernels are h_{1B} (and h_{2B}). No assumptions are made, as yet, concerning the equality between Y's and B's kernels of the same order. Assume, for the moment, that Y and B are linear (i.e., they do not possess second order kernels).

Excitation of system S with monochromatic 600 (or 583) nm light would excite sub-system Y only resulting, upon appropriate cross-

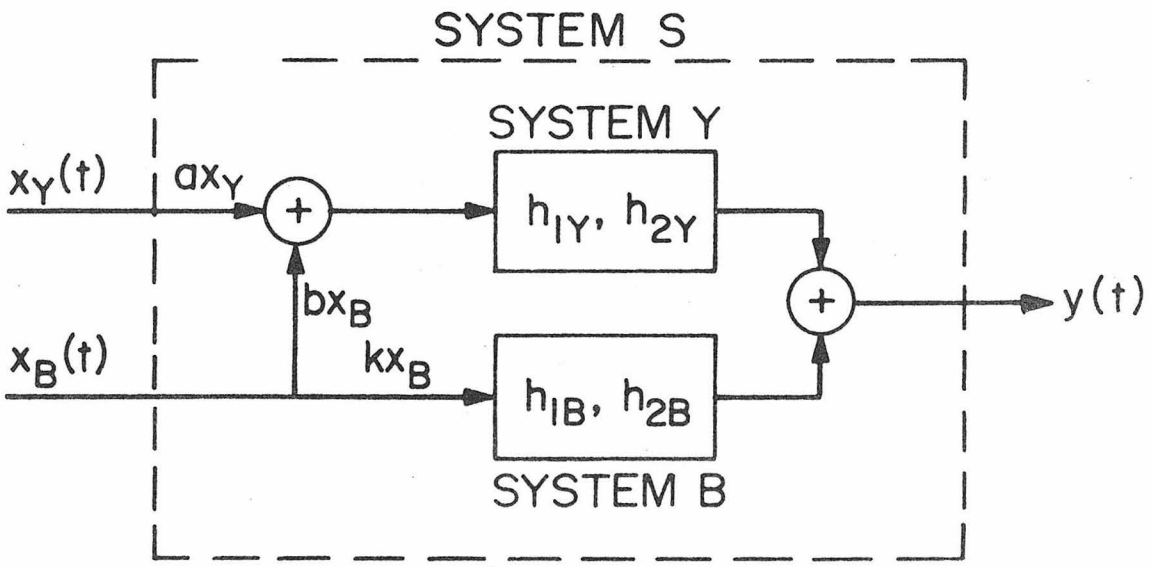

Fig. 6.3.1 System for Testing "Swamping Hypothesis". (See Text.)

correlation between the system response and x_Y, in a computed Wiener kernel $h_{1y}^{(S)}$ for S, reflecting its yellow sensitive channel. Monochromatic blue light excites both Y and B and results in a Wiener kernel $h_{1b}^{(S)}$. Simultaneous excitation with red and blue light results in kernels $h_{1y(b)}^{(S)}$ and $h_{1b(y)}^{(S)}$, reflecting the red and blue channels of S, respectively. Appropriate cross-correlations between input signals and system responses result in the relations:

$$h_{1y(b)}^{(S)} = h_{1y}^{(S)} = ah_{1Y} \tag{6.3.1}$$

and

$$h_{1b(y)}^{(S)} = h_{1b}^{(S)} = bh_{1Y} + kh_{1B} \tag{6.3.2}$$

If a swamping mechanism was at work, then equation 6.3.1 correctly predicts the Y-system's first order kernel. The kernel $h_{1b}^{(S)}$ would also reflect the yellow system's dominance if $k < b$. For the two-input experiments, however, the data unequivocally show that $h_{1b(y)}^{(S)}$ is unequal to h_{1B}; in fact, $h_{1b(y)}^{(S)}$ appears to be non-existent--a result unexpected and unacceptable for the swamping hypothesis!

The fact that second-order kernels have been observed in the above experiments, and that retinula cells are known to contain second-order nonlinearities (McCann, et al (1976)) suggests that second-order kernels be considered in the swamping model even though the second-order contribution is small. In that case the first-order Wiener kernels, $h_{1y(b)}^{(S)}$ and $h_{1b(y)}^{(S)}$ remain unchanged but now we have the second-order kernels:

$$h_{2y}^{(S)} = h_{2y(b)}^{(S)} = a^2h_{2Y} \tag{6.3.3}$$

and

$$h_{2b}^{(S)} = h_{2b(y)}^{(S)} = b^2 h_{2Y} + k^2 h_{2B} \qquad (6.3.4)$$

and a cross-kernel of the form

$$h_{2yb}^{(S)} = abh_{2Y} \qquad (6.3.5)$$

As before, swamping hypothesis predictions for monochromatic single-input experiments are upheld by the observed results, but for the 2-input test $h_{2b(y)}^{(S)}$ disappears, and more important, there is no sign of the cross kernel composed (entirely) of the dominant yellow receptors' second-order kernel h_{2Y}. [cf. Koblasz's (1976) Chapter 5 for related discussions about color cross kernels taken from human EEG analyses].

6.4 Miscellaneous Comments

If blue channel inhibition by yellow channels is what is witnessed, it would not necessarily conflict with the limited observations concerning color discrimination in the crayfish. First, it has not been established that 038 provides any input (major or minor) into the optokinetic response, hence the behavior of its color channels need not affect the outcome of such experiments. If 038 did provide an important input, then it might be possible that resultant phenomena from the inhibition (such as "blank" field portions indicative of blue objects) might be behaviorally relevant; hence, discrimination between red and blue stripes results in a response to red stripes separated by "blank" fields.

Recently, Olivo (unpublished, personal communication) has examined the spectral sensitivity of the crayfish's optokinetic response while

the rotating drum was flooded with a background red adapting light. Under these conditions the spectral sensitivity of the response demonstrated a peak in the blue (near 460 nm), which otherwise resembled the sensitivity curve for the dark-adapted crayfish ERG. The blue peak (presumably resulting from a depressed activity from red adapted yellow receptors) should not be expected if yellow channels in the entire visual system inhibited blue channels. Olivo's comments apply to my observations as well. If the described inhibition phenomenon is global, it might be possible that a strong background adaptation can sufficiently depress the yellow channels' inhibition so as to allow the blue channels to operate undisturbed.

Furthermore, it must be remembered that 038 is an area observed by Woodcock and Goldsmith (1973) to be particularly blue sensitive. Hence there is plenty of freedom for establishing the relative weighting of the coefficient k with respect to a and b (Figure 6.3.1) in developing any models (cf. Woodcock and Goldsmith's (1970) Figure 2) of crayfish color processing.

One phenomenon that is not observed in the kernels for blue-only excitation is the long after-discharge component seen in "blue" impulse responses (Trevino and Larimer's (1970) Figure 1). First and second-order Wiener kernels were computed for τ values up to 250 milliseconds without indications of the mechanism underlying the after-discharge. There is no explanation as yet for its absence.

An interesting observation is that the kernel dynamics of the small and large field experiments appear nearly identical except for a scaling factor.

6.5 Conclusion: Inhibition versus Swamping--An Additional Test

If 038's blue response is determined by the yellow-sensitive receptor population, then the 2-input fiber optic experiments eliminate "swamping" as an explanation for the above results. From values taken off spectral sensitivity curves for dark adapted isolated eyestalk preparation (Wald, 1968) the differences in the Y-system's sensitivities to 583 nm and 423 nm light is 0.6 log units (i.e., a fourfold difference).

A different type of two-input test was performed to determine if the differences in quantal absorption explained the above results. The sources feeding into the two fibers were both yellow LEDs, but they were driven with different bias currents such that a fourfold difference existed in their emitted intensities at their respective fiber exit apertures (50 $\mu w/cm^2$ and 12.5 $\mu w/cm^2$). The LEDs were driven by independent noise sources.

Figure 6.5.1 shows the kernels computed from the simultaneous presentation of the unmatched yellow intensities to 038. The kernels for each excited channel do not disappear, although they are unequal in amplitude due to the mismatched intensities exciting each channel.

Hence it appears that 038 is fed by a discrete blue channel that is inhibited by 038's input yellow channel (when both are simultaneously excited) although it is not clear from the available data, how or where this is done. Possible interactions that might lead to these results are explored in Chapter 8's model for 038's receptive field microstructure.

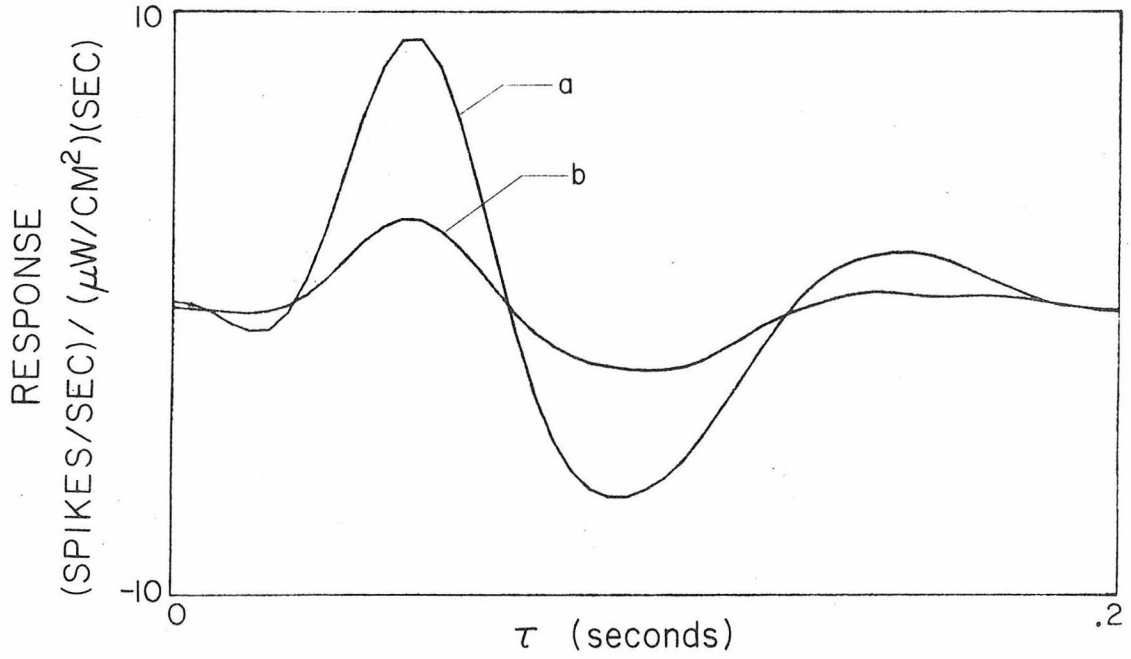

Fig. 6.5.1 Two-Input "Yellow" Experiment: First-Order Kernels Computed from a) 50 $\mu w/cm^2$ and b) 12.5 $\mu w/cm^2$ Output Fiber Intensities

Chapter 7

3-, 4-, AND MULTI-INPUT TESTS

7.1 Introduction

Most investigations on lateral interactions in visual systems have been limited to studying the interaction of, at most, two independently excited retinal regions. When three or more spots have been introduced to the eye, they have been modulated by a common source (e.g., Hartline, et al. (1961)), usually dc, and the underlying neural "dynamics" have been observed by noting gross changes in the optic nerve's firing pattern. The limitations of such a methodology have been discussed in Chapter 5. Recently, Von Seelen and Hoffman (1976) attempted to stimulate the cat's visual system with multiple random stimuli constructed from a Julesz random texture driven by a single Gaussian white noise source. This approach assures that the intensity seen, at any moment, by any point on the retina is "different" from that seen by any other point, but the problem with such an approach is that the time course of the signals is identical. Hence, each point source of white noise falling on the eye is merely a scalar variant of the noise falling on any other retinal area. Stimulation with such a common source makes computation of cross kernels impossible: Von Seelen and Hoffman (1976) were only able to compute (noisy) first order self kernels for single or small clusters of retinal points and to compare among them their kernels' amplitudes and dynamics (cf. Figures 10-13 in Van Seelen and Hoffman (1976)).

To compute cross kernels describing the interactions among multiple retinal channels it is necessary to drive each retinal area (channel)

with an independent Gaussian white noise stimulus. Such a capability is inherent with the LED/fiber optic stimulus package used throughout this thesis(cf. Figure 7.1.1).

7.2 Four Spot Stimuli--Symmetric Configurations

As a first step in studying the lateral interactions induced by a pattern incident upon the eye, four small stimulus spots arranged in a square configuration were presented to ommatidia at coordinates A = (2,27), B = (8,26), C = (2,21), and D = (7,12), such that each side of the square measured 5 ommatidial widths. Upon simultaneous excitation of all four ommatidia, four first order self kernels, four second order self kernels, and six second order cross kernels were computed from 038's response. A model response for each kernel was then computed and the predicted responses for all the first order kernels were summed together to form a single first order model. Similarly, the second order self and cross kernel models were summed together.

Figure 7.2.1a shows a one-second record of 038's binned response to simultaneous excitation by the four stimuli of Figure 7.1.1: the first order model (Figure 7.2.1b) reveals a poor ability to mimic 038's response. The mse for that model is 87.3%. The combined first and second order model (Figure 7.2.1c), however, shows a remarkable improvement in following 038's responses: all false firings have been eliminated and every burst from 038 is well represented in the model. The mean square error is reduced to 60.5%. The effect of the cross kernels is noted in Figure 7.2.1d. They narrow the width of the model's predicted peak firing pattern to more closely follow the time course of 038's

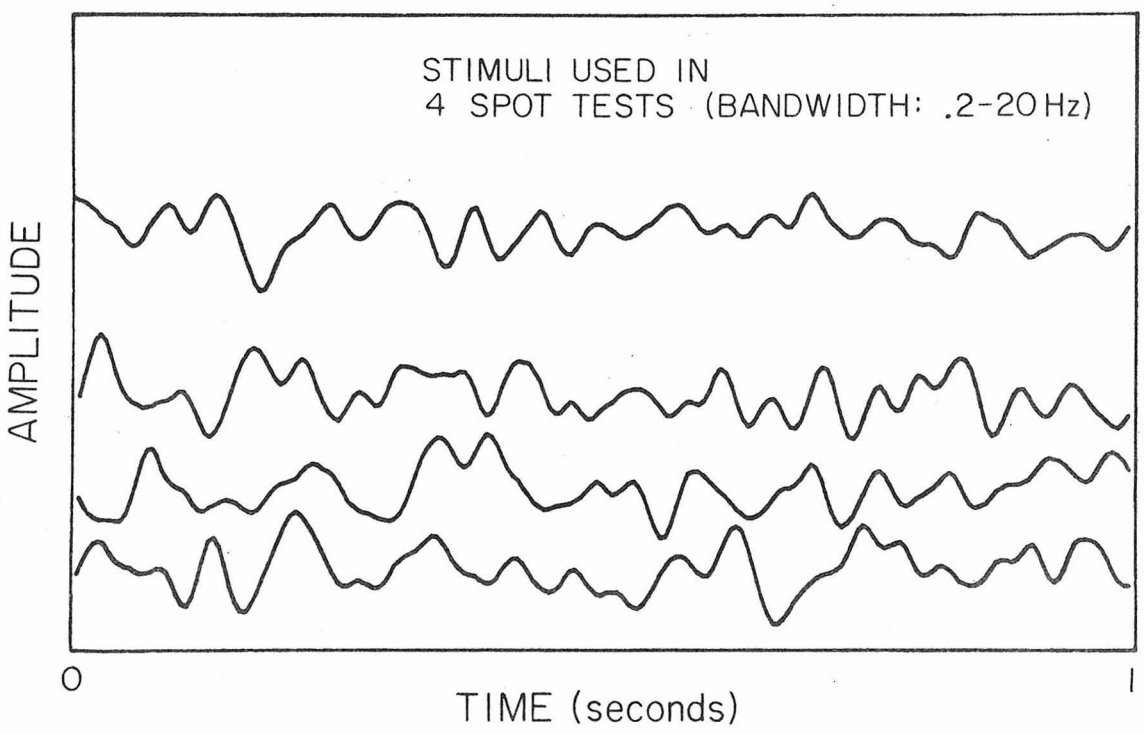

Fig. 7.1.1 Stimuli Used in 4-Input Tests

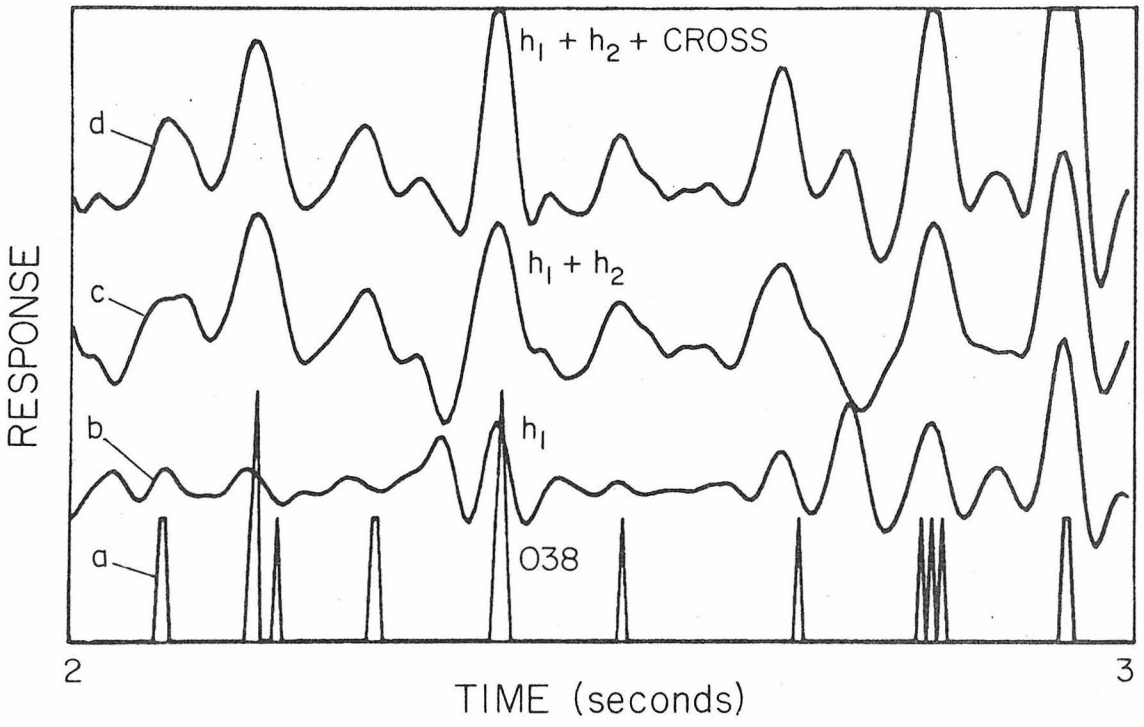

Fig. 7.2.1 4-Input Test. 038's Response (a) vs. Kernel Model Predictions: b) Σh_1, (4 Channels); c) $\Sigma(h_1+h_2)$ (4 Channels); d) $\Sigma(h_1+h_2)$ + 6 Cross Terms

bursts. The cross kernels greatly add to the amplitude of the response to match 038's peak activity as well as smooth the silent periods between bursts. The cross kernels also add 6.7% to the model's accuracy, thus bringing the total mse to 53.8%.

Figure 7.2.2 compares, with greater clarity, 038's response with the responses predicted by the: h_1; the h_1+h_2; and h_1+h_2+ cross kernel models. In fact an interesting observation is made in Figure 7.2.2: 038 appears to be firing in regular bursts at a rate of almost seven per second in the second order model without the cross kernels. A histogram of 038's interspike interval indicates this phenomenon (Figure 7.2.3a) by a minor peak at 120 msec (i.e., 8.3 Hz); however, an autocorrelation of 038's raw spike response to the four stimuli does not reveal any long term cyclic behavior. The power spectrum of 038's spike response, however, indicates a definite peak at 6.47 Hz (Figure 7.2.3).

The kernels underlying this behavior closely resemble those computed for 2-input tests. The six cross kernels representing the interactions between AB, AC, AD, CD, BD and BC are shown in Figures 7.2.4a-f. There appear to be no major differences among the amplitudes or shapes of these kernels except that the two sets of diagonal kernels (AD and BC) appear to undershoot slightly more than the remaining "edge kernels". The standard deviation for a typical cross kernel is shown in Figure 7.2.5. The second order kernels for each spot resemble the cross kernels--a typical kernel is shown in Figure 7.2.5. Interestingly, the dynamics of the first order kernels match those of the second order self

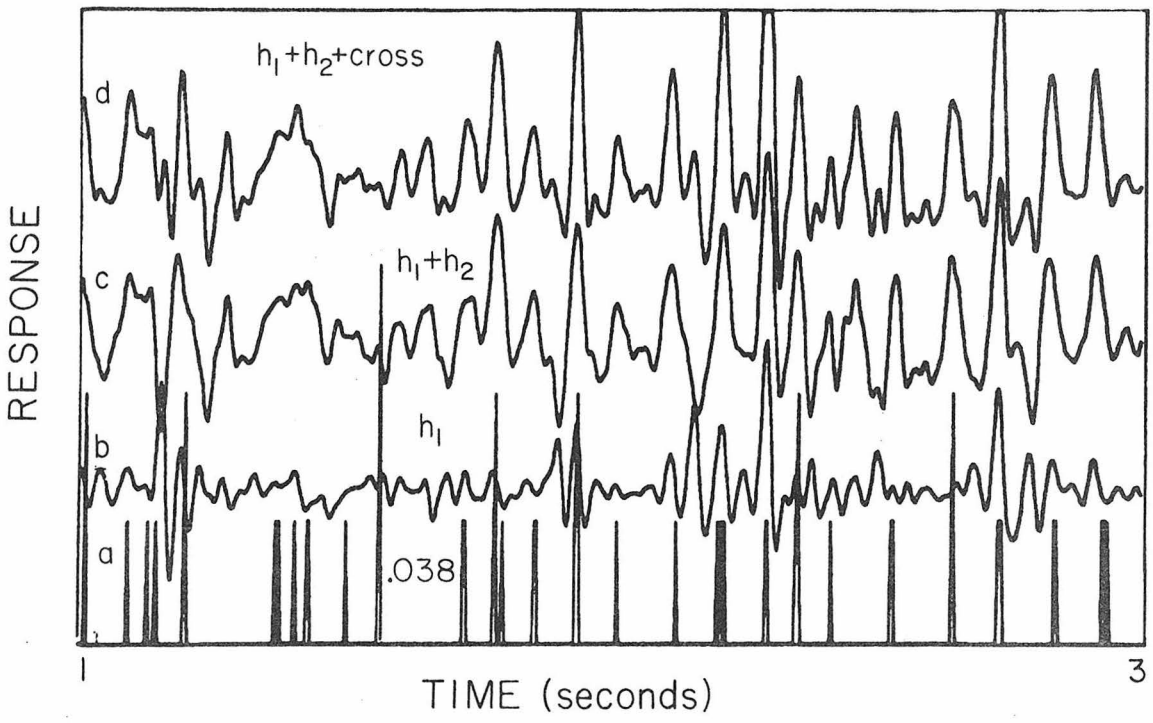

Fig. 7.2.2 4-Input Test. 038's Response (a) vs. Kernel Model Predictions: b) Σh_1, (4 Channels); c) $\Sigma(h_1+h_2)$ (4 Channels); d) $\Sigma(h_1+h_2)$ + 6 Cross Terms

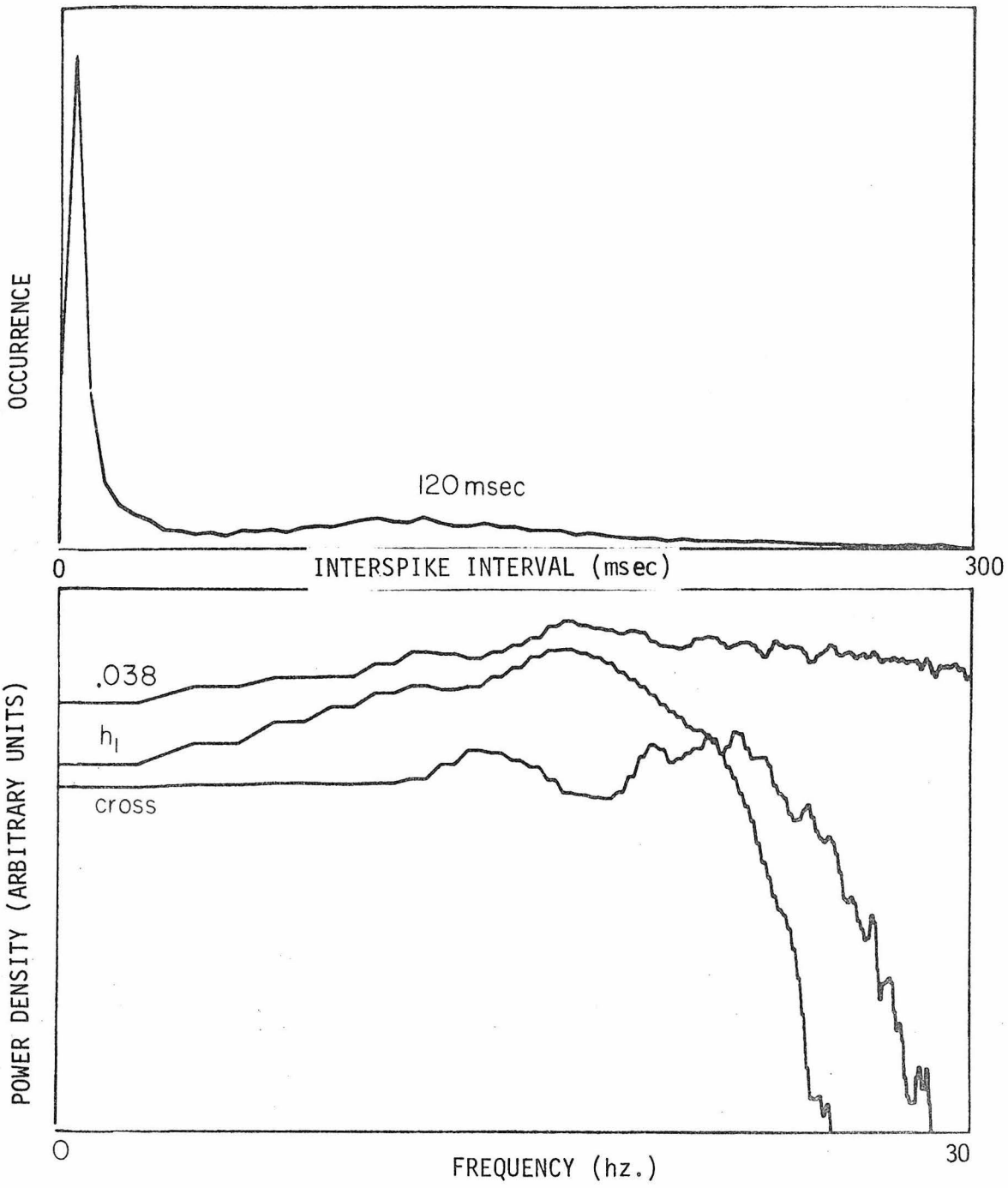

Fig. 7.2.3 ~ 7 Hz. Phenomena in 038.
Upper: Interspike Interval Histogram
Lower: Response Power Spectrum

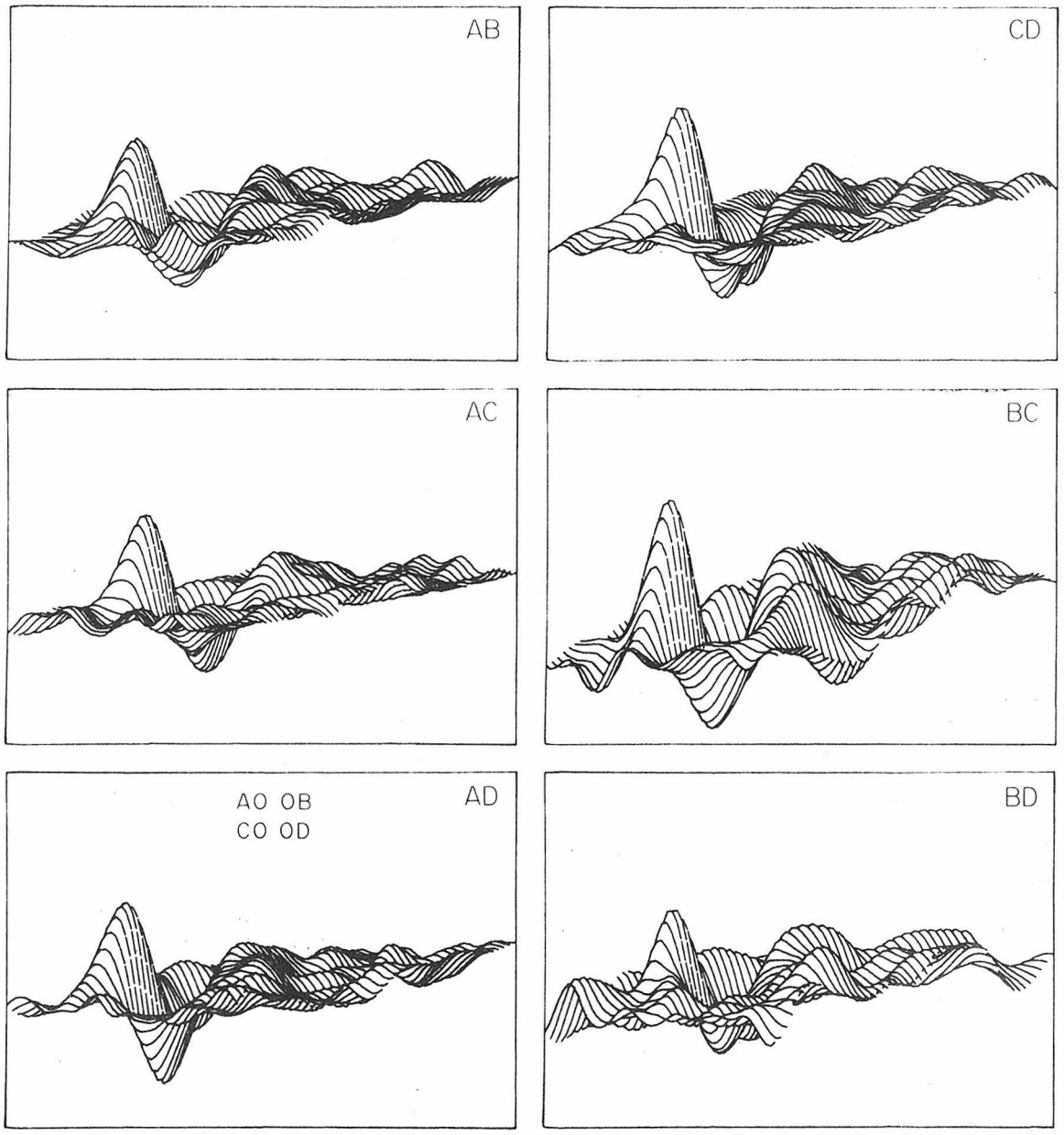

Fig. 7.2.4 Six Cross Kernels from 4-spot Tests.

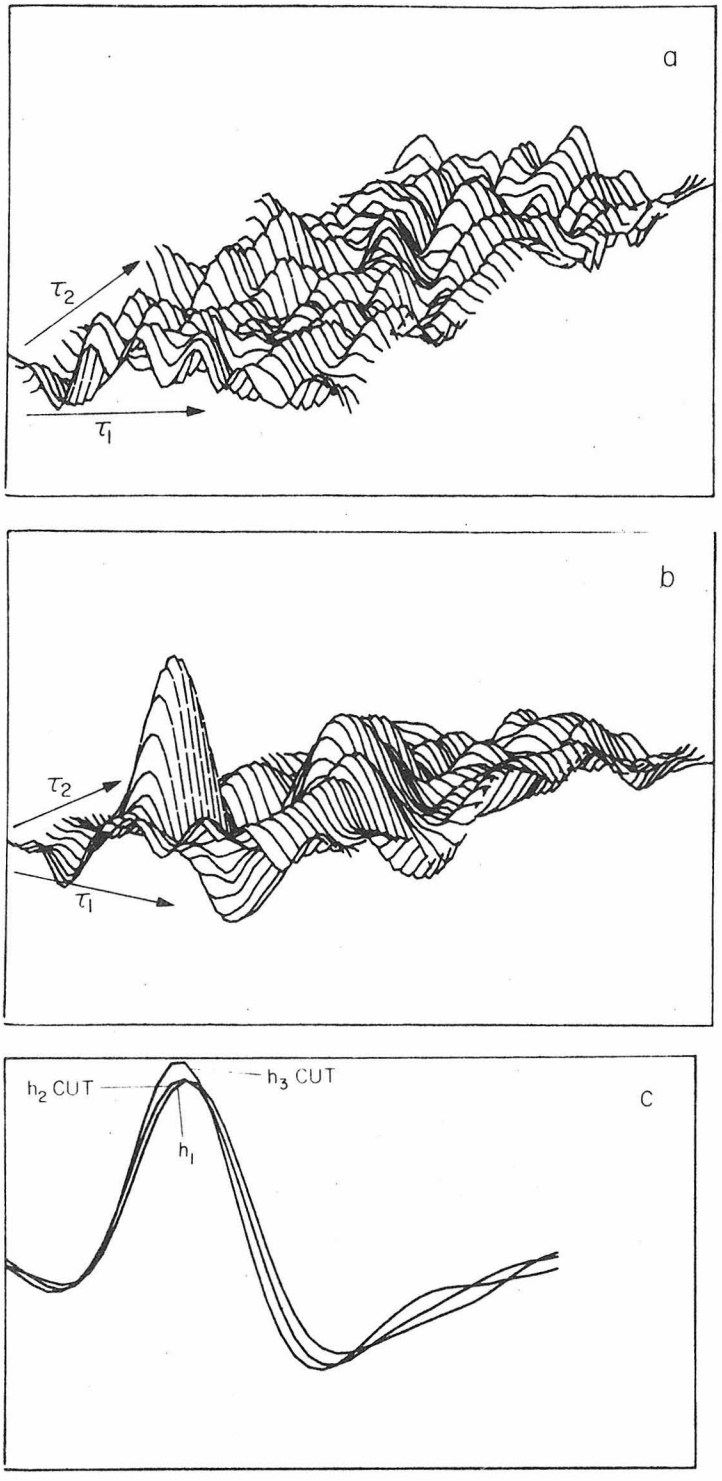

Fig. 7.2.5 4-Spot Tests: Miscellania. a)Standard Deviation of a Cross Kernel. b) Second-Order Self Kernel. c) h_1 vs. cuts through h_2 and h_3 (See Text).

and cross terms (Figure 7.2.5).

Changing the circular orientation of the four spots in 20 shifts did not result in any obvious changes in the self or cross kernels. Changing the configuration of four spots does, however, change the cross kernels when their fiber geometries are asymmetric.

7.3 Four Spot Excitation--Asymmetric Configuration

To completely identify 038's spatial characteristics, one would have to theoretically, exhaustively test it with all possible configurations of 1,2,···, and n spots. To eliminate that exhaustive (and exhausting) necessity, an attempt was made to stimulate 038 with the white spatio-temporal noise scheme recently introduced by Yasui (1975). Unfortunately, 038 would not respond to the field of noise presented to it and the reasons for this are unknown. Hence 038's response to a few representative configurations was tested to ascertain the basic spatial-dependent characteristics of the system.

One question of interest is how asymmetric stimulus configurations affect the dynamics of the various lateral interactions previously computed for symmetric configurations. One way of studying this is to move, for example, point C along the paths AC or BC of the last section's 4-spot square configuration. As C is moved towards B along the path BC through the center of the square, the cross kernels AD and CB remain symmetric, but channel B's second order self kernel is systematically reduced ;as C moves away from B the latter's second order self kernel once again increases in amplitude. That B's amplitude

decreased as C approached it is very surprising, since Chapter 5's 2-spot experiments gave no hint of a lateral inhibition between two close spots. Hence, it appears that some other interaction involving spots A and D is manifesting itself on the second order kernel of channel B.

. These results suggest a strong lateral inhibitory network probably exists in the sustaining fiber's excitatory field but that its effects are minimally seen due to symmetric cancellations in the presence of symmetric stimulus configurations. Appropriate asymmetric stimulus configurations appear to be able to set up unequal strengths of mutual inhibition in different directions that can cancel each other but also enhance other effects.

As spot C is moved along the path AC (parallel to BD) the cross kernel AC takes on completely new characteristics. As C moves towards A we see that the kernel AC diminishes in amplitude but that it takes on very definite asymmetric dynamics (Figure 7.3.2) not related to unequal light fluxes entering points A and D. (The basic shape of the cross kernel is of the form

$$h_2(\tau_1,\tau_2) = \alpha h_1(\tau_1)\ \beta h_1(\tau_2)$$

where α and β ($\alpha \neq \beta$) are channel gains reflecting unequal light flux inputs.) For unequal light fluxes we would expect the gain of the first order kernels to be different, thus keeping the basic topology of the kernel but making its amplitude distribution asymmetric. Again the reduced amplitude is suggestive of an inhibition phenomenon. The kernel

also appears to take on a double peak near the origin but this may be due to noise resulting from the kernel's greatly reduced amplitude. Surprisingly the first order kernels are not greatly affected; Figure 7.3.1 shows the first order kernels computed for spots A, B,C, and D. D's kernel is slightly greater in amplitude, but both A's and C's share equal heights. In all cases the dynamics remain the same. Model responses for these kernels do not indicate any inhibitory behavior from any of the self or cross kernels.

Under no circumstances could a 4-spot configuration within 038's hot spot be found to alter the basic dynamics found in the self kernels (first or second order).

7.4 Three-Channel Inputs

Symmetric configurations of 3-spots in 038's hot spot yielded symmetric kernels with characteristics similar to those presented in the preceding section. An interesting phenomenon, however, is clearly

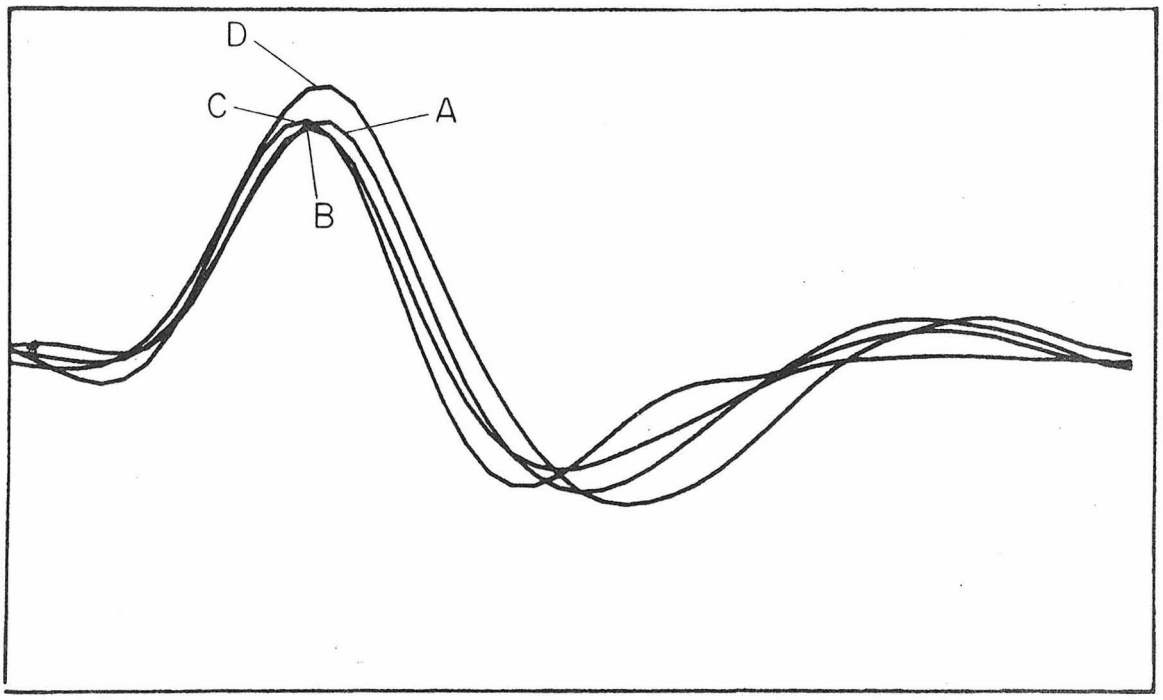

Fig. 7.3.3 Self Kernels in 4-Spot Tests (See Text)

indicated with three fibers (column 4, row 19) and (column 4, row 25), that is not so clearly shown with four. When two spots are excited within 038's hot spots, a typical cross kernel of Chapter 5 results. When a third spot was introduced right on the rim (column 4, row 19) with an output light intensity of 65 w/cm^2 the cross kernel for the other two spots could be wiped out completely (Figure 7.4.1). Figure 7.4.1 however, reveals that there is still some minor activity in its cross kernel. This phenomenon begins to explain some of the observations in the previous section providing certain assumptions are allowed. Assuming that ommatidia near the rim do not receive strong inhibition from the rim where there is no neural network, it is conceivable that they exert a powerful inhibitory influence on the ommatidial channels immediately adjacent to them. This inhibition is not second order as we know from Chapter 5. It appears to be at least third order (which also means that it is capable of demonstrating complex dynamics). 038's hot spot is right next to the rim and it is possible that the changes in second order kernels as a function of stimulus configuration are setting up strong or weak effects from the rim region. Ideally, one would hope to map these interactions as a function of all ommatidial configurations. The ultimate question, however, would be--what is this interaction's functional significance? The next section hopes to provide some insight into this question.

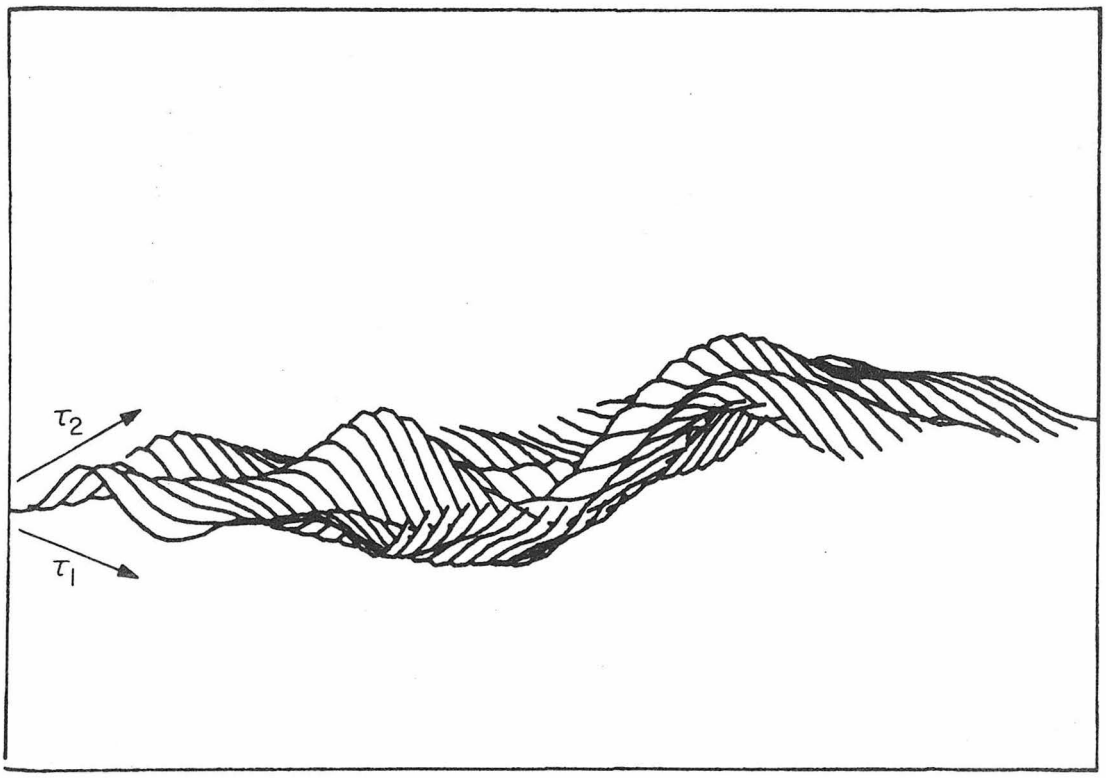

Fig. 7.4.1 See Text

7.5 Multi-Spot Experiments

Ideally one would hope to have a complete catalog of interactions underlying 038's receptive field so that predictions could be made of 038's response to various stimuli. Glantz (Glantz and Nudelman, 1976; Nudelman and Glantz, 1977) has forwarded the idea that 038 might be able to encode the properties of various stimuli as a function of its bursting properties.

An alternative method for testing 038's receptive field uses the idea of Julesz's random textures introduced briefly in Chapter 1. To test for such a capability in 038, and to unify the results of the preceding sections with the ideas of Chapter 1, 038 was tested with a special configuration of "random" textures designed by Julesz (1975) for human texture discrimination experiments.

If the cross kernels of 038 play any role in encoding patterns then we would like to see 038 respond to two different sets of patterns. From the field plots of Chapter 4, this can be achieved if one or two ommatidia are selectively stimulated at widely disparate retinal regions. What happens, though, when 038 sees a full field pattern?

To test 038's spatial encoding ability two "random" textures were designed so that accidental stimulation of 038 in a preferred horizontal or vertical direction would not occur. The patterns were constructed from the fiber optic array shown in Figure 2.1.4a in which selective combinations of sixteen LEDs could be driven to mimic any spatial configuration desired. All sixteen LEDs, however, were driven by a common source signal so that the temporal properties at each point were the same.

The random features used were taken from subregions of the textures that Julesz (1975; his page 9, left pattern, middle row) designed and used for his studies on the texture discrimination ability of humans. The patterns, when complete, ideally have identical first and second order statistics (i.e., the probability of nearest neighbors being close) but the third order statistics are different. When a small subregion of the type shown in Figure 7.5.1 is used, these relations fall apart but they serve as an easily duplicated standard for other investigators to use. When presented to 038's asymmetric field profile (Chapter 4) any remaining statistical similarities quickly disappear.

To test for 038's discrimination ability the two textures, designated 1 and 2, were presented in ten different orientations within the area of 038's field delineated by the points (column 3, row 9), (column 10, row 10), (column 3, row 27), and (column 14, row 19). For each stimulus presentation 038's interspike interval distribution was computed and the averages of these ten distributions were taken. Figure 7.5.1 shows nearly identical results except that pattern 2 appears to result in a slightly greater concentration of interspike intervals of 30 msec. When compared, however, to the average + 1 standard deviation histogram of texture 1, it is seen that there is no difference in 034's response to the two patterns.

A closer analysis of 038's firing pattern response to the identical temporal signal driving the two different patterns show that 038's response is nearly identical to both!

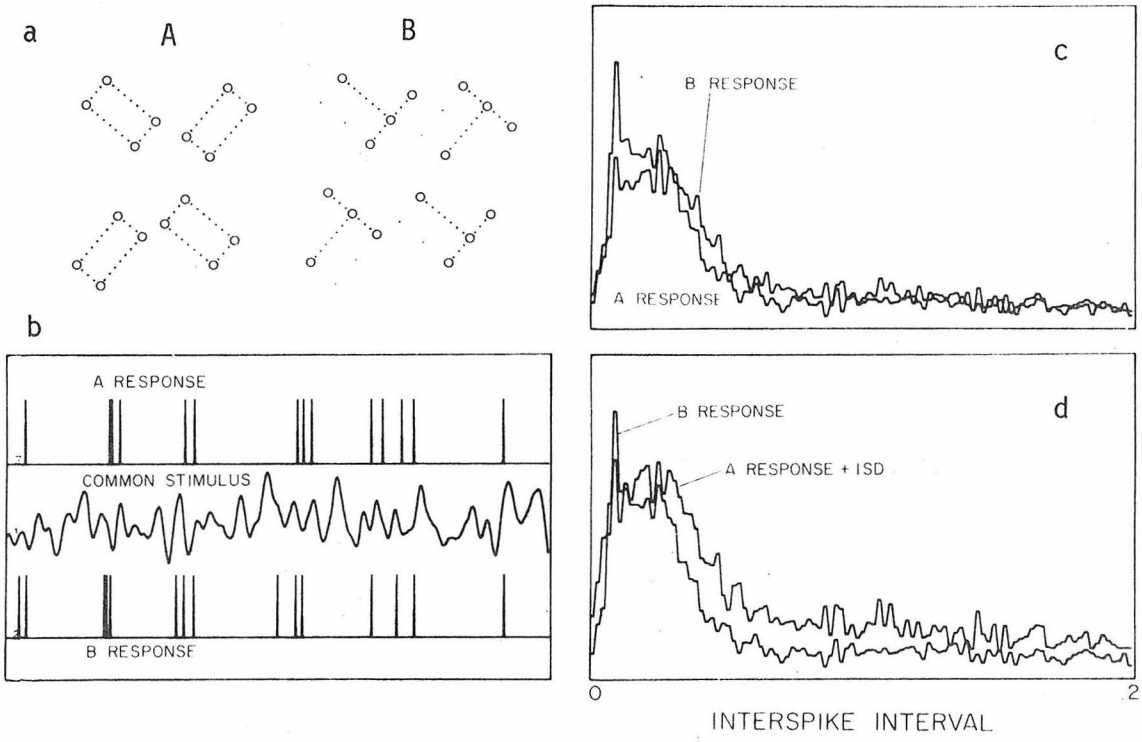

Fig. 7.5.1 "Pattern Analysis" in 038.
a) Patterns "A" and "B" presented to 038; b) Segment of 038's Response to each Pattern; c) 038's (A and B Pattern) Response Interspike Interval Histograms; d) B (from (c)) vs. 1 Standard Deviation of the A-Response (from (c)). (See Text.)

It appears then that 038 cannot tell large field objects apart from each other and is primarily concerned with the presence of light. From this rather coarse test it would seem that there is little justification to pursue a cataloging of 038's higher order interactions since, en toto, they do not appear to assist the animal in telling patterns apart.

Chapter 8

SUMMARY AND CONCLUSIONS: A MODEL FOR 038's RECEPTIVE FIELD MICROSTRUCTURE

8.1 Introduction

The Wiener kernels identified in the previous chapters have proven to be excellent descriptors of 038's functional characteristics as evidenced by their ability to accurately predict 038's response to various stimuli. The match in dynamics between 038's first order kernels and cuts through to higher order kernels suggests that the single channels of 038 can be "modeled" as a linear system cascaded with a zero order nonlinearity (Caughey, 1975; McCann, et al, 1976). While such a model is mathematically correct in that it yields kernels of equivalent orders and properties as 038's, it offers little insight into the actual anatomical substrate underlying the sustaining fiber system. A biologist may wish to know, for example, which of the neural elements lying between, and including the retinular cells (delineating 038's receptive field) and 038 itself, is associated with the model's linear system and memoryless nonlinearity. Upon examining the literature he may find that retinular cells have been modeled by this linear-nonlinear cascade (McCann et al, 1976) and wonder how a higher-order neuron is modeled like its own first stage. While such questions may seem naive to the nonlinear systems analyst, they are the real barriers to the widespread acceptance of the techniques used in this thesis.

This chapter attempts to combine the results of Chapters 3 through 7 in a comprehensive model of 038's receptive field microstructure. In

addition to presenting the results in Chapter 1's kernel formalism, an attempt will be made to identify the various interactions that reside in the crayfish's visual system. All the results will be shown to be consistent with what is actually known about the crayfish or reasonably extrapolated from studies on other arthropods.

8.2 The Single Channels of 038: A Model

The first stage of data processing in the crayfish sustaining fiber system takes place in the retinular cells, whose functional characteristics determine the signals processed by the more distal regions of the visual system.

Unfortunately, however, the frequency response of crayfish retinular cells have not been reported in the literature. It is not unreasonable, however, to suspect that their frequency characteristics do not differ significantly from those reported for other arthropods (e.g., insects; Wiersma, personal communication). Thus far, however, flies are the only arthropods whose retinula have been studied by Wiener kernels. In an attempt to understand what contribution a retinular cell has on 038's system kernels, a typical set of first and second order kernels identified for the fly Calliphora were studied. It is important to emphasize that these fly kernels were extracted in experimental conditions closely related to those used on the crayfish (i.e., a light with absolute intensity 30×10^{-6} $\mu w/cm^2$. These kernels were provided by Dr. McCann and are known to accurately model the fly's retinular cell to frequencies beyond 100 Hz (R. Fargason, personal communication). The total mse for these kernels

is about 5% and the second order kernel h_2 contributes only about 10-15% to the total model response (R. Fargason, personal communication).

Compared to 038's narrow band characteristics, the retinular cell appears to act as a wide band-pass filter. Compared to the kernels computed for 038, the retinular cell's first order kernel appears to resemble a delta function. If the retinular cell were strictly linear, then it could be modelled by a Dirac delta function (as far as 038 is concerned). But the retinular cell has a second order kernel; could this be the source for the second order kernel obtained for 038? It appears unlikely. The fact that h_2 contributes so little, at the experimental light levels, suggests that the retinular system in toto is acting as a linear filter, thus insuring that any Gaussian signal passing through it comes out Gaussian. Figure 8.2.1c shows the amplitude distribution of a signal exciting the retinular cell's kernels and Figure 8.2.1d shows the amplitude distribution of the kernels' predicted response which is also Gaussian.

How can we be certain that the linearity criterion is satisfied in the crayfish? To do so requires some effort. In their study on bursting properties of sustaining fibers, Glantz and Nudelman (1976, p. 1264) used stimulus intensities of .35 mw/cm^2 - 4.79 mw/cm^2 which were 100 to 1000 times the threshold needed to excite 038 (Glantz and Nudelman, 1976, p. 1257). This means that the 038 kernels were computed (using Glantz's numbers) about 1 log unit above threshold. Comparison of 038's relative threshold with that determined for an intracellularly recorded crayfish retinula cell (cf. Figures 1 and 3 in Glantz, 1971) suggests that the crayfish retinula cells are working in a fairly linear range at the stimulus intensities used in these experiments.

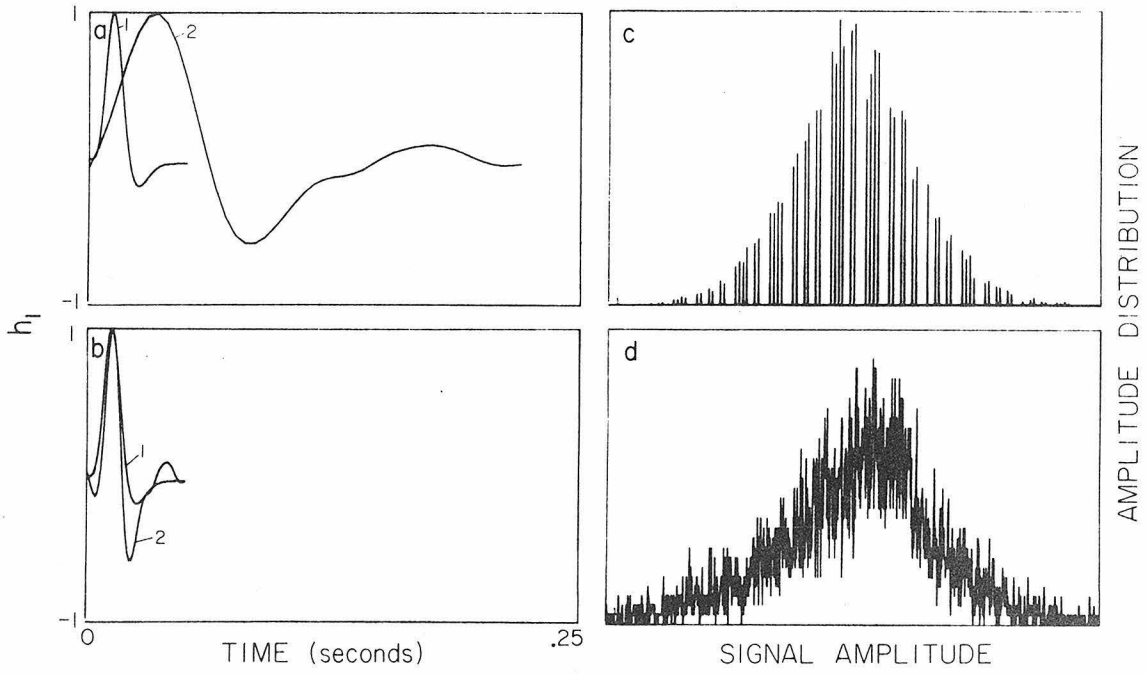

Fig. 8.2.1 Properties of Retinular Cells vs. 038 (See Text)

Hence we expect the crayfish's retinular cells to behave linearly in the intensity range studied. From comparison with the overall system kernels for 038 (Figure 8.2.2b) it looks as if the retinula cell can be treated as a signal processing box whose impulse response is a delta function (at these light intensities). This result suggests that the effect of the retinular cells on 038's dynamics are minimal--that only those cells postsynaptic to the retinula are reflected in 038's kernels. Can we localize the sources contributing to the kernels?

Figure 8.2.1a shows 038s h_1 compared to the retinular cell's h_1; if 038's kernel is time compressed by a factor of 5, then we see the result in Figure 8.2.1b. If the retinula cell's h_1 could be considered an impulse, then 038's kernel resembles that of a unit doublet impulse--the sign of a differentiator.

It is easily shown that in linear systems a differentiator response to a square pulse stimulus will Laplace transform

$$\frac{e^{-as} - e^{-bs}}{s} \tag{8.2.1}$$

is

$$e^{-as} - e^{-bs} \tag{8.2.2}$$

i.e., an upward impulse at time a and a downward impulse at time b.

It is well known that the monopolar cells in a large variety of orthropods (e.g., bees, flies, and locusts) respond to square pulses of light with a triphasic hyperpolarization that is characterized by the upward and downward spike phenomena described in equation 8.2.2 (e.g., Laughlin, 1973; Menzel, 1974)

It is not unreasonable, therefore, to suppose that the monopolar cells in the lamina of the crayfish display a similar behavior. But those cells would need dynamics to match those dictated by equation 4.3.1. It is not unreasonable to attribute these dynamics to the lamina for two reasons. First, there appears to be a general tendency for the memories of neurons to increase as does their position order in a visual system (cf. Figure 3c in McCann (1974)). Secondly, kernels with approximately the same dynamics have been found for third order neurons (i.e., horizontal cells) in vertebrate eyes (cf. Fukurotani & Hara, 1975; Marmarelis & Naka, 1975b).

A source for a second order nonlinearity is now required for the lamina. This mechanism can manifest itself in any number of ways: rectification by a synapse, or multiplication by correlation units of the type envisioned by McCann (1974).

It seems unlikely that the second order kernel arises in 038. The reason for this stems from Chapter 4. It was commented that the amplitude profiles for the second order kernels matched those for the first order kernels. Histological investigations in the crayfish eye reveal no inhomogeneous concentration of laminar neuron types that would explain the receptive field profile found for 038 (Nassel, personal communication; Niersma, personal communication). Hence it appears likely that the sensitivity profiles arise from a skewness in 038's dendritic tree which sums inputs from neurons in the lamina. If the relative weight of each dendritic branch preceded a second order nonlinearity in 038, then the profile for the h_2 amplitudes would be a quadratic function. But the profile for h_2 amplitudes appears to fall off linearly.

Let's assume, for simplicity, that 038's dendritic branch concentration is some linear function of position in the optic ganglia. If we assume that 038's dendritic branch is nonlinear, we would have to invoke some complex summing functions in 038's dendritic tree, preceding the nonlinearity, that would give the impression of a linear falloff in sensitivity. Hence the profile data suggest that 038 sees a nonlinearity before its dendritic tree.

The only available neuroanatomy left, assuming the previous assumptions to be correct, is the complex plexus of lateral interactory pathways perfusing the crayfish lamina (Nassel 1976, 1977; Hafner, 1973)

Although the previous discussion is based on speculation, the speculation is not specious. The model then envisioned for each channel of 038 is that depicted in Figure 8.2.2. It consists of a retinular cell which essentially senses the input light stimulus and converts it into an electrical signal for processing in the lamina. The lamina cells act as differentiation and their output feed into local rectifiers of as yet unknown nature. The various dendritic branches of 038 samples the inputs from cells presynaptic to 038 in a linear fashion. A simple IPFM would be all that is required to generate spikes (cf. Chapters 3 and 4).

An interesting aspect of the model is that it supports Gordon's (1975) notion that a differentiator exists in the 038 system as evidenced by Glantz's (1973) results, indicating AC coupling between 038 and the retinular cells. Furthermore, the model suggests that the basic resonant phenomenon of 038's spike train bursts resides in a process already contained in the single channels. If 038's dynamics are modeled by a second

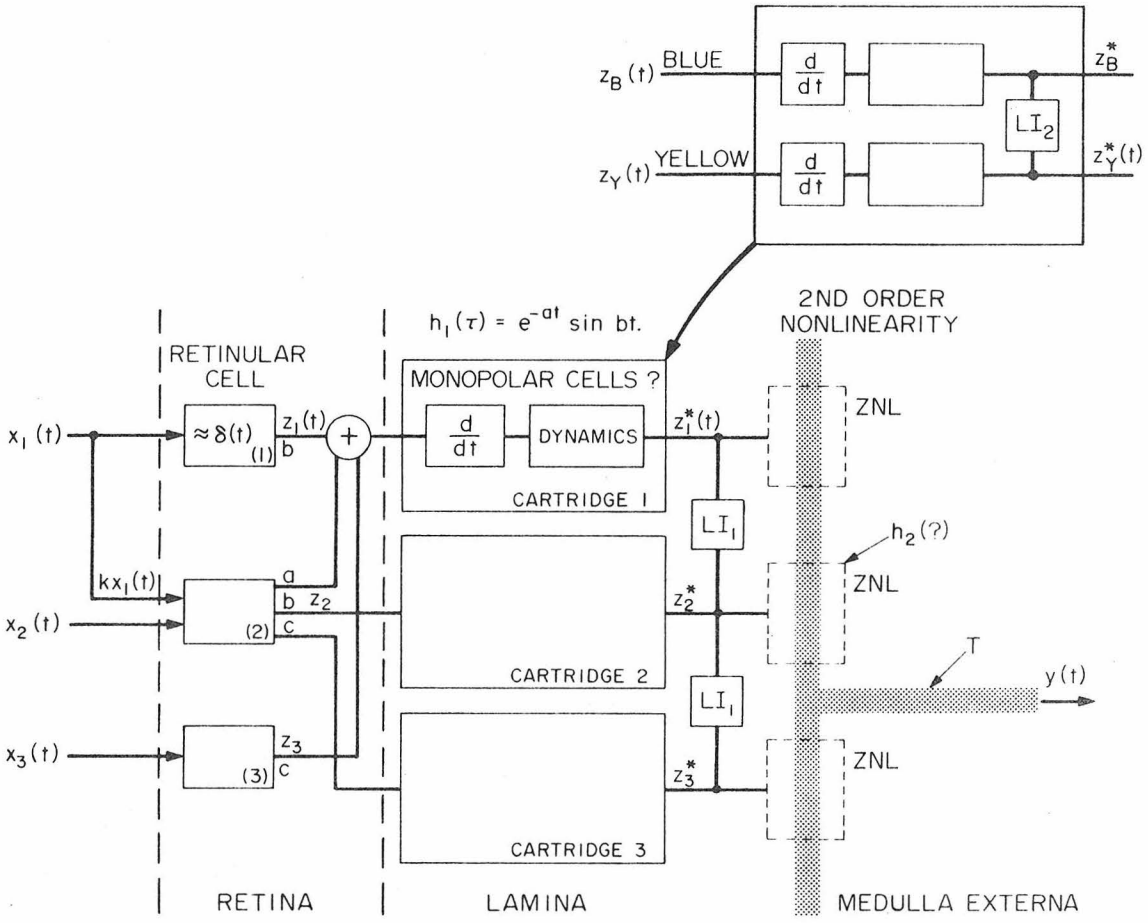

Fig. 8.2.2 Functional Model of 038's Receptive Field

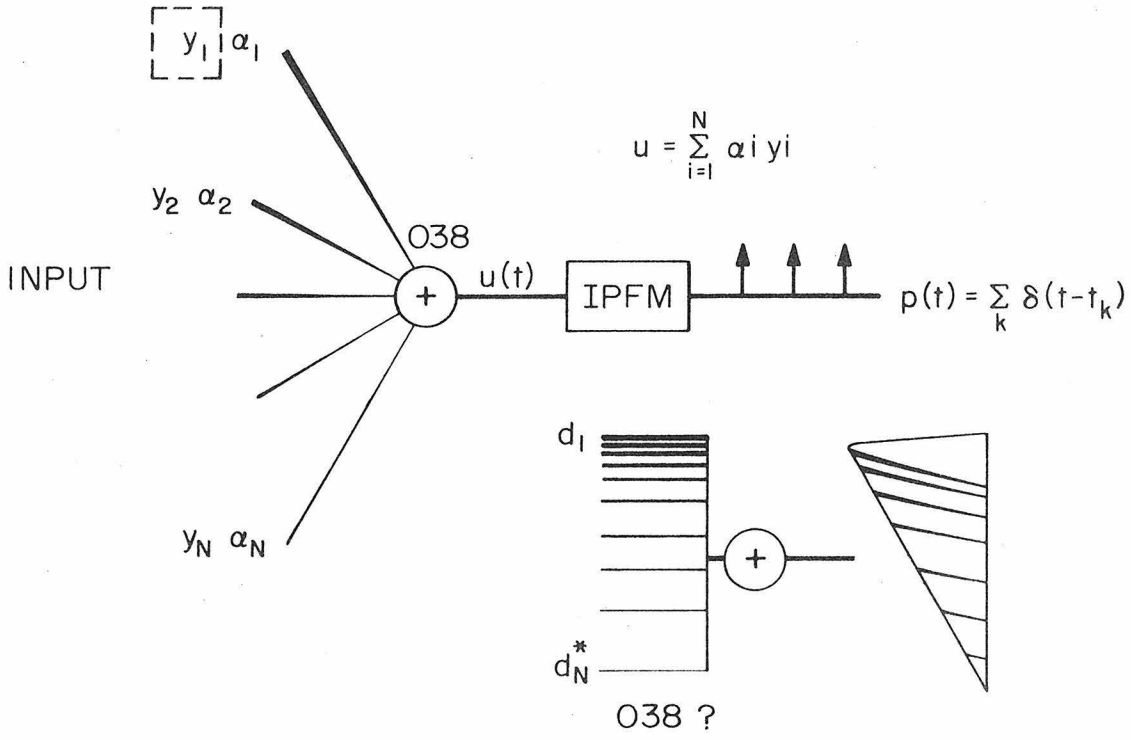

Fig. 8.2.3 Field Summation in 038

order differential equation

$$\frac{M d^2y}{dt^2} = x(t) - K_y(t) - \frac{B dy}{dt}$$

then it is well known that the damping coefficient is what controls oscillations in the impulse response of 038's first order kernel as the dynamics of an underdamped system. If, however, the section is undamped, the system oscillates with a frequency of sin bt, where b is defined by

$$(K/M)^{1/2}$$

(Hence it seems that if a lateral inhibitory system could set B to zero then sustained bursting in 038 could be observed.)

Modeling such a system electrically, however, would require an inductor--something hard to imagine in a neuron. Is there another way that one can get the dynamics observed herein? The answer, again speculative, may lie in the kernels that McCann and Gemperlein (1974) published. They bear a striking resemblance to the kernels computed for horizontal cells in the carp by Fukurotani and Hara (1975) when a very small size stimulus (with respect to the size of the receptive field) was used. As the stimulus size increased so did the first order kernels change into a form closely resembling that of equation 4.3.1. Fukurotani and Hara postulated that feedback loops between neighboring horizontal cells were becoming activated. Perhaps a similar mechanism is at work in the crayfish lamina. There the neural component underlying each retinular cell of the retina is composed of a minimum of 5 monopolar cells and two wide field tangential cells--one of which branches for 300μ on all sides.

The cell types found in the crayfish lamina are depicted in Figure 8.3.1, demonstrating the complex anatomy available for supporting almost any conceivable type of lateral interaction.

8.4 Color Phenomena

Woodcock and Goldsmith (1973) reported an unusual blue sensitivity in the dorsal regions of the crayfish eye. It is known that other arthropods have structural specializations in the dorsal regions in their compound eyes. Bees, for example (Schinz, 1975) have distinct structural specializations in that eye region as manifested by: 1) microvilli arranged in more than two directions, and 2) the 9th retinula cell (which is ultraviolet sensitive) and its microvilli are not restricted to the distal part of the rhabdom but extend over the full length of the retinula.

Recent work by Goldsmith (unpublished communication) has suggested that the 8th retinula cell in the crayfish compound eye is the blue sensitive retinular cell, and that R1-7 (Eguichi (1971)) are all yellow sensitive. Such a conclusion would be welcomed to this study. It is well known that R8 in crayfish projects into the (lamina and) medulla separately from R1-R7.

In bees it is known that the monopolar cells respond to square wave retinal illumination with triphasic hyperpolarization. Although most inputs to these monopolar cells come from the bee's dominant blue and green receptors, there are indications of low sensitivity in the ultraviolet. The blue and green receptors supply excitatory inputs to the monopolar cells with equal weighting: the ultraviolet receptors appear to

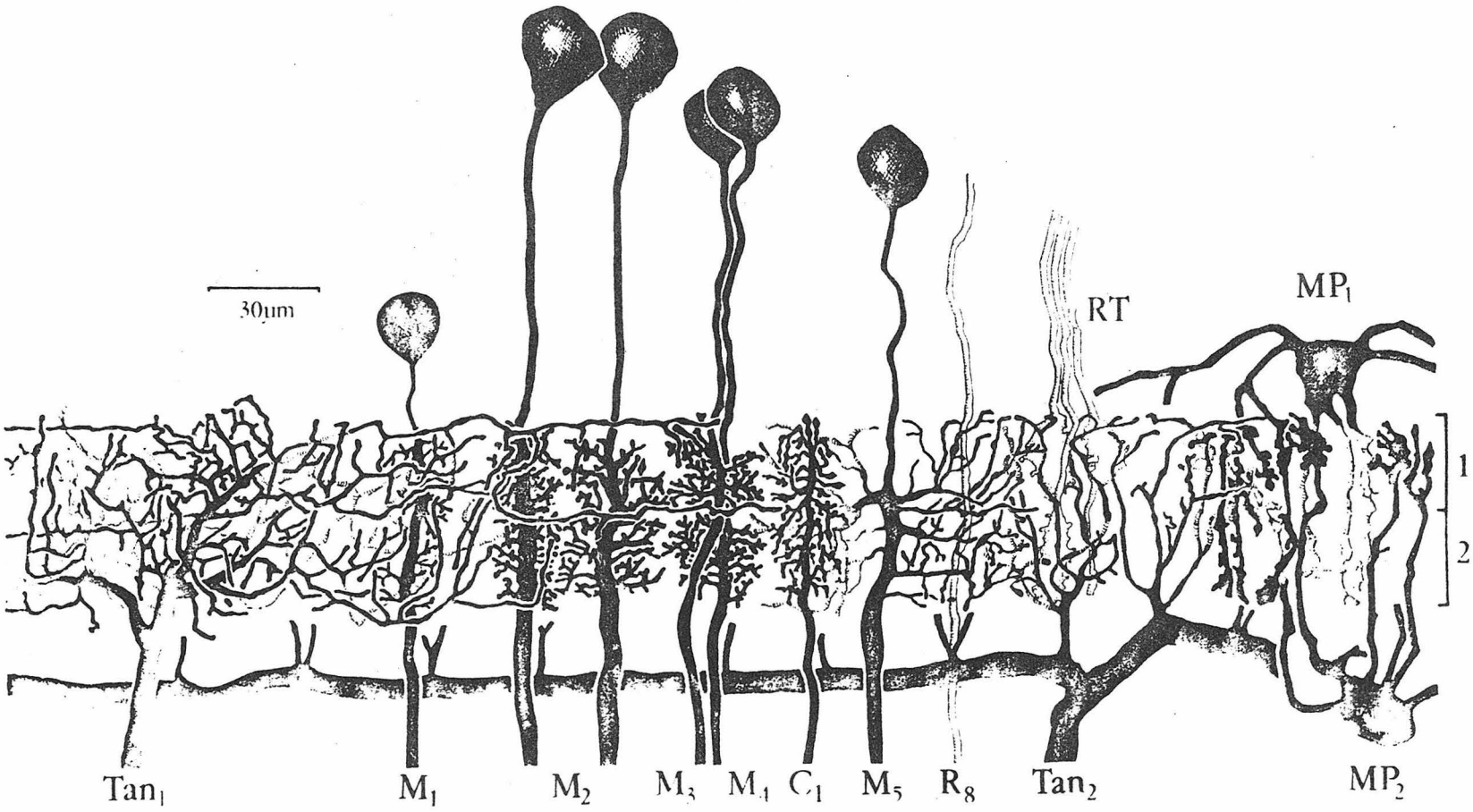

Fig. 8.3.1 Cell Types in the Crayfish Lamina (from Nassel (1976)). M_{1-5} = Monopolar Cells. Tan_2 is a Large Field Tangential Cell.

supply an inhibitory input of less weight than those of the other receptors.

From bee data we can draw two conjectures about 038's color channels. First, the similarity in dynamics between the yellow and blue channels (Chapter 6) suggests that the processing of yellow and blue light processes in similar stages. The evidence that the triphasic (i.e., differentiating) behavior in monophase cells is activated by the bees small retinular cell R9 suggests that the crayfish's R8 cell may also feed into the lamina. That the two channels can have opposite effects on the monopolar cells suggests that it is not unreasonable to suspect a similar laminar mechanism in the crayfish.

The inhibition of channels must be accomplished by a process greater than second order. A mechanism for that is as yet unknown, since there is no way to tell where the inhibition is coming from.

Conjecture 1 is easily tested by histological studies. Recently, Nassel (1976) reported finding two distinct types of retinular cell endings terminating in the lamina cartridges. Although R8 is well known to project directly into the medulla, Nassel (1976) suggests the real possibility that R8 might be in the lamina. This, coupled with Menzel's work (1974) yields a nonzero possibility of finding a laminar interaction responsible for the color inhibition described herein.

8.5 Lateral Interactions in 038

Aside from the color interactions that have been described there appear to be at least two other types of lateral interactions subserving

038's receptive field. The first is the excitatory interaction captured in the cross kernels computed in Chapters 5 and 7. The second interaction is observed indirectly; it is seen through its effect on h_1's amplitude (Chapter 5) and h_2's dynamics (Chapter 7). If p-order 2 cross kernels of n order 3rd or 4th could be computed (they can't due to the algorithms not being currently running in our computer) then their existence might be verified.

What role the interactions play in contributing to 038's encoding behavior is still a matter of speculation, but some ideas can be advanced about it. First, lateral inhibition appears to play a minor role in the sustaining fiber as evidenced by the inability to detect inhibition in the second order cross kernel. While it is true that most other studies on sustaining fibers have found evidence for a lateral inhibition field connecting a sustaining fiber's excitatory field to an inhibitory surround, none, with the exception of Glantz (1971), have studied the details of 038's excitatory field as has this thesis.

Secondly, all studies on crayfish fibers have studied the dynamics of sustaining fibers through crude counting methods on the sustaining fibers' spike train. With Wiener kernels we have gotten to the heart of the system's dynamics with a powerful probing technique.

The fact that the four input white noise was able to excite a rhythmic spike output in 038 and that the 4 sets of self kernels and 6 sets of cross kernels were able to model it suggests that inhibition, of the type envisioned by Glantz and Nudelman, is not required to explain bursting in the sustaining fibers.

The kernels of Chapter 4 clearly show that the 7 Hz natural frequency described by Glantz and Nudelman is found in Wiener kernels computed from light stimuli 10-100 times less bright than required by them to observe bursting.

It would be very interesting, however, to place a microelectrode in a large field fiber such as a laminar tangential cell to ascertain, by Wiener kernel analysis, if the excitatory phenomena observed were localized to this cell.

8.6 The Model: Underlying Neuroanatomy

Figure 8.2.2 is a schematic of the interactions conjectured to underlie 038's excitatory field, incorporating known physiology and the speculations arising from this thesis. The retinular cells act as ideal delta functions (for a narrow intensity range) and project their outputs, through 3 axon bundles (R8 is not included) (Nassel, 1975) to three adjacent cartridges composed of the cell types shown in Figure 8.3.1. (This may account for the strong cross kernels for small interommatidial distances alluded to in Chapter 5.) The cartridges, in toto, supply the e^{-at} sin bt dynamics invoked in Chapter 4 (and possibly incurred through complex feedback loops). The large lateral extent of the excitatory interaction requires a pathway capable of subserving the observed distances: the wide-field tangential cells of Figure 8.3.1 are, herein, imagined to be capable of supporting such a function. It is also conjectured that some as yet unknown mechanism underlies the excitatory cross kernel in these cells, and the second order self nonlinearity. It is assumed that

the lateral inhibition seen indirectly through first order kernels is also at work through some as yet unknown pathway LI_1, and that a second, independent, pathway LI_2 exists for the color channel interaction observed in Chapter 6. Furthermore, 038's dendritic field is envisioned to be asymmetric with a distribution following the profile schematized in Figure 8.2.3. Until more is known about the physiology and histology of the cell types in the crayfish lamina, it is difficult to speculate with any greater specificity than has been done thus far.

8.7 Conclusion

This thesis has introduced a new approach to Wiener kernel analysis. By recognizing how higher order kernels manifest themselves, one can do an extensive analysis on the system in a brief period of time and extract information of a higher quality than previously available to the field.

REFERENCES

Abelson, H. (1977): Computational geometry of linear threshold functions. Information and Control. 34:66-92.

Abramou, I. and M. W. Levine (1975): On the lack of lateral inhibition within the receptive fields of goldfish retinal ganglion cells. Vision Res.15:791-798.

Arechiga, H. et al. (1973): Circadian rhythm of responsiveness in the visual system of the crayfish. Neurobiology of Invertebrates. 403-427.

Arechiga, H. and K. Yanagisawa (1973: Inhibition of visual units in the crayfish. Vision Res. 13:731-744.

Arechiga, H. et al. (1974): Influence of retinal shielding pigments on light sensitivity in the crayfish. Acta Physiologica Latino Americana. 24:601-611.

Arnett, D. W. (1972): Spatial and temporal integration properties of units in first optic ganglion of Dipterans. J. Neurophysiology. 35:429-444.

Barlow, R. B., Jr. (1969): Inhibitory fields in the Limulus lateral eye. J. Gen. Physiol. 54:383-396.

Barlow, R. B. Jr. and G. D. Lange (1974): A nonlinearity in the inhibitory interactions in the lateral eye of Limulus. J. Gen. Physiol. 63:579-589.

Barlow, R. B., Jr. and D. A. Quarles (1975): Mach bands in the lateral eye of Limulus. Comparison of theory and experiment. J. Gen. Physiol. 65:709-730.

Bedrosian, E. and S. O. Rice (1971): The output properties of Volterra systems (nonlinear systems with memory) driven by harmonic and Gaussian inputs. Proc. IEEE. 59:1688-1707.

Bryant, H. L. and J. P. Segundo (1975): How does the neuronal spike trigger zone read transmembrane current? In: Proc. First Symp. on Testing and Identification of Nonlinear Systems, Marmarelis, P. Z. and G. D. McCann, eds., Pasadena, California: California Institute of Technology, pp. 236-256.

Bryant, H. L. and J. P. Segundo (1976): Spike initiation by transmembrane current: A white-noise analysis. J. Physiology. 290:279-313.

Buttner, C., et al. (1971): Interaction of excitation and direct inhibition in the receptive field center of retinal neurons. Pflugers Arch. 322:1-21.

Caughey, T. K. (1975): Nonlinear analysis, synthesis and identification theory. In: Proc. First Symp. on Testing and Identification of Nonlinear Systems, Marmarelis, P. Z. and G. D. McCann, eds. Pasadena, California: California Institute of Technology, pp. 1-14.

Coggshall, J. C. (1973): Linear models for biological transducers and impulse train spectra: General formulation and review. Kybernetik. 13:30-37.

Coleman, B. D. and G. H. Renninger (1974): Theory of delayed lateral inhibition in the compound eye of Limulus. Proc. Nat'l. Acad. Sci. 71:2887-2891.

DeBoer, E. (1976): Cross-correlation function of a bandpass nonlinear network. Proc. IEEE (Lett.) 64:1443-1444.

Easter, S. S., Jr. (1968): Excitation in the goldfish retina: Evidence for a nonlinear intensity code. J. Physiol. 195:253-271.

Enroth-Cugell, C. and J. G. Robson (1966): The contrast sensitivity of retinal ganglion cells of the cat. J. Physiol. 187:517-552.

Euguichi, E., et al. (1973): Localization of the violet and yellow receptor cells in the crayfish retinula. J. Gen. Physiology. 62:355-374.

French, A. S. (1976): Practical nonlinear system analysis by Wiener kernel estimation in the frequency domain. Biol. Cybernetics. 24:111-119.

Fukurotani, K. and K. I. Hara (1975): A dynamic model of the receptive field of L-cells in the carp retina. Biol. Cybernetics. 20:1-8.

Gemperlein, R. and G. D. McCann (1975): A study of the response properties of retinula cells of flies using nonlinear identification theory. Biol. Cybernetics. 19:147-158.

Glantz, R. M. (1968): Light adaptation in the photoreceptor of the crayfish, Procambarus clarkii. Vision Res. 8:1407-1421.

Glantz, R. M. (1971): Peripheral vs. central adaptation in the crustacean visual system. J. Neurophysiology. 34:485-492.

Glantz, R. M. (1972): Visual adaptation: A case of nonlinear summation. Vision Res. 12:103-109.

Glantz, R. M. (1973): Spatial integration in the crustacean visual system: peripheral and central sources of nonlinear summation. Vision Res. 13:1801-1814.

Glantz, R. M. and H. B. Nudelman (1976): Sustained, synchronous oscillations in discharge of sustaining fibers of crayfish optic nerve. J. Neurophysiology. 39:1257-1271.

Goldman, J. (1973): Volterra series description of crosstalk interference in communication systems. Bell System Tech. J. 52:649-668.

Goldsmith, T. H. (1972): The natural history of invertebrate visual pigments. In: Handbook of Sensory Physiology, Vol. VII/1. Dartnall, H.J.A., ed. Berlin-Heidelberg-New York: Springer, pp. 685-719.

Goldsmith, T. H. (in press): The spectral absorption of crayfish rhabdoms: Pigment, photoproduct and pH sensitivity. J. Comp. Physiol.

Goldsmith, T. H. and H. R. Fernandez (1966): Some photochemical and physiological aspects of visual excitation in compound eyes. In: The Functional Organization of the Compound Eye, Bernhard, C. G., ed. Oxford: Pergamon Press, pp. 125-143.

Gordon, W. (1975): A Nonlinear Model of the "Sustaining" Visual Interneurons of the Crayfish Optic Nerve. Ph.D. thesis, Rice University Houston, Texas.

Grusser, O.-J., et al. (1970): A quantitative analysis of the spatial summation of excitation within the receptive field centers of retinal neurons. Pflugers Arch. 319:101-121.

Hafner, G. S. (1973): The neural organization of the lamina ganglionaris in the crayfish: A Gulgi and EM study. J. Comp. Neurol. 152:255-280.

Hafner, G. S. (1973): The ultrastructure of retinula cell endings in the compound eye of the crayfish. J. Neurocytology. 3:295-311.

Hartline, H. K. (1938): The response of single optic nerve fibers of the vertebrate eye to illumination of the retina. Am. J. Physiol. 121:400-415.

Hochstein, S. and R. M. Shapley (1976a): Quantitative analysis of retinal ganglion cell classifications. J. Physiology. 262:237-264.

Hochstein, S. and R. M. Shapley (1976b): Linear and nonlinear spatial subunits in Y-cat retinal ganglion cells. J. Physiology. 262: 265-284.

Hudson, M. C. (1974): Calculation of the maximum optical coupling efficiency into multimode optical waveguides. Applied Optics. 13:1029.

Jarvilento, M. and F. Zettler (1973): Electrophysiological-histological studies on some functional properties of visual cells and second order neurons of an insect retina. Z. Zellforsch. 136:291-306.

Johnston, D. and H. Wachtel (1976): Electrophysiological basis for the spatial dependence of the inhibitory coupling in the Limulus retina. J. Gen. Physiol. 67:1-25.

Jowett, J. and D. Vere-Jones (1972): The prediction of stationary point processes. In: Stochastic Point Processes: Statistical Analysis, Theory and Applications. Lewis, P.A.W., ed. New York: Wiley, pp. 405-435.

Julesz, B. (1975): Experiments in the visual perception of texture. Scientific American. 232:34-43.

Kennedy, D. and M. S. Bruno (1961): The spectral sensitivity of crayfish and lobster vision. J. Gen. Physiol. 44:1089-1102.

Knight, B. W. (1969): Frequency response for sampling integrator and for voltage to frequency convertor. In: Systems Analysis in Neurophysiology. Terzuolo, C. A., ed. Minneapolis: University of Minnesota, pp. 61-72.

Koblasz, A. J. (1977): Nonlinear Analysis of the Human Electroretinogram. Ph.D. thesis, Calif. Inst. of Technology, Pasadena, CA.

Land, H. F. (1976): Superposition images are formed by reflection in the eyes of some oceanic decapod crustacea. Nature. 263:764-765.

Laughlin, S. B. (1973): Neural integration in the first optic neuropile of dragonflies. I. Signal amplification in dark-adapted second-order neurons. J. Comp. Physiol. 84:335-355.

Laughlin, S. B. (1974): Neural integration in the first optic neuropile of dragonflies. III. The transfer of angular information. J. Comp. Physiol. 92:377-396.

Lee, Y. W. and M. Schetzen (1965): Measurement of the Wiener kernels of a nonlinear system by cross-correlation. Int'l. J. Control. 2:237-254.

Levine, M. W. and I. Abramov (1975): An analysis of spatial summation in the receptive fields of goldfish retinal ganglion cells. Vision Res. 15:777-789.

Marmarelis, P. Z. (1971): Nonlinear Dynamic Transfer Functions for Certain Retinal Neuronal Systems. Ph.D. thesis, Calif. Inst. of Technology, Pasadena, CA.

Marmarelis, P. Z. and G. D. McCann (1973): Development and application of white-noise modeling techniques for studies of insect visual nervous systems. Kybernetik. 12:74-89.

Marmarelis, P. Z. and K. I. Naka (1973): Nonlinear analysis and synthesis of receptive-field responses in the catfish retina. I. Horizontal cell → ganglion cell chain. J. Neurophysiology 36:605-618.

Marmarelis, P. Z. and K. I. Naka (1974): Identification of multi-input biological systems. IEEE Trans. Biomedical Engineering. BME-21: 88-101.

Marmarelis, P. Z. and G. D. McCann (1975): Optimization of test parameters in the identification of spike train responses of biological systems through random test signals. In: Proc. First Symp. on Testing and Identification of Nonlinear Systems. Marmarelis, P. Z. and G. D. McCann, eds. Pasadena, California: California Institute of Technology, pp. 325-338.

Menzel, R. (1974): Spectral sensitivity of monopolar cells in the bee lamina. J. Comp. Physiol. 93:337-346.

Mimuro, K. (1976): Some spatial properties in the first optic ganglion of the fly. J. Comp. Physiol. 105:65-82.

Minsky, M. and S. Papert (1969): Perceptrons. An Introduction to Computational Geometry. Cambridge, Mass: MIT Press.

McCann, G. D. (1974): Nonlinear identification theory models for successive stages of visual nervous systems of flies. J. Neurophysiology. 37:869-895.

McCann, G. D. et al. (1976): The response properties of retinula cells in the fly Calliphora erythrocephala as a function of the wavelength and polarization properties of visible and ultraviolet light. Biol. Cybernetics. 26:93-107.

McCann, G. D. and C.A.G. Wiersma (in preparation): Application of nonlinear identification theory to studies of visual fibers in the crayfish.

McKean, T. A., et al. (1970): The biologically relevant parameter in nerve impulse trains. Kybernetik. 6:168-170.

Naka, K. I. (1975): Identification of function and structure in the central nervous system. In: Proc. First Symp. on Testing and Identification of Nonlinear Systems. Marmarelis, P. Z. and G. D. McCann, eds. Pasadena, California: California Institute of Technology, pp. 205-220.

Nassel, D. R. (1975): The organization of the lamina ganglionaris of the prawn, Pandalus borealis (Kroyer). Cell Tiss. Res. 163:445-464.

Nassel, D. R. (1976): The retina and retinal projection on the lamina ganglionaris of the crayfish Pacifastacus leniusculus (Dana). J. Comp. Neur. 167:341-360.

Nassel, D. R. (1977): Types and arrangements of neurons in the crayfish optic lamina. Cell Tiss. Res. 179:45-75.

Nisio, M. (1960): On polynomial approximation for strictly stationary processes. J. Math. Soc. Japan. 12:207-226.

Nosaki, H. (1969): Electrophysiological study of color encoding in the compound eye of crayfish, Procambarus clarkii. Z. Vergl. Physiologie. 64:318-323.

Nudelman, H. B. and R. M. Glantz (1977): Sustained oscillations, entrainment and lateral inhibition in the crayfish visual system. Federation Proc. 36:2042-2044.

Nunnemacher, R. F. et al. (1962): The fine structure of the crayfish nervous system. V. Int. Cong. for Electron Microscopy. 2:N-11.

O'Leary, D. P. and V. Honrubia (1976): Analysis of afferent responses from isolated semicircular canal of the guitarfish using rotational acceleration white-noise inputs. II. Estimation of linear system parameters and gain and phase spectra. J. Neurophysiology. 39:645-659.

Parente, R. B. (1970). Nonlinear differential equations and analytic system theory. SIAM J. Applied Math. 18:41-66.

Paek, U. C. and A. L. Weaver (1975): Formation of a spherical lens at optical fiber ends with a CO_2 laser. Appl. Optics. 14:294-298.

Perkel, D. H. and T. H. Bullock (1968). Neural coding. Neurosciences Research Program Bull. 6:221-348.

Poggio, T. and W. Reichardt (1976): Visual control of orientation behavior in the fly. Part II. Towards the underlying neural interactions. Quart. Rev. Biophys. 9:377-438.

Ratliff, F. (ed.) (1974): Studies on Excitation and Inhibition in the Retina. New York: The Rockefeller University Press.

Roach, J.L.M. and C.A.G. Wiersma (1974): Differentiation and degeneration of crayfish photoreceptors in darkness. Cell Tissue Res. 153:137-144.

Roberts, G. E. and H. Kaufman (1966): Table of Laplace Transforms. Philadelphia: W. B. Saunders.

Rodieck, R. W. and W. E. Stone (1965): Analysis of receptive fields of cat retinal ganglion cells. J. Neurophysiology. 28:833-849.

Schetzen, M. (1974): A theory of nonlinear system identification. Int'l. J. Control. 20:577-592.

Schinz, R. H. (1975): Structural specialization in the dorsal retina of the bee, Apis mellifera. Cell Tiss. Res. 162:23-34.

Shapley, R. (1971): Fluctuations of the impulse rate in Limulus eccentric cells. J. Gen. Physiol. 57:539-556.

Shaw, S. R. (1969): Interreceptor coupling of an ommatidia of drone honey bee and locust compound eyes. Vision Res. 9:999-1029.

Shaw, S. R. (1969): Optics of arthropod compound eye. Science. 165:88-90.

Sheby, D. and G. D. McCann (1976): Nonlinear analysis of visual systems using LEDs and optic fibers. Proc. Soc. Photo-Optical Instrum. Engrs. 89:51-58.

Smith, H. W. (1966): Approximate Analysis of Randomly Excited Nonlinear Controls. Cambridge, Mass: M.I.T. Press.

Stone, J. and M. Fabian (1968): Summing properties of the cat's retinal ganglion cell. Vision Res. 8:1023-1040.

Strausfeld, N. J. and J. A. Campos-Ortega (1977): Vision in insects: pathways possibly underlying neural adaptation and lateral inhibition. Science. 195:894-897.

Trevino, D. L. and J. L. Larimer (1970): The responses of one class of neurons in the optic tract of crayfish (Procambarus) to monochromatic light. Z. Vergl. Physiologie. 69:139-149.

von Seelen, W. and K.-P. Hoffman (1976): Analysis of neuronal networks in the visual system of the cat using statistical signals. Biol. Cybernetics. 22:7-20.

Wald, G. (1968): Single and multiple visual systems in arthropods. J. Gen. Physiol. 51:125-156.

Waterman, T. H. and H. R. Fernandez (1970): E-vector and wavelength discrimination by retinular cells of the crayfish Procambarus. Z. Vergl. Physiologie. 68:154-174.

Wiener, N. (1958): Nonlinear Problems in Random Theory. Cambridge, Mass: M.I.T. Press.

Wiersma, C.A.G. and T. Yamaguichi (1966): The neuronal components of the optic nerve of the crayfish as studied by single unit analysis. J. Comp. Neur. 128:333-358.

Wiersma, C.A.G. and T. Yamaguichi (1967): Integration of visual stimuli by the crayfish central nervous system. J. Exp. Biol. 47:409-431.

Wiitanen, W. (1973): Some aspects of visual physiology of the honeybee. J. Neurophysiology. 36:1080-1089.

Woodcock, A.E.R. and T. H. Goldsmith (1970): Spectral responses of sustaining fibers in the optic tracts of crayfish (Procambarus). Z. Vergl. Physiologie. 69:117-133.

Woodcock, A.E.R. and T. H. Goldsmith (1973): Differential wavelength sensitivity in the receptive fields of sustaining fibers in the optic tract of the crayfish Procambarus. J. Comp. Physiol. 87:247-257.

Yamaguchi, T. and T. Ohtsuka (1973): Dual channelling mechanism of brightness and dimness information in the crayfish visual system. J. Fac. Sci. Hokkaido Univ. Ser. VI, Zool. 19:15-30.

Yasui, S. (in preparation): Stochastic functional Fourier series, Volterra series and nonlinear system analysis.

York, B. (1972): Sustaining fibers in the rock lobster. J. Neurobiology. 3:303-309.

Zettler, F. and H. Autrum (1975): Chromatic properties of lateral inhibition in the eye of a fly. J. Comp. Physiol. 97:181-188.

Zettler, F. and M. Jaruilehto (1972): Lateral inhibition in an insect eye. Z. Vergl. Physiologie. 76:233-244.